Critical Normal Traffic Loading for Flexure of Bridges according to TMH7

by

Andreas Dawid Malan

Thesis presented in partial fulfillment of the requirements for the degree of

Master of Science in Civil Engineering

at the University of Stellenbosch

Department of Civil Engineering
University of Stellenbosch
Private Bag X1, 7602 Matieland, South Africa

Study leader: Dr. G.C. van Rooyen

March 2013

Declaration

By submitting this thesis/dissertation electronically, I declare that the entirety of the work contained therein is my own, original work, that I am the sole author thereof (save to the extent explicitly otherwise stated), that reproduction and publication thereof by Stellenbosch University will not infringe any third party rights and that I have not previously in its entirety or in part submitted it for obtaining any qualification.

Date: March 2013

Synopsis

Critical Normal Traffic Loading for Flexure of Bridges according to TMH7

A.D. Malan

Department of Civil Engineering
University of Stellenbosch
Private Bag X1, 7602 Matieland, South Africa

Thesis: MScEng (Civil)

March 2013

Different types of live loading due to traffic may act on bridges. The focus of this study is on normal traffic loading according to the South African specification of TMH7. Heavy vehicles are not included in normal traffic loading. TMH7 represents the code of practice for the design of highway bridges and culverts in South Africa. The aim of the study is to provide an insight into the flexural analysis of skew bridges, under the effects of normal traffic loading.

The need for the study arose since the specification of TMH7 does not explicitly specify application patterns for normal traffic loading. Only the intensity of normal traffic loading is specified and it should be applied to yield the most adverse effects. For these reasons, a set of so-called standard application patterns are investigated and developed through the course of this study. The envelope of the values from the standard application patterns are compared to the most adverse application pattern for flexural effects in certain design regions of the bridge deck. Flexure, as in the context of this study, translates into the bending and twisting of the bridge deck under loads.

A number of numerical experiments are performed for typical single span and multi-span continuous carriageways, where the standard application patterns are compared to the most adverse application patterns. The results from the numerical experiments are documented and compared as the angle of skew of the bridge deck increases in plan-view. For this purpose, the development of effective and specialized software was necessary.

It was found that the set of standard application patterns can be used as a preliminary approximation for the most adverse effects of normal traffic loading, for specific flexural resultants in certain design regions of a bridge deck. However, for a large number of secondary flexural effects, the set of standard application patterns did not represent a good approximation for the most adverse values.

Sinopsis

Kritiese Normale Verkeers-belasting vir Buig-effekte van Brûe volgens TMH7

A.D. Malan

Departement van Siviele Ingenieurswese
Universiteit van Stellenbosch
Privaatsak X1, 7602 Matieland, Suid-Afrika

Tesis: MScIng (Siviel)

Maart 2013

Verskillende tipes lewendige belasting, as gevolg van verkeer, kan op brûe inwerk. Die fokus van die studie is op normale verkeers-belasting volgens die Suid-Afrikaanse spesifikasie van TMH7. Swaar-voertuie word nie ingesluit by normale verkeers-belasting nie. TMH7 verteenwoordig die kode vir die ontwerp van padbrûe en duikers in Suid-Afrika. Die doel van die studie is om insig te verskaf in die buig-analise van skewe brûe, as gevolg van die werking van normale verkeers-belasting.

Die rede vir hierdie studie ontstaan aangesien die spesifikasie van TMH7 nie eksplisiet aanwendings-patrone vir normale verkeers-belasting voorskryf nie. Slegs die intensiteit van normale verkeers-belasting word voorgeskryf en dit moet aangewend word om die negatiefste effekte te verkry. Vir hierdie redes word 'n versameling van sogenaamde standaard aanwendings-patrone deur die loop van die studie ondersoek en ontwikkel. Die omhullings-kurwe van die waardes wat deur die standaard patrone gelewer word, word vergelyk met die waarde van die aanwendings-patroon wat die negatiefste buig-effek in sekere ontwerp-areas van die brugdek veroorsaak. Buig-effekte, soos van toepassing op hierdie studie, verwys na buig en wring van die brugdek as gevolg van belastings.

'n Aantal numeriese eksperimente, vir enkel-span sowel as multi-span deurlopende brugdekke, word uitgevoer en die standaard aanwendings-patrone word vergelyk met die aanwendings-patrone wat die negatiefste waardes lewer. Die resultate van die numeriese eksperimente word gedokumenteer en vergelyk soos die hoek van skeefheid van die brugdek in plan-aansig toeneem. Vir hierdie doel is die ontwikkeling van effektiewe en gespesialiseerde sagteware dus nodig.

Daar is gevind dat die standaard aanwendings-patrone, vir spesifieke buig-resultante in sekere ontwerp-areas van die brugdek, as 'n voorlopige benadering vir die negatiefste effekte van normale verkeers-belasting gebruik kan word. Dit was egter verder gevind dat vir 'n groot aantal sekondêre buig-effekte, die versameling standaard aanwendings-patrone nie as 'n goeie benadering vir die negatiefste waardes dien nie.

Acknowledgments

To my study leader, Dr. Gert van Rooyen, for the pleasant and challenging learning experience. Thank you for your expert guidance in the exciting field of civil engineering informatics.

Fritz and Jackie Malan, my father and mother, for providing me with the opportunity to attend university. Thank you to my brother, Johann Malan and all my other family and friends for your inspiration and loving support.

Jeanine Bekker, for your patience and support.

Thank you to the following people for providing me with the opportunity to interview them:

- Mr. Frans Kromhout (BKS, Pretoria)
- Mr. Johan Kotzé (Aurecon, Pretoria)
- Prof. Jan Wium (University of Stellenbosch)
- Mr. Andri van Blerk (Antro Enterprises Limited, New Zealand)
- Mr. Pieter Louw (Pieter Louw and Associates, STRAP Software, Pretoria)
- Mr. Johan Swart (WSP, Bloemfontein)

Thank you to the following people for attending the talk on bridge deck analysis, for providing feedback and ideas on the software development:

- Mr. Bennie Zietsman (Element Consulting Engineers, Stellenbosch)
- Dr. Celeste Barnardo-Viljoen (University of Stellenbosch)
- Mr. Pierre van der Spuy (Aurecon, Cape Town)
- Mr. Rossouw Conradie (Aurecon, Cape Town)
- Mr. Harry Viljoen (Provincial Government, Western Cape)

I greatly acknowledge the OSP funding from the University of Stellenbosch, without which this study would not have been possible.

Thank you to the following people for testing the prototype software and verifying the user guide:

- Johann Malan: Windows system
- Johann Potgieter: Linux system

Dedicated to my father, Dr. Fritz Johannes Malan. The inspiration you provided will always be with me.

Contents

List of Figures

List of Tables

List of Abbreviations

2D	Two Dimensional
3D	Three Dimensional
API	Application Programming Interface
CAD	Computer Aided Design
DKT	Discrete Kirchoff Triangle
NA	Normal Traffic Loading
NB	Abnormal Traffic Loading
NC	Super Traffic Loading
TMH	Technical Methods for Highways
UML	Unified Modeling Language
W & A	Wood and Armer Moments

List of Symbols

General

$^\circ$	Degrees
m	Meter
N	Newton

Set Theory

$E\left(x\right)$	Logical expression
$\in$	Element of
$\notin$	Not an element of
$\subseteq$	Subset
$\subset$	Proper subset
$\cup$	Union
$\cap$	Intersection
$\emptyset$	Empty set
$\wedge$	Universal quantifier
$\vee$	Existential quantifier

Plate Theory

A_e	Area of the element
E	Modulus of elasticity
t	Plate thickness
u_3	Transverse displacement perpendicular to the plane of the element
ν	Poisson's ratio
$\left\{q\right\}$	The vector containing the intensities of the load at each node
$\left\{w_e\right\}$	Element load vector
$\left[S_e\right]$	Displacement-interpolation matrix
M_{11}	Twisting moment
M_{12}	Transverse bending moment
M_{21}	Longitudinal bending moment

1 Introduction

An introduction to the study of critical normal traffic loading for flexure of bridges is presented in this chapter. Normal traffic loading is described according to the South African specification of TMH7, from the range of TMH's (Technical Methods for Highways). The following definitions are presented:

TMH7: TMH7 represents the code of practice for the design of highway bridges and culverts in South Africa.

Normal Traffic: Normal traffic represents a formula loading consisting of the most severe arrangement of legal vehicles that are probable [14].

The incorporation of heavy vehicles are excluded from normal traffic loading. The problem statement and the aim of the study are presented in this chapter. The layout and organization of the document are also described. Electronic media, as an aid to this document, is discussed at the end of this chapter.

1.1 Problem Statement

Bridge structures are subject to dead loads and live loads. Dead loads refer to permanent loads, e.g. the own weight of the structure. Live loads, such as live loads due to traffic, refer to loads which may act in various possible locations on the bridge deck. Without the aid of specialist software, the determination of the positions where the traffic loads should be placed to produce the most adverse effects are not always obvious, except for simple structures with simple loading arrangements. The problem statement is presented below:

- The most adverse effects are not *necessarily* obtained when the bridge deck is fully loaded.
- The South African specification of TMH7 does not explicitly specify application patterns for live loading due to normal traffic.
- Published influence surfaces are not available for all types of structural geometries, or for all the modes of failure in each of the regions of the bridge deck (Refer to Chapter 2).

The problem arises how the traffic loads *should* be applied to produce the most adverse effects. From the three statements mentioned above, the aim of the study is formulated in the next section.

1.2 Aim of the Study

The aim of the study is to provide an insight into the flexural analysis of skew bridges, under the effects of normal traffic loading according to TMH7. In the context of this study, flexure of bridges translates into the bending and twisting of the bridge deck under loads. The aim of the study is further described in the paragraphs below:

Most Adverse Effects: Since the most adverse effects are not necessarily obtained when all the loadable parts of the bridge deck are loaded, the following topics will be investigated:

- The possibility to determine certain design regions in the bridge deck where the flexural modes of failure are critical, i.e. a specific mode of failure reaches its absolute maximum value in that region.
- The possibility to formulate certain guidelines regarding which parts of the bridge deck should be loaded to produce the most adverse effects for a selected mode of failure in a specific design region.

Application Patterns: Since TMH7 does not explicitly specify application patterns for normal traffic loading, the following questions should be asked:

- Is it possible to develop a certain set of standard application patterns and can the envelope of these patterns be used to approximate the most adverse effects of normal traffic loading?
- If these standard patterns are used, by how much will their values differ from the most adverse values?
- Can the set of standard application patterns be used as the angle of skew of the bridge deck increases in plan-view?
- Will the standard application patterns be applicable to both single span and multi-span continuous carriageways?

From the questions formulated above, it becomes clear that a procedure must first be developed to produce the most adverse application pattern in a selected region of the bridge deck. Thereafter, the formulation of a set of standard application patterns can be pursued. A number of numerical experiments will then be performed for typical bridges and the values produced by the set of standard application patterns will be compared to the values produced by the most adverse application patterns. For this purpose, qualitative comparative analysis will be performed. The application patterns will be compared as the angle of skew of the bridge deck increases in plan-view. The application patterns will also be compared for single span and multi-span continuous carriageways.

Software Development: The development and implementation of effective and specialized software is a prerequisite to the study of flexure of skew bridges according to TMH7. It will be necessary to perform a large amount of numerical experiments for typical carriageways. Furthermore, a large number of load cases will have to be compared to each other, in order to determine if a set of standard application patterns can be developed and used to approximate the most adverse effects of normal traffic loading.

1.3 Layout and Organization

This document consists of 9 chapters including the introduction. Six appendices from A to F are also included.

An overview of the literature is presented in Chapter 2. A continuation of the literature, pertaining specifically to normal traffic loading according to the South African specification of TMH7, is presented in Chapter 3. The interpretation of the results is presented in Chapter 4. Two approaches regarding the generation of normal traffic loading patterns are described in Chapter 5.

The implementation, using object-orientated methods of software technique, is presented in Chapter 6. After the theory and technical requirements are described and the implementation presented, the results from detailed analysis for single span and multi-span continuous carriageways are presented in Chapter 7 and Chapter 8 respectively. The conclusions and recommendations are presented in Chapter 9.

Additional results for single span carriageways and multi-span continuous carriageways are presented in Appendix A and Appendix B respectively. The formulas for the Wood and Armer design moments are presented in Appendix C. A user guide describing the operation of the software is presented in Appendix D. An overview of the elements of the software model, developed for the purpose of this study, is presented in Appendix E. Lastly, electronic media is attached to this document in Appendix F. The electronic media contains the software, source code, results and files in digital format.

1.4 Electronic Media

Through the course of this document, the generation and comparison of critical normal traffic loading for flexure of bridges will be presented. It is not always possible to present these critical normal traffic loading patterns for large bridges, or bridges with complex traffic loading patterns, with a sufficient level of detail in printed media, e.g. an A4 page. For the purpose of providing a sufficient level of detail, the traffic loading patterns can be viewed in a digital graphical environment. All the data files are attached to this document in digital format in Appendix F. Each loading pattern is associated with a specific file as well as a loading pattern number. The associated files and loading pattern numbers are indicated in the tables that present the results of the various carriageways treated in this study. The procedure for viewing the data files are explained in the user guide of Appendix D.

2 Literature Review

A review of the literature is presented in this chapter. This chapter deals with TMH7 in general and the underlying principles of limit state design applicable to the work in this document. The characteristics of skew bridges and the use of influence surfaces are also described. A continuation of the literature, pertaining specifically to normal traffic loading, is presented in the next chapter, Chapter 3.

2.1 Bridge Traffic Loading

Different types of traffic loads act on bridges. Live loading due to traffic on highway bridges consists of three types [14]:

NA Normal Loading

NB Abnormal Loading

NC Super Loading

The specific focus of this study is on type NA loading. Type NA loading represents live loading due to normal traffic and is further discussed in Chapter 3. Type NB loading is a unit loading representing a single abnormally heavy vehicle. Type NC loading is a loading representing multi-wheeled trailer combinations (or self-propelled multi-wheeled vehicles) with controlled hydraulic suspension and steering intended to transport very heavy indivisible payloads.

The NA, NB and NC loadings are applied separately according to TMH7, except in the case where dual carriageways are carried by a single substructure, or when a unified substructure carries separate superstructures of a dual carriageway. The exceptions, where type NA, NB and NC loadings are not applied separately, are not treated in this study.

2.2 Limit State Design

The definition of limit state design according to TMH7 is presented below [14]:

> "Limit state design is the logical and practical procedure that has been evolved to achieve acceptable probabilities so that the structure being designed will remain fit for the required purpose during some reference period with its intended life taken into consideration. A structure, or part of a structure, is considered unfit for use when it exceeds a particular state, called a limit state, beyond which it infringes one of the criteria governing its performance or use."

The limit states can be placed in two categories [14]:

Ultimate Limit State: The ultimate limit state corresponds to the maximum load carrying capacity.

Serviceability Limit State: The serviceability limit state is related to the criteria governing the normal use and durability of structure.

TMH7 is based on the principles of limit state design, which can be considered to be a semi-probabilistic procedure using partial safety factors to determine design effects and involves checking for the ultimate limit state and the serviceability limit state.

2.3 Skew Bridges

The majority of bridges built today have some form of skew, taper or curve. Due to the increasing restriction on available space for traffic schemes, the alignment of a transport system can seldom be adjusted for the purpose of reducing the skew or complexity of bridges. In addition to introducing problems in the design details of a bridge deck, skew has a considerable effect on the behaviour of the bridge deck and the critical stresses. The special characteristics of skew of a slab are presented below [7]:

- variation in the direction of maximum bending moments across the width
- hogging moments in the region of the obtuse corner
- considerable torsion of the deck
- high reactions and shear forces near the obtuse corner
- low reactions and possibly uplift in the acute corner

The magnitude of these effects depend on the angle of skew, the ratio of width to span length and particularly on the type of construction of the bridge deck and the supports.

2.4 Influence Surfaces

Live loads due to traffic refer to loads which may act in various possible locations on the bridge deck. The determination of the positions where the traffic loads should be placed to produce the most adverse effects are not always obvious for complex structures with complex loading arrangements.

Influence surfaces and design charts can be used to determine the effect in a specific region, resulting from the application of a load in another region. For example, an influence surface and the application of a vehicle loading is shown in Figure 2.1.

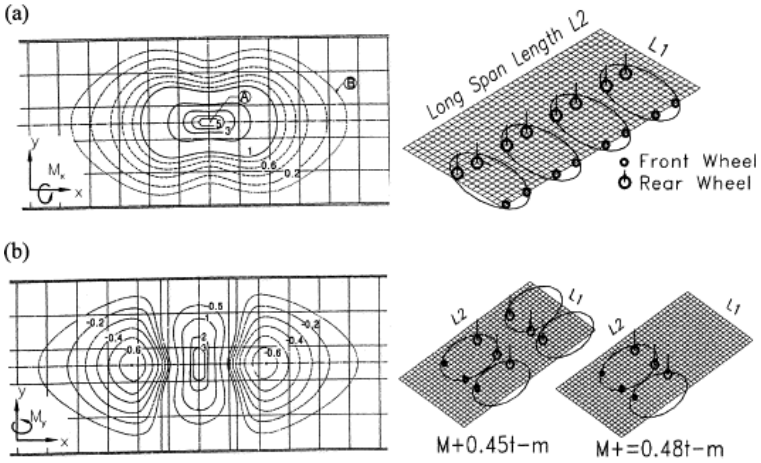

Figure 2.1: Influence surface (Source: Pucher [16])

However, influence surfaces and design charts have the following disadvantages [7]:

- They are not always easy to use.

- They do not give the user a complete picture of the force system in the bridge deck under the effects of a particular load case.
- They cannot be used for orthotropic, cellular or beam-and-slab decks due to their different distortional and torsional characteristics.

Furthermore, published influence surfaces and design charts are not available for all types of structural geometries and support conditions in each of the regions of the bridge deck.

2.5 Methods of Analysis

According to TMH7, the methods of analysis used to assess compliance with the requirements of the various limit states should be based on as accurate a representation of the behaviour of the structure as is practicable. The methods used and the degree of sophistication, or refinement thereof, will depend on the nature, purpose and configuration of the structure. The effects under the most adverse conditions, appropriate to the ultimate limit state, should be calculated by a method satisfying equilibrium requirements, all effects being shown to be in equilibrium with the applied actions [14]:

- Elastic methods are acceptable as lower-bound collapse solutions. They will also lead to solutions less likely to violate serviceability criteria.
- Non-linear plastic or yield-line methods may be adopted when appropriate to the type of structural material and the response of the structure to actions and imposed deformations.

Linear elastic first order finite element analysis are used throughout this study for comparative qualitative analysis. The finite element modeling and analysis are further described in section 3.4.

3 Normal Traffic Loading

The different types of live loading due to traffic on highway bridges were discussed in Chapter 2. Normal (NA) traffic loading, the specific focus of this study, is presented in this chapter.

The geometry of the components of the bridge deck is presented in this chapter. Thereafter, the definition and application of type NA loading to produce the most adverse effects are described. Mesh and load considerations, regarding the finite element modeling of type NA loading are presented at the end of this chapter.

3.1 Bridge Deck Geometry

The investigation of critical normal traffic loading is restricted to the modeling and analysis of the *bridge deck*, i.e. the whole bridge structure is not considered. The geometry and layout of the bridge deck, for the application of type NA loading is presented in this section. The carriageway, supports and notional lanes are defined below:

Carriageway: The carriageway is that part of the bridge deck that includes all traffic lanes and shoulders. The carriageway represents that part of the bridge deck for the application of traffic loads.

Support: Supports are represented as line-type supports beneath the carriageway. Vertical displacement is restricted by the supports, i.e. the displacement perpendicular to the plane of the bridge deck. The supports run through the entire carriageway in the transverse direction.

Notional Lane: Notional lanes represent longitudinal strips along the carriageway, used for the purpose of applying the specified vehicle traffic loading.

The bridge geometry, as defined above, is presented in Figure 3.1 for a skew bridge deck in plan-view.

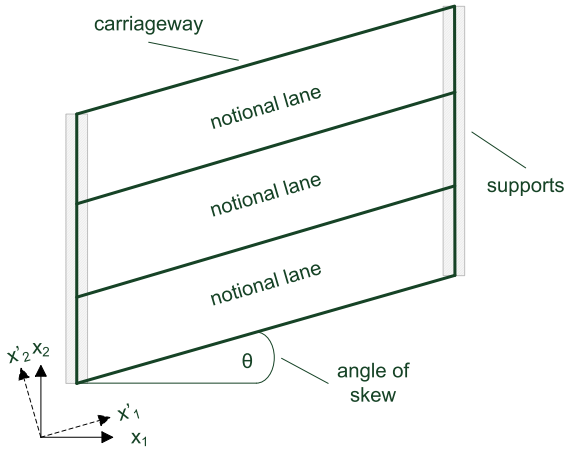

Figure 3.1: Bridge deck geometry

The notional lanes do not represent the actual traffic lanes. The width and number of notional lanes are specified by TMH7 and they are only dependent on the effective width[1] of the carriageway.

[1]Carriageways with an effective width less than $4.8\,m$, with a non-integral number of notional lanes are not considered in this study.

3.2 Definition of NA Loading

Type NA loading represents normal traffic without the incorporation of heavy vehicles. NA loading is a formula loading representing normal traffic consisting of the most severe arrangement of legal vehicles that are probable, as defined in the introduction of Chapter 1. The layout and intensity of type NA loading is presented in this section, as specified according to TMH7.

Type NA loading consists of a distributed part and a concentrated part acting in conjunction with each other. The distributed part can either be in the form of two equal and parallel line loads spaced 1.9 m apart, or a uniformly distributed load over the full width of the notional lane. The concentrated part of type NA loading can either be in the form of two equal point loads spaced 1.9 m apart, or in the form of a knife-edge load over the full width of the notional lane. Two possible methods of application of normal traffic loading are illustrated in Figure 3.2.

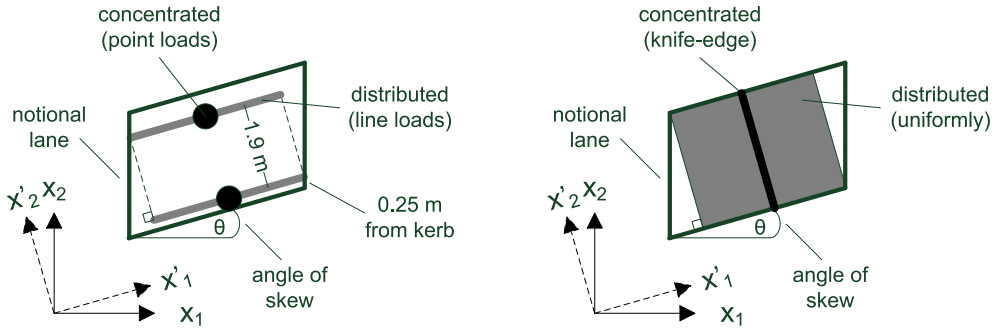

(a) Spaced 1.9 m apart **(b)** Over full width

Figure 3.2: Normal traffic loading

The distributed part is dependent on the effective loaded length of the relevant part where it is applied. The concentrated axle part is dependent on the loading sequence of the relevant notional lane. The intensities of type NA loading, pertaining to the distributed part and the concentrated part are described further in the subsections below.

3.2.1 Distributed Load

The distributed part of type NA loading represents a nominal distributed lane loading $Q_a = Q_a(L_e)$, acting on the whole or parts of the length of any notional lane or combination of such lanes. In the longitudinal direction the loading is uniformly distributed for any continuous part of a notional lane, but the intensity may be different for separate parts:

$$\begin{aligned} &\text{for } L_e < 36\,m && Q_a = 36\,kN/m \\ &\text{for } L_e \geq 36\,m && Q_a = \tfrac{180}{\sqrt{L_e}} + 6\,kN/m \end{aligned}$$

with,

L_e the effective loaded length in m
Q_a the intensity of the loading kN/m

The specification of TMH7 provides a procedure whereby the loading intensities are based on the assumption that the total loading is dependent on the aggregate loaded length of all the notional lanes being considered (Refer to section 2.A.2.1 of TMH7). The intensities of the uniformly distributed loadings in these separate parts are not necessarily equal. The loading procedure for the distributed part is presented according to method A(i) of TMH7:

Loading Procedure for the Distributed Loads: That part of any notional lane, which has the maximum average influence value (positive or negative as the case may be), is loaded at an intensity determined by the NA uniformly distributed loading formula for that loaded length. Thereafter, that part of the same or any other notional lane with the next highest average influence value of similar sign is loaded at an intensity such that the total load on the two loaded parts correspond to the formula loading for a loaded length equal to the sum of the two loaded lengths.

If $\sum_{i=1}^{p} L_i$ is the sum of all the loaded lengths up to and including the p^{th} part, the intensity of loading Q_{ap} on the p^{th} part of length L_p is defined as follows:

$$Q_{ap} = \left(Q_a \sum_{i=1}^{p} L_i - \sum_{i=1}^{p-1} Q_i L_i \right) / L_p$$

with,

Q_a	the intensity of loading for a length of $\sum_{i=1}^{p} L_i$
Q_i	the intensity of loading applied to any previously calculated base length portion i
L_i	is the dimension of any previously calculated base length portion i

In this procedure Q_{ap} reduces as p increases with no limiting value.

3.2.2 Concentrated Load

The concentrated part of type NA loading is in the form of one nominal axle load[2] per notional lane with the following intensity:

$$\frac{144}{\sqrt{n}}\, kN$$

with,

n	the loading sequence number of the relevant notional lane

For example, $n = 1$ for the first lane loaded with the axle load, $n = 2$ for the second loaded lane, etc. The concentrated axle part of type NA loading is applied in conjunction with the distributed loading defined in the previous subsection.

No additional allowances need to be made for the effects of wheel impact. The effects of wheel impact, together with an allowance for the dynamic effect of moving traffic, are included in NA loading [14].

[2]Two nominal $100\,kN$ wheel loads that provide for local impact effects are not treated in this study.

3.3 Application of NA Loading

The definition and intensities of type NA loading were presented in the previous section. Certain specifications regarding the application of type NA loading according to TMH7 are presented in the subsections below.

3.3.1 Distributed Load

In the longitudinal direction, the distributed part of type NA loading should be applied to those parts of any combination of notional lanes which will result in the most adverse effect for the member or structure under consideration (Refer to section 2.6.3.2.1 in Part 2 of TMH7). The effective loaded length L_e consists of the aggregate length of all the parts loaded in any single notional lane, or combination of notional lanes in one or more carriageways. The distributed part of type NA loading should be applied as two equal and parallel line loads of $Q_a/2\,kN/m$, to represent the effect of two longitudinal lines of wheels spaced $1.9\,m$ apart.

The loading should be applied in such a transverse position as to represent the most severe effect on the member being analyzed. The line loads on separate parts of any single notional lane may act in different transverse positions, but always parallel to the longitudinal direction of a lane. The two line loads acting on separate parts should be of equal length, terminating at each end on a line orthogonal to the direction of the lane. In the case where type NA loading is applied as two equal and parallel line loads, the loading may not be placed closer than $0.25\,m$ from the face of a kerb, as indicated in Figure 3.2.

3.3.2 Concentrated Load

The axle loads equal to $144/\sqrt{n}\,kN$ per notional lane, act in conjunction with the distributed loads. The axle loads are applied in the form of two equal point loads, to represent the effect of two wheel loads spaced $1.9\,m$ apart (Refer to section 2.6.3.2.2 in Part 2 of TMH7). Only one axle load is applied to any single notional lane, in such a position that the point loads coincides with the transverse position of the line loads. The loading sequence n for the different lanes must be selected to cause the most severe effect. The axle loads in the adjacent notional lanes do not necessarily act in a single line and shall be taken as acting at such positions as to cause the most severe effect on the member being analyzed.

3.3.3 Specification for Loads

The specification for the application of type NA loading according to TMH7 was presented in the subsections above. In short, the South African specification of TMH7 does not explicitly specify application patterns for type NA loading. Only the intensity of NA loading is specified and it should be applied to yield the most adverse total effect, bound by some geometric restrictions. For these reasons, an investigation for the development of critical and standard application patterns are pursued. The load application patterns are presented in Chapter 5.

3.4 Finite Element Modeling

The definition and application of type NA loading were presented in the previous sections. The finite element modeling, regarding certain mesh considerations and the use of consistent point loads

in combination with consistent line loads are described in this section.

Comparative Qualitative Analysis: The finite element modeling of the bridge deck and the application of type NA loading is done for the purpose of performing comparative qualitative analysis. The finite element results that are produced are qualitative, not quantitative. For the purpose of performing comparative qualitative analysis, the exact section of the bridge deck is not taken into consideration. The bridge deck is modeled as a slab with a constant thickness. The different patterns of type NA loading are applied to the slab-deck and the values are compared relative to each other as the angle of skew of the bridge deck increases in plan-view. The application patterns of type NA loading are presented in Chapter 5.

3.4.1 Plate Bending Element

Thin displacement-based plate bending elements are used to approximate the geometry and physical state of the bridge deck. The plate bending element used for the finite element modeling of the bridge deck is the DKT (Discrete Kirchoff Triangle) plate bending element. The DKT element consists of one transverse displacement degree of freedom and two in-plane rotational degrees of freedom per node. The theory, implementation and verification of the element can be found in references [11, 17].

The specific DKT plate element behaves well in bending and is ideally suited for flexural analysis. The element load vector is represented by the following expression [11]:

$$\left\{w_e\right\} = \int_{A_e} \left[S_e\right] \left\{q\right\} \, \mathrm{dA_e}$$

with,

w_e	the element load vector
A_e	the area of the plate element
$\left[S_e\right]$	the displacement-interpolation matrix
$\left\{q\right\}$	the vector containing the intensities of the load at each node

The element load vector $\left\{w_e\right\}$, as presented above, is only applicable for loads over the area of the element A_e, with the intensities of the load at each node contained in $\left\{q\right\}$. The modification of the expression for the element load vector, pertaining to the application of type NA loading as two line loads in combination with two point loads are presented in the next subsection.

3.4.2 Mesh and Load Considerations

The application of type NA loading over the full width of a notional lane is a permissible simplification only when the transverse distribution in a lane has no significant effect on the member being analyzed (Refer to Figure 3.2). The application of type NA loading over the full width of a notional lane will not be considered further in this study. The application of type NA loading as two equal and parallel line loads spaced $1.9\,m$ apart, acting in conjunction with two equal point loads spaced $1.9\,m$ apart, will further be used for the finite element modeling of type NA loading.

Certain aspects, regarding the generation of the mesh and the application of the loads, have to be considered for the use of line loads and point loads:

- Traditionally a point load is applied in the form of a node load, i.e. at a specific finite element system node.
- Line loads can be approximated as a collection of node loads, where the effect of the line load is distributed among the nodes beneath/above the line load. Again a line-of-nodes are required for the application of a line load.

Should the application of type NA loading be done according to the procedures described above, the generation of the mesh and the application of the loads may become overly complicated. The generation of the mesh, to ensure that a point load is applied at a node and a line load is applied at a line-of-nodes, will result in a non-regular and warped mesh. Undesirable aspect ratios may also develop. These effects increase as the angle of skew increases, from the specification that the loads should end on a line orthogonal to the direction of a lane (Refer to Figure 3.2). Further complications arise from the specification that the line loads may not be placed closer than $0.25\,m$ from the face of a kerb.

For the reasons mentioned above, consistent point loads and consistent line loads are developed and implemented. Consistent point loads and line loads can be applied on the element, independent of the layout of the nodes of the element. Consistent element loads provide technically correct load application procedures, i.e. the loads are not simply lumped on the nodes, but incorporated in the integration of the element load vector $\left\{w_e\right\}$. The development of consistent point loads and consistent line loads, for the DKT plate bending element, are presented in the paragraphs below:

Consistent Point Load: A consistent point load, in the local area-coordinate system $\left\{z\right\} = \left\{z_1 \quad z_2 \quad z_3\right\}^T$, is shown in Figure 3.3.

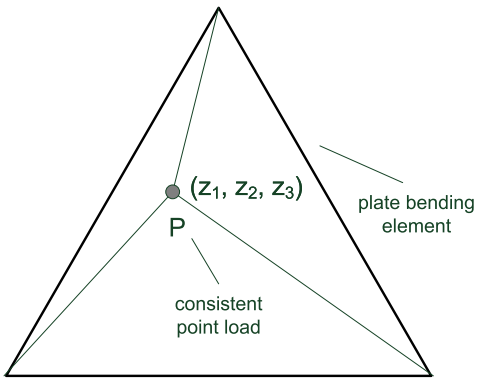

Figure 3.3: Consistent point load

Since the intensity of the load is constant, the integration of the element load vector simply reduces to the value of the displacement interpolation matrix $\left[S_e\right]$, at the location of the point load, scaled with the intensity of the load q:

$$\{w_e\} = q\left[S_e\right]_{at}\left\{z\right\}$$

Consistent Line Load: A consistent line load, with a mapping to the normalized coordinate system, is shown in Figure 3.4.

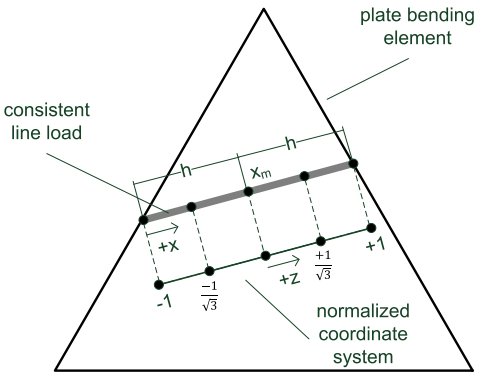

Figure 3.4: Consistent line load

Since the intensity of the load q is constant, it can be removed from the integral as a scalar:

$$\{w_e\} = q \int_x \left[S_e\right] \, \mathrm{dx}$$

The integral can be converted to the normalized coordinate system, by scaling the element load vector with half of the physical length of the line load h:

$$\{w_e\} = qh \int_{-1}^{+1} \left[S_e\right] \, \mathrm{dz}$$

The line integral reduces to the value of the displacement interpolation matrix $\left[S_e\right]$ at the two Gauss[3] points, gp_1 and gp_2, scaled with the intensity of the line load q and half the physical length of the line load h:

$$\{w_e\} = qh \left[\left[S_e\right]_{at\ gp_1} + \left[S_e\right]_{at\ gp_2} \right]$$

The procedures described in the paragraphs above, regarding the use of consistent point loads and consistent line loads, are ideally suited for the modeling of type NA loading. The consistent element loads provide technically correct loading procedures and the loads can be applied independent of the layout of the finite element nodes.

[3]For two point numerical integration, the Gauss weight is 1.0 and the two Gauss points are $\frac{\pm 1}{\sqrt{3}}$.

4 Interpretation of Results

The definition, application and finite element modeling of type NA loading were described in Chapter 3. The finite element modeling of type NA loading was done by making use of consistent point loads in combination with consistent line loads.

The method by which the finite element results are extracted, in which regions of the carriageway they are extracted, as well as the definition of the different moment resultants are presented in this chapter.

4.1 Actual and Median Results

For a specific finite element model of the bridge structure, i.e. a specific carriageway with a certain angle of skew, the finite element results are extracted in two ways for each of the selected resultants[4]:

- The *actual* point value at the monitored finite element node is extracted.
- The *median* of the values in the region of the monitored finite element node is extracted.

When the median value is used, the values from the neighboring nodes around the monitored finite element node are also included in the sample. The acquiring of point and median results are illustrated in Figure 4.1.

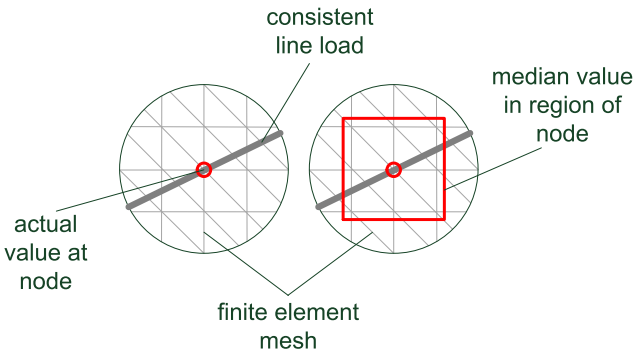

Figure 4.1: Actual and median results

When the monitored finite element node falls directly under a point or line load, local stress concentrations can occur at that node. The median-approach is adopted in order to avoid the effect of local stress concentrations, e.g. directly under a point or line load. The median definition is given below [18]:

Median: In statistics and probability theory, the median is described as the numerical value separating the higher half of a sample, a population, or a probability distribution from the lower half.

If the median value is to be used, the values in the sample are sorted from small to large. If the number of values in the selection is odd, the median is the middle value, else the median is represented by the average of the two middle values.

[4]The stress resultant definition is given in section 4.2.

4.2 Moment Resultants

As explained in the introduction, in Chapter 1, this study is concerned with the flexural analysis of skew bridges. The concept of flexure, for the purpose of this study, corresponds to the twisting and bending of the carriageway. The twisting and bending of the carriageway translates into twisting and bending moment resultants. The moment resultant definition is given below:

Bending Moment Vector: A bending moment vector is defined as M_{ij}, where i indicates the direction of the moment vector and j indicates the relevant face.

The different moment resultants are illustrated in Figure 4.2.

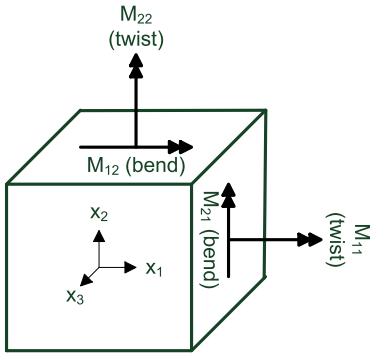

Figure 4.2: Moment resultants

The two twisting moment vectors are defined as M_{ii} or M_{jj}. They are of equal magnitude and opposite sign. The derivation of the moment resultants for thin plate theory can be found in reference [17].

4.2.1 Wood and Armer Moments

Wood and Armer proposed one of the most popular design methods that explicitly incorporate twisting moments in slab design [10]. The Wood and Armer approach apportions the twisting moment between the transverse bending and longitudinal bending terms, based on the reinforcement directions. From the Lagrange equation for elastic plates, the M_{11} twisting moment term can be written as follows:

$$M_{11} = -D\frac{\partial^2 u_3}{\partial x_1 \partial x_2}(1-\nu)$$

where D represents:

$$D = \frac{Et^3}{12\,(1-\nu^2)}$$

with,

u_3	the transverse displacement perpendicular to the plane of the element
E	the modulus of elasticity
t	the thickness of the plate
ν	Poisson's ratio

The Wood and Armer values incorporate the twisting moment, as presented in the equation above, into the M_{12} and M_{21} bending terms. As a result, ultimate design moments of resistance, M_{ux} and $M_{u\alpha}$ are produced, corresponding to the reinforcement layout in the x-direction and α-direction respectively. The Wood and Armer formulas can be found in Appendix C.

For the results presented in this study, the Wood and Armer values are acquired with an assumed reinforcement layout parallel to the edges of the carriageway in the longitudinal and transverse directions, as indicated in Figure 4.3 in the next section.

4.3 Critical Regions

Through the course of this study certain critical design regions were identified. Three main design regions were chosen and are marked with an "x" in Figure 4.3. The moment resultants that should be measured in each of the critical regions are also indicated in the figure, along with the assumed reinforcement layout.

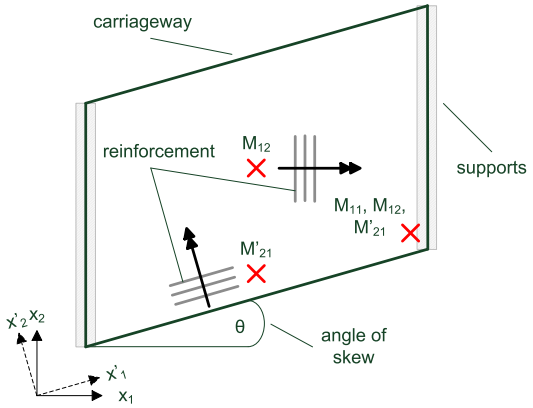

Figure 4.3: Critical regions and corresponding moment resultants

The three main design regions and corresponding moment resultants indicated in Figure 4.3 are described below:

Mid-span Edge: The longitudinal bending moment is measured in this region. As illustrated in Figure 4.3, the accented axes represent rotated axes, which corresponds with the angle of skew. Moment resultant M'_{21} represents the bending moment vector in the rotated x'_2-direction on the rotated x'_1-face. It is assumed that the reinforcement will be placed in the rotated longitudinal direction, parallel to the edge of the carriageway.

Mid-span Centre: The transverse bending moment is measured in this region. Moment resultant M_{12} represents the bending moment vector in the x_1-direction on the x_2-face. The transverse bending moment corresponds to the moment to be resisted by the reinforcement in the transverse direction.

Obtuse Corner: The twisting moment M_{11}, the transverse bending moment M_{12} and the longitudinal bending moment M'_{21} are measured in this region.

In order to improve the legibility of this document, M_{11} will be referred to as the twisting moment, M_{12} will be referred to as the transverse bending moment and M'_{21} will be referred to as the longitudinal bending moment.

5 Loading Patterns

The definition, application and finite element modeling of type NA loading were described in Chapter 3. Two approaches regarding the application of normal traffic loading are developed, namely the *standard* patterns and the *extreme* patterns. These patterns and a comparison of their results are presented in this chapter.

5.1 Standard Patterns

The South African specification of TMH7 for bridge loading does not specify application patterns for normal traffic loading. Only the loading intensities are prescribed and they should be applied to yield the most adverse effect in a specific region for a selected mode of failure.

The so-called standard patterns are based on intuition, i.e. how an engineer can consider placing type NA loading to yield the most adverse effect, if he/she did not have access to influence surface-based software. The standard patterns are illustrated in Figure 5.1 for a single span simply supported carriageway. Standard patterns for continuous multi-span carriageways are described on the next page.

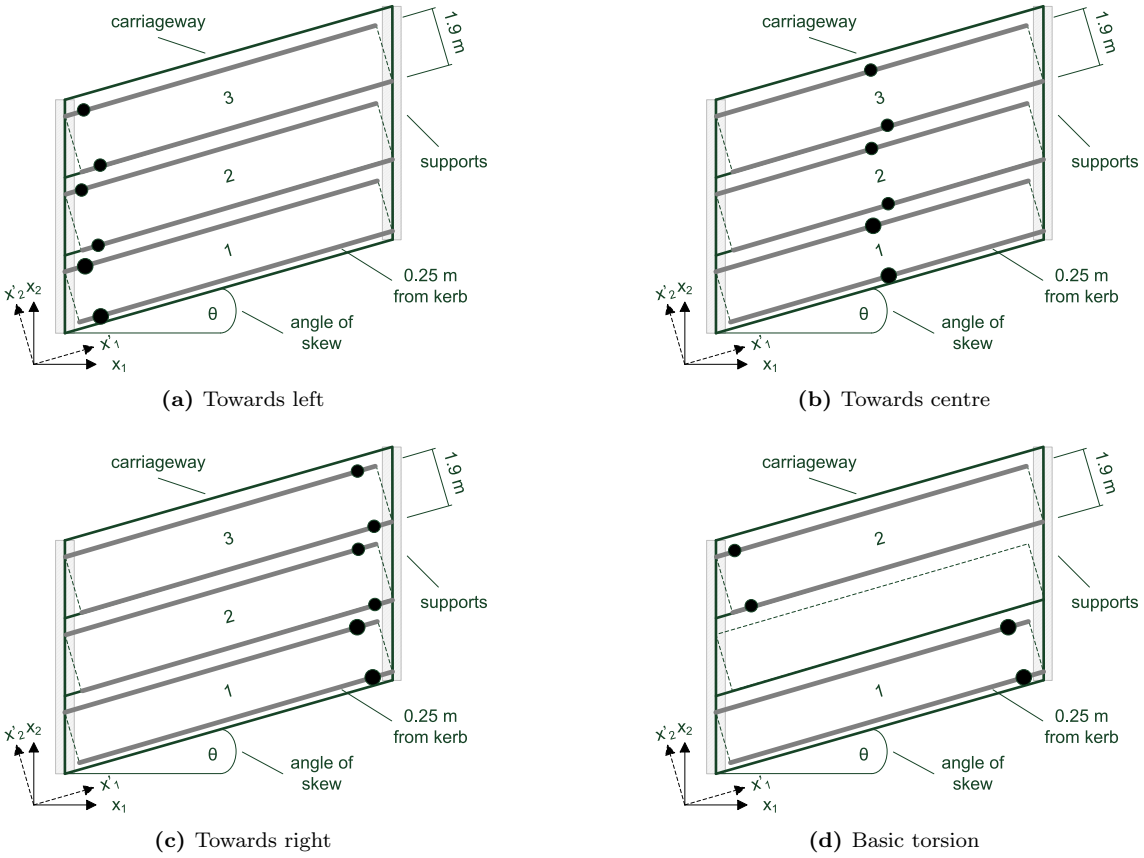

(a) Towards left

(b) Towards centre

(c) Towards right

(d) Basic torsion

Figure 5.1: Standard patterns

In the case of the standard patterns, as illustrated in Figure 5.1, the heaviest loading is placed towards the bottom edge of the carriageway in the transverse direction. The concentrated axle part

of type NA loading is placed towards the left, the centre and the right respectively. A basic torsion load is also included. When the standard patterns are used, all the loadable parts of the notional lanes are loaded, with a decreasing intensity when applicable, as described in section 3.2.1.

The standard patterns for continuous multi-span carriageways are similar to the standard patterns illustrated in Figure 5.1 for a single span carriageway. The loading with the highest intensity is placed towards the bottom edge of the carriageway in the transverse direction. In the longitudinal direction, the following pattern loading is applied with regard to the spans of the carriageway:

- each span is loaded individually
- adjacent spans are loaded incrementally
- odd spans are loaded incrementally
- even spans are loaded incrementally

The pattern loading applied to continuous carriageways in the longitudinal direction is similar to the pattern loading applied to continuous beams. For each of the spans loaded by the distributed part of type NA loading, the concentrated axle loads are placed towards the left, the centre and the right of each loaded span. It is not practical to illustrate all the standard patterns graphically in this text for a continuous multi-span carriageway. The number of standard NA loading patterns increase rapidly as the number of spans of the carriageway increase. The reader is referred to the user guide in Appendix D and the following example file:

StandardContinuousPatternsExample.load

The example file can be found in the electronic media of Appendix F. The example file illustrates the standard loading patterns for a skew continuous multi-span carriageway with three spans. When the continuous carriageway under consideration has an angle of skew larger than 0°, or the carriageway is not span-wise symmetric, the pattern loading is applied from both the left and the right side of the carriageway in the longitudinal direction.

The generation of standard NA loading patterns provide a systematic, programmatic procedure for loading a carriageway. The loading procedure is implemented in the software and can be used to generate standard NA loading patterns for any carriageway with any number of spans and any number of notional lanes.

5.2 Extreme Patterns

The standard NA loading patterns, as described in the previous section, loads all the loadable parts of a notional lane for a specific span. As a result, certain regions that provide a relieving effect may also be loaded, which results in less adverse values. For these reasons, a method is presented that generates *extreme* positive or negative loading patterns in a specific region of the carriageway for a selected mode of failure[5]. Extreme NA loading patterns provide the most adverse positive or negative effect in a specific region for a selected mode of failure.

Extreme NA loading patterns are based on the influence value of a specific incremental load, placed in certain positions. Consistent line loads move over all the loadable parts of the notional

[5]Only flexural modes of failure are considered in this study.

lanes of the carriageway in small increments. The generation of an extreme pattern is illustrated in Figure 5.2.

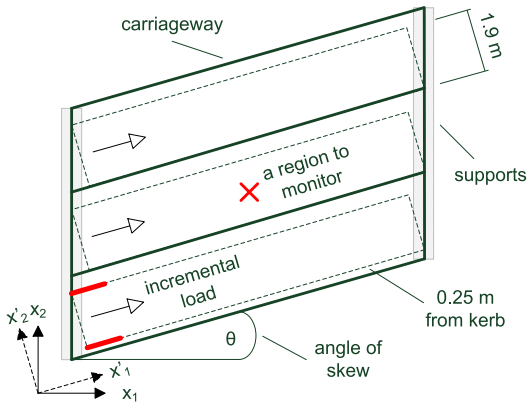

Figure 5.2: The generation of an extreme pattern

The generation of an extreme pattern, as illustrated in Figure 5.2, is described below:

- Select a region in the carriageway for which the extreme pattern should be generated.
- Select a mode of failure.
- The incremental load moves over all the loadable parts of the carriageway, as indicated by the arrows in Figure 5.2.
- The influence of the currently applied load is documented for the following effects:
  - If the currently applied load is causing a positive or a negative effect at the selected region.
  - The relative order of magnitude of the currently applied load, relative to the previously applied loads.

In order to produce the extreme positive pattern for the selected region and the selected mode of failure, all the loads that cause a positive effect will be applied in their decreasing order of magnitude. In this way, the load that has the largest influence value will be applied first, at the position where it causes the most adverse effect. The concentrated axle part of type NA loading will be placed at the position with the highest influence value in each of the notional lanes that should be loaded.

Similarly, in order to produce the extreme negative loading pattern for a specific region and a selected mode of failure, the incremental load with the largest negative effect will be applied first. Thereafter the incremental load with the second largest negative effect will be applied, until all the incremental loads that cause a negative effect have been applied. This approach produces an extreme loading pattern for a selected region and a selected mode of failure.

5.2.1 The K-factor of TMH7

The k-factor of TMH7 is a correction factor used to compensate for the effects of partial loading of parts of influence lines (Refer to section 2.A.2.2 of TMH7). The complication arises from the

fact that partial loading of an influence line may result in a more severe effect than that caused by loading the whole base of the relevant part of the influence line with a corresponding lower intensity. The challenge is to determine if a more severe effect will be obtained if the whole base of the influence line is to be loaded at a reduced intensity (when the loaded length exceeds $36\,m$) or if just the peak of the influence line should be loaded at the full intensity of $36\,kN/m$. Figure 5.3 illustrates this problem.

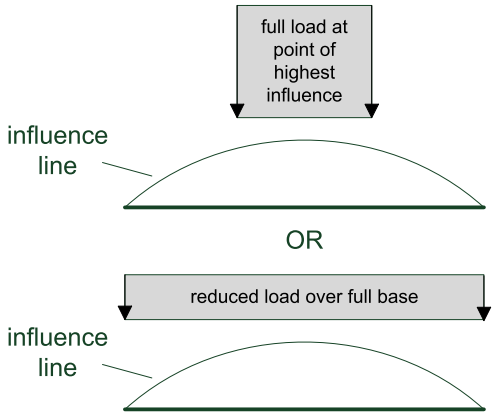

Figure 5.3: K-factor: The challenge

TMH7 introduces certain correction factors (k-factors) to compensate for the effects illustrated in Figure 5.3. The k-factors depend on the tails of the influence lines, which can be difficult to incorporate in software. The procedure developed during this study, with the incremental generation of extreme NA loading patterns, provides a solution where the k-factor is no longer required. With the incremental generation of extreme patterns the area with the most severe effect (the peak of the influence line) will be loaded with the full intensity of type NA loading. The parts with decreasing influence values are loaded with correspondingly lower intensities (when this becomes applicable). The solution is illustrated in Figure 5.4.

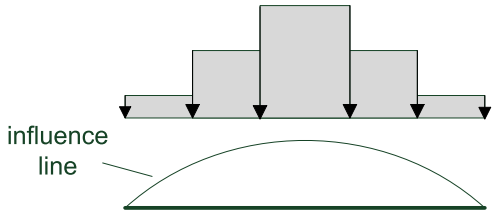

Figure 5.4: K-factor: The solution

The procedure adopted in this study, with the incremental generation of extreme patterns, effectively eliminates the need for the k-factor.

5.3 Critical Patterns

The critical NA loading pattern corresponds to the extreme pattern in one of the critical regions, as defined in section 4.3. Two approaches regarding the application of normal traffic loading, i.e. the standard patterns and the extreme patterns, were discussed in the previous sections. The extreme pattern in a critical region will be referred to as the critical NA loading pattern in that region:

Critical NA Loading Pattern: The extreme pattern in a critical region is defined as the critical NA loading pattern in that region. The critical NA loading pattern is the loading pattern that produces the most adverse effect for a selected mode of failure in that critical region.

The critical NA loading pattern will provide the following information, regarding a selected mode of failure and a specific critical region:

- Which loadable parts of the notional lanes should be loaded to produce the most adverse effect:
  - Which of these parts should be loaded first with the highest intensity loading.
  - Which of the remaining parts should be loaded with decreasing intensities and in what sequence.
- Which loadable parts of the notional lanes should not be loaded:
  - The parts that should not be loaded provide a relieving effect, or a less adverse effect, when they are loaded.

5.4 The Process of Comparative Analysis

A comparative finite element analysis is performed between the standard patterns and the extreme patterns. The comparative analysis is performed for a range of typical carriageways. The percentage error between the two sets of results is documented as the angle of skew increases form 0° to 40° in increments of 10°. The percentage error is measured for each of the moment resultants in the corresponding critical regions. The percentage error is defined as:

$$Error\,(\%) = \frac{v_1 - v_0}{v_0}$$

with,

v_0	represents the value produced by the extreme pattern
v_1	represents the value produced by the envelope of the standard patterns

The value from the extreme pattern is compared to the value from the *envelope* of the standard patterns. The envelope of the standard patterns represent the highest and lowest values from the standard patterns, i.e. the extreme value is compared to the nearest value from one of the standard patterns. In the context of this study the error between these values should always be negative or zero. A zero or negative error will indicate that the value produced by the envelope of the standard patterns is smaller than or equal to the value produced by the extreme pattern in a specific region for a selected mode of failure.

Presentation of Results: During the process of comparative analysis, the critical NA loading patterns are presented for a specific moment resultant in a corresponding critical region, as the angle of skew of the carriageway increases. In order to present a large amount of numerical data in a compact way, the critical NA loading patterns are only shown for three of the increments between between 0° and 40° in this document. The presentation of the critical NA loading patterns at 10°

and 30° are omitted since the progression of the critical NA loading patterns become clear at 0°, 20° and 40° angles of skew. However, the errors are still compared and presented as the angle of skew increase form 0° to 40° in increments of 10°. The omitted NA loading patterns are included in the electronic media in Appendix F. Each loading pattern is associated with a specific file and NA loading pattern number. The associated files and NA loading pattern numbers are indicated in the tables that present the results of the various carriageways treated in this study.

6 Implementation

The theory and technical requirements, regarding the definition, generation and application of type NA loading, were described in Chapter 3, Chapter 4 and Chapter 5. These requirements are now implemented using state of the art object-orientated methods of software technique. This chapter focuses on the implementation at model level.

The implementation at component level, i.e. the elements of the model, is not described in detail in this document. The components of the models are however presented in Appendix E, in the form of UML (Unified Modeling Language) diagrams [1]. The reader is referred to the attached source code and the documentation thereof in Appendix F, if more detail is required. The following topics are presented in this chapter:

- The mathematical fundamentals of object modeling.
- The requirements of the object model for the purpose of this study.
- The implementation of the models.
- An overview of the model architecture.

All implementations of concepts and algorithms use the Java [6] platform. The reader who is not interested in the development of the software for the purpose of this study can omit the reading of this chapter and continue to the discussion of the results in Chapter 7.

6.1 Object Modeling

In object-orientation *objects* play the central role. An object can be characterized by the flowing [5]:

State: In the form of the attributes or properties of the object.

Behaviour: In the form of the methods of the object.

Identification: An object can be distinguished uniquely amongst all other objects.

Classification: Objects can be classified, i.e. an object is an instance of a class.

The mathematical fundamentals of object modeling using set theory and the description of the object model is presented in the next subsections.

6.1.1 Set Theory

The *set* is a fundamental concept of mathematics and computer science [15]. The definition of a set, the rules for the formation of sets and the relationship between the elements of sets are described in the following paragraphs of this subsection.

Formation of Sets: Objects which are separable and can be identified uniquely are called elements. A collection of elements with similar properties is called a set. Each element of the set is uniquely identified using a property called the name, label or identifier of the element. The formation of sets is defined below:

$M = \{ a,\ b,\ c \}$	the set M consists of the elements a, b and c
$M = \{ x \mid E(x) \}$	the set M contains every element for which the logical expression $E(x)$ is true

The set without elements is called the empty set and designated by $\emptyset$:

$$\emptyset := \{ x \mid x \neq x \}$$

The membership of an element a in a set M is represented as follows:

$a \in M$	a is an element of M
$a \notin M$	a is not an element of M

Quantifiers: There are statements which are true for certain elements of a set M and false for other elements of M. Relationships between statements and elements are represented using the universal quantifier $\wedge$ and the existential quantifier $\vee$.

$\underset{x \in M}{\wedge} f(x)$	for every x in the set M $f(x)$ holds
$\underset{x \in M}{\vee} f(x)$	there is an x in the set M for which $f(x)$ holds

Subset: A set A is called a subset of a set B if every element of A is also an element of B. If the set B contains at least one element not contained in A, then A is called a proper subset of B.

$A \subseteq B$	A is a subset of B
$A \subset B$	A is a proper subset of B

Operations on Sets: An operation on sets yields exactly one set as a result for two given sets. The intersection between set A and set B is defined as follows:

$$A \cap B := \{ x \mid x \in A \ \wedge \ x \in B \}$$

The union between set A and set B is defined as follows:

$$A \cup B := \{ x \mid x \in A \ \vee \ x \in B \}$$

Disjoint Sets: The sets A and B are said to be disjoint if they have no elements in common.

$A \cap B = \emptyset$	the intersection between set A and set B is the empty set $\emptyset$

6.1.2 Description of the Object Model

The description of the object model is presented in the paragraphs of this subsection. The object model is described with emphasis on the object set, the set of object types and the sub-sets of the object set. The subsets of the object set represent the sub-models of the object model.

Object Set: The set of objects that represent the state of a model is called the object set M:

$$M := \{\, a \in M \mid a \text{ is an object of the model} \,\}$$

Set of Object Types: The set of object types T comprise the disjoint sets K of all classes and I of all interfaces:

$T := K \cup I$ the set of object types T represent the union between the set of all classes K and the set of all interfaces I

The set of object types T has the following properties:

$K \subset T$ K is a proper subset of T
$I \subset T$ I is a proper subset of T

The set of all classes K and the set of all interfaces I have no elements in common:

$K \cap I = \emptyset$ the intersection between the set of all classes K and the set of all interfaces I is the empty set $\emptyset$

Sub-models: A sub-model represents a subset of elements from the object model, i.e. a subset of the object set M. A specific subset representing a specific sub-model i of the object model is designated by M_{sub_i}:

$$M_{sub_i} := \{\, a_{sub_i} \in M_{sub_i} \mid a_{sub_i} \text{ is an object of sub-model } i \,\}$$

The following sub-models were developed for the purpose of generating critical normal traffic loading for flexure of bridges:

- M_{bridge}
- M_{load}
- M_{mesh}
- M_{fem}

A graphical representation of the sub-models of the object model is given in Figure 6.1.

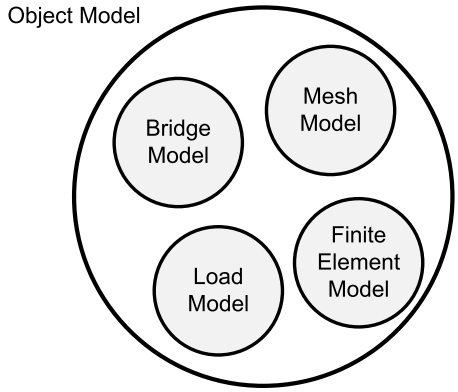

Figure 6.1: Sub-models of the object model

The purpose and functionality of each of the sub-models are described in section 6.3 on page 29 of this chapter. It can be seen from Figure 6.1 that the sub-models represent proper subsets of the object set M:

$M_{bridge} \subset M$	M_{bridge} is a proper subset of M
$M_{load} \subset M$	M_{load} is a proper subset of M
$M_{mesh} \subset M$	M_{mesh} is a proper subset of M
$M_{fem} \subset M$	M_{fem} is a proper subset of M

All the subsets M_{sub_i} of the object set M are disjoint:

$M_{bridge} \cap M_{load} \cap M_{mesh} \cap M_{fem} = \emptyset$	the intersection[6] between all the subsets M_{sub_i} of the object set M is the empty set $\emptyset$

6.2 Requirements of the Object Model

The concept of object modeling and the description of the object model for the purpose of this study were presented in the previous section of this chapter. A software model can be seen as a representation of concepts, relationships, constraints, rules and operations that specify data semantics for a chosen domain of discourse [9]. A software model should provide a sharable, stable and organized structure of information requirements for the domain context.

Two requirements pertaining to the sub-models of the object model were identified and they are presented below:

- Requirements for sub-model interaction:
  - A procedure for specifying the interaction amongst sub-models while maintaining a sufficient level of separation between the various sub-models of the object model.

[6] The intersection is an associative operation.

- Requirements for sub-model functionality:
  - A sub-model structure that provides the functionality for the addition, removal, extraction and modification of objects of a sub-model.

These two requirements of the object model are described in the following subsections.

6.2.1 Sub-model Interaction

To manage interaction amongst sub-models or a subset of sub-models the concept of a linkable model is introduced as an interface. The concept of a linkable model provides formalism to the interaction amongst sub-models, without constraining how the description is mapped to an actual implementation. Figure 6.2 shows a graphical representation of linkable models.

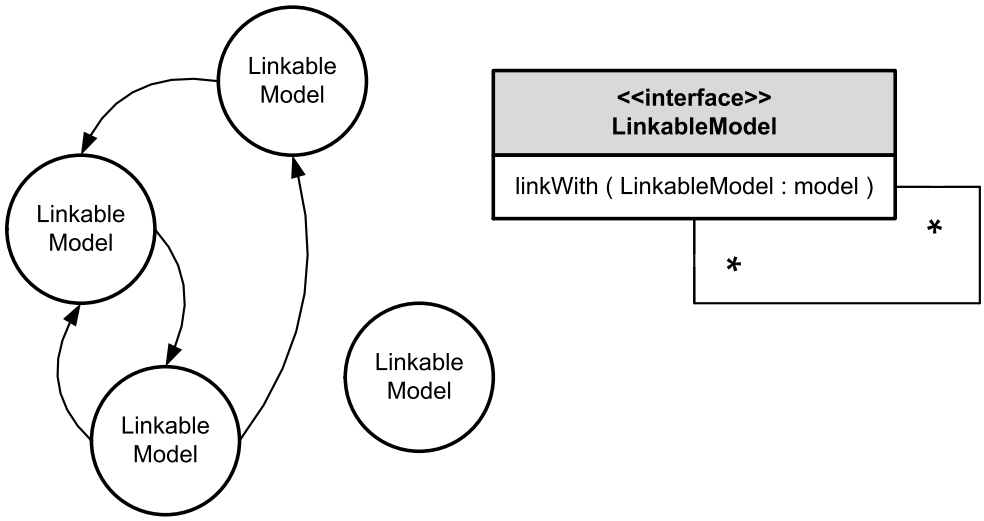

Figure 6.2: Linkable models

The following can be observed from Figure 6.2:

- A linkable model does not need to be linked at the time of software development:
  - Effective change accommodation is possible by adding additional sub-models and functionality at a later stage without changing the core structure of the existing application.
- The linkable model interface represents a reflexive association:
  - Both classes are aware of each other and their relationship.
  - An instance of a linkable model is related to *another* instance of a linkable model.

It remains the responsibility of the implementer to make effective use of the functionality provided by the linkable model interface in order to avoid cyclic anti-patterns [8]. The implementation of the linkable model interface is presented in the following paragraph:

Interface LinkableModel

The interface provides the functionality for a model to be linked with another model. The interface specifies the following method:

> `public void linkWith(LinkableModel model)`
> The method provides the functionality for a model to be linked to another model.

Linkable models can be linked as is needed via a graphical user interface, allowing a user to interact with multiple models which co-exist inside an application during run time, switching dynamically between models and transferring information between them. The user parameters are set and applied to the specific model and the link-with functionality is executed.

6.2.2 Sub-model Functionality

The structure and functionality required by a sub-model is presented in this subsection. The set of objects that represent the state of the object model M was presented in the previous section, section 6.1.2. When a method is executed operations on the object set may take place. A sub-model structure is required that provides the functionality for the following operations on the object set M:

- objects are added to M
- objects are removed from M
- objects in M are modified
- objects are uniquely extracted from M

Sub-models encapsulate a typical mapping, where components or objects contained within the model are mapped to their respective persistent identifiers by making use of a parametrized or generic class. The implementation of a sub-model structure that provides the necessary functionality, as described above, is presented in the following paragraph:

Abstract Class SubModel

Class `SubModel` represents the class for managing the collection of elements of a sub-model. The class encapsulates a `java.util.Map` for managing collections with given keys and values. The keys are mapped to the values and each key can map to at most one value. The methods of the class are described below:

> `protected boolean add(K key, V value)`
> Adds a value to the collection with a given key. Returns `true` if the value was successfully added, `false` otherwise. The method is override in the subclasses.
>
> `protected boolean remove(K key)`
> Removes a value from the collection with a given key. Returns `true` if the value was successfully removed, `false` otherwise. The method is overridden in the subclasses.

`protected boolean change(K old, K new, Method method, Object par)`
`throws Exception`

Changes the value corresponding with the old key in the collection. The value is changed by invoking the specified method with the given parameters on it. A new key is also specified if it is different from the old key, i.e. the key can also change. Returns `true` if the value was successfully changed, `false` otherwise. A `java.lang.Exception` is thrown for invalid method definitions.

`public V get(K key)`

Returns the value from the collection corresponding with the given parameter key.

Generic type parameters are used to maintain an acceptable level of separation between cooperative sub-models. In this way, if the implementation compiles without warnings, the compiler can guarantee type correctness at compile time [2] in order to ensure that the type constraints are not violated at run time. When the linkable model functionality is executed and the sub-models are linked, this restriction ensures that the bridge model can only contain bridge components and the mesh model can only contain mesh components etc. This restriction ensures an acceptable level of separation between cooperative sub-models, i.e. all the subsets M_{sub_i} of the object set M are disjoint:

$$M_{bridge} \cap M_{load} \cap M_{mesh} \cap M_{fem} = \emptyset$$

Elements from a specific sub-model are however still used by other sub-models, but storing these elements internally is not allowed.

6.3 Sub-model Implementation

A sub-model structure that provides the functionality for the addition, removal, extraction and modification of elements of the object model was described in the previous section. The purpose and functionality of each of the sub-models are described in this section. Each sub-model comprises a collection of elements specific to that sub-model. The implementation of the sub-models of the object model is presented in the following subsections.

6.3.1 Bridge Model

The bridge model is concerned with the definition and layout of the geometry of the bridge deck, e.g. the definition of the carriageway, supports and notional lanes. The following class and interfaces relevant to the bridge model implementation were developed:

Interface MeshableBridgeModel

A `MeshableBridgeModel` specifies the functionality for a bridge model to be meshed by a mesh model. The interface definition is given below:

```
public interface MeshableBridgeModel extends LinkableModel
```

The interface specifies the functionality for bridge components to be meshed by a mesh model. The interface extends the `LinkableModel` interface for providing the functionality for the `MeshableBridgeModel` to be linked to other models.

Class BridgeModel

The bridge model comprises a collection of bridge components (Refer to Figure E.1 on page E-1). The class definition is given below:

```
public class BridgeModel extends SubModel<String, BridgeComponent>
      implements MeshableBridgeModel
```

The class extends the `SubModel` super class. The keys are represented by character strings and the values by bridge components. The class implements the `MeshableBridgeModel` interface for providing the functionality for the bridge components to be meshed.

Interface BridgeModel.Listener

The bridge model declares a nested listener interface for the notification of bridge component events:

```
public static interface Listener {
    public void bridgeComponentAddedEvent();
    public void bridgeComponentChangedEvent();
    public void bridgeComponentRemovedEvent();
}
```

Classes that implement the `BridgeModel.Listener` interface are added to the set of listeners of the bridge model. Objects of the classes that implement the interface are notified when a bridge component is added to the bridge model, removed from the bridge model or changed inside the bridge model. When either of these events take place the notional lanes are recalculated and the graphical user interface is updated.

6.3.2 Load Model

The load model consists of the functionality for the the generation of standard and extreme NA loading patterns. The following class and interface relevant to the load model implementation were developed:

Class LoadModel

The load model comprises a collection of load components (Refer to Figure E.2 on page E-1). The class definition is given below:

```
public class LoadModel extends SubModel<String, LoadComponent>
      implements LinkableModel
```

The class extends the `SubModel` super class. The keys are represented by character strings and the values by load components. The class implements the `LinkableModel` interface for providing the functionality for the load model to be linked to other models.

Interface LoadModel.Listener

The load model specifies the following nested listener interface:

```
public static interface Listener {
   public void naLoadPatternsClearedEvent();
   public void naLoadPatternAddedEvent(NaLoadPattern naLoadPattern);
}
```

Classes that implement the `LoadModel.Listener` interface are added to the set of listeners for the load model. Objects of the classes that implement the interface are notified when the NA load patterns are cleared or when a new NA load pattern is added to the load model. When either of these events take place the graphical user interface is updated.

6.3.3 Mesh Model

The mesh model consists of the functionality for the piecewise approximation of the geometry and physical state of the components contained in the bridge model. The following interface and classes relevant to the mesh model implementation were developed:

Interface AnalysableMeshModel

The interface specifies the functionality for a finite element analysis to be performed from the data contained in mesh model. The interface definition is given below:

`public interface AnalysableMeshModel`
The interface specifies the functionality for a mesh model to by analyzed by a finite element model.

Class MeshModel

The mesh model comprises a collection of mesh components (Refer to Figure E.3 on page E-2). The class definition is given below:

```
public class MeshModel extends SubModel<String, MeshComponent>
      implements AnalysableMeshModel
```
The class extends the `SubModel` super class. The keys are represented by character strings and the values by mesh components. The class implements the `AnalysableMeshModel` interface for providing the functionality for a finite element model to perform a finite element analysis from the data contained in the mesh model.

Class BridgeMeshModel

The class provides the bridge-specific mesh model implementation, i.e. the class is used specifically to mesh bridge components. The class definition is given below:

```
public class BridgeMeshModel extends
      MeshModel implements LinkableModel
```

The class extends the `MeshModel` to provide the bridge-specific mesh model implementation. The `LinkableModel` interface is implemented for providing the functionality for the mesh model to be linked to other models.

6.3.4 Finite Element Model

The finite element model consists of the functionality to perform a finite element analysis. The following classes relevant to the finite element model implementation were developed:

Class FemModel

The finite element model comprises a collection of finite element components (Refer to Figure E.4 on page E-2). The class definition is given below:

```
public class FemModel extends SubModel<String, FemComponent>
```

The class extends the `SubModel` super class. The keys are represented by character strings and the values by finite element components.

Class BridgeFemModel

The class provides the bridge-specific finite element implementation. The class definition is given below:

```
public class BridgeFemModel extends
      FemModel implements LinkableModel
```

The class extends the `FemModel` to provide the bridge-specific finite element implementation. The `LinkableModel` interface is implemented by the class for providing the functionality of the finite element model to be linked to other models.

6.4 Model Architecture

The basic function and implementation of the sub-models M_{sub_i} of the object model M were described in the previous sections. An overview of the architecture and interaction between the cooperative sub-models are presented in this section in the form of an UML (Unified Modeling

Language) diagram. A class diagram representing an overview of the sub-models are presented in Figure 6.3.

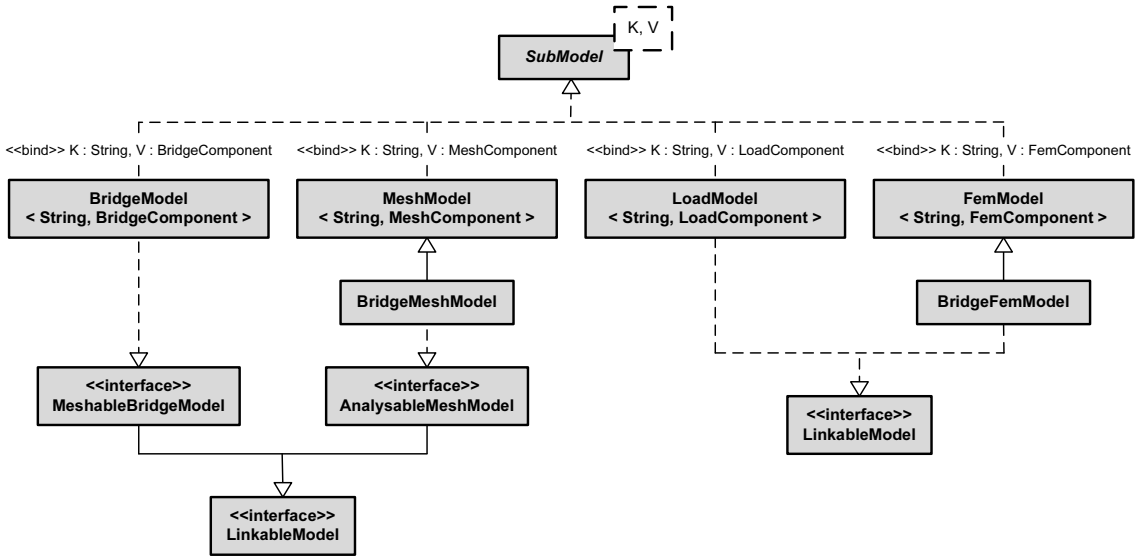

Figure 6.3: Class diagram: Model architecture

The concepts of achieving specialization through inheritance and ensuring compatibility, pertaining to the model architecture illustrated in Figure 6.3 are described below:

Specialization through Inheritance: It can be seen from Figure 6.3 that the inheritance shows specialization, following Coad's criteria for inheritance [3]. The specialized models inherit from the more general models. The specialization-generalization relation can be seen from the following:

- The `BridgeMeshModel` extends the `MeshModel`:
  - The `BridgeMeshModel` is used specifically to mesh the geometry of bridge components.
- The `BridgeFemModel` extends the `FemModel`:
  - The `BridgeFemModel` is used specifically for the finite element computations of the bridge model.

The specialization-generalization relation can be seen from the procedure described above. The derived classes model an *"is a special kind"* of relationship to the more general base classes.

Ensuring Compatibility: For the purpose of ensuring compatibility between cooperative sub-models, the functionality of each linkable sub-model is extended and specified in the form of an interface:

- The `BridgeModel` *is also* a `MeshableBridgeModel`:
  - The functionality specified by the `MeshableBridgeModel` interface allows the geometry of the `BridgeModel` to be meshed.

- The `BridgeMeshModel` *is also* an `AnalysableMeshModel`:
  - The functionality specified by the `AnalysableMeshModel` interface allows the finite element model to perform a finite element analysis from the data contained in the `BridgeMeshModel`.

The procedure described above ensures that when two `LinkableModels` are linked, e.g. the `MeshableBridgeModel` and the `BridgeMeshModel`, both consists of the necessary functionality to execute the link effectively.

6.5 Graphical User Interface

The graphical user interface is used to change and control the state of the models during execution. The graphical user interface was developed using a 2D projection model and the Java 2D API (Application Programming Interface). Modeling of the graphical user interface is not described in detail in this document. The layout and operation of the graphical user interface is however described in the user guide of Appendix D. The reader is referred to the attached source code in Appendix F, should more detail be required.

7 Detailed Results: Single Span

The results from a detailed analysis for a typical single span carriageway[7] are presented in this chapter. Critical NA loading patterns are presented and compared to the standard NA loading patterns, as discussed in Chapter 5. The results are compared for each of the moment resultants in the different critical regions, as discussed in Chapter 4. The results are compared as the angle of skew of the carriageway increases. A typical single span carriageway with the following geometry will be considered:

- span length of $15\,m$
- effective width of $10\,m$
- angle of skew from 0° to 40°
- angle of skew increases in increments of 10°

Critical NA loading patterns for an additional single span carriageway and the comparison of its results can be found in Appendix A. The critical NA loading patterns for the different moment resultants in each of the critical regions will be presented in this chapter as the angle of skew increases.

7.1 Twisting Moment

The critical twisting moment is measured in the region of the obtuse corner of a skew carriageway. The critical NA loading patterns and resulting contour plots are illustrated in Table 7.1 for the twisting moment in the obtuse corner. The errors are measured as the angle of skew increases from 0° to 40° in increments of 10°. To conserve space, the critical NA loading patterns are only shown for three of the increments between 0° and 40° in this document. The critical NA loading patterns at 10° and 30° are omitted since the progression of the critical NA loading pattern for the twisting moment in the obtuse corner becomes clear at 0°, 20° and 40° angles of skew.

Angle of Skew ($^{\circ}$)	Critical NA Loading Pattern	Resulting Contour Plot (Nm)
0°	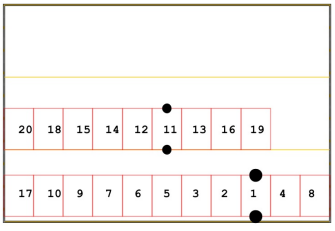 File: 10x15x00.load NA Load Pattern Number: 1	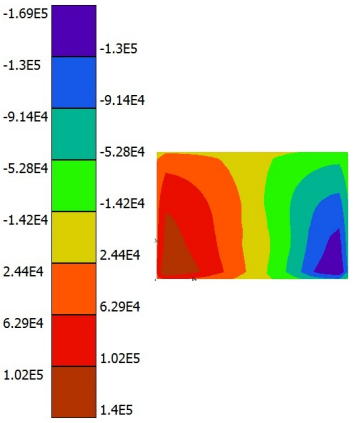

Table 7.1: Carriageway $10\,m \times 15\,m$: Critical NA loading patterns and resulting contour plots for the twisting moment in the obtuse corner (Continued on the next page)

[7]Detailed results for a typical multi-span continuous carriageway are presented in Chapter 8.

Angle of Skew (°)	Critical NA Loading Pattern	Resulting Contour Plot (Nm)
20°	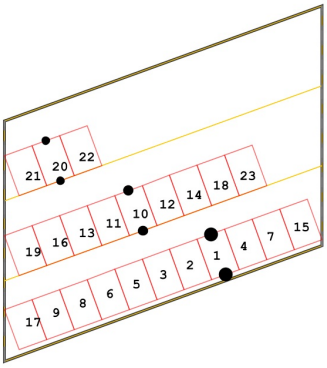 File: 10x15x20.load NA Load Pattern Number: 1	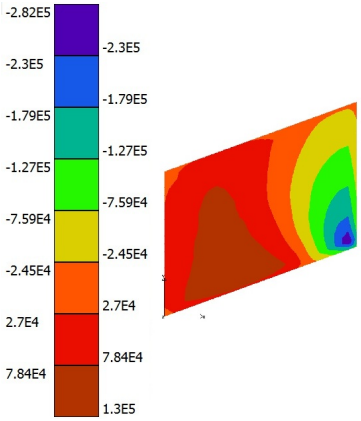
40°	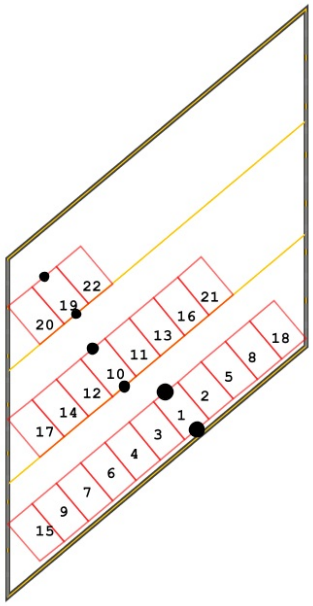 File: 10x15x40.load NA Load Pattern Number: 1	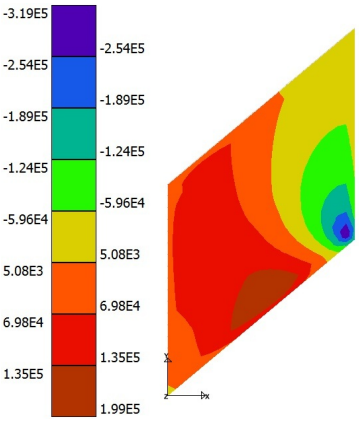

Table 7.2: Carriageway $10\,m \times 15\,m$: Critical NA loading patterns and resulting contour plots for the twisting moment in the obtuse corner (Continued from the previous page)

The following can be observed from Table 7.1 on the preceding page regarding the twisting moment in the obtuse corner:

- To produce the critical NA loading pattern for the twisting moment in the bottom right obtuse corner of the carriageway, the top right acute corner of the carriageway should not be loaded.
- It can be seen from the load indices that the heaviest loading should be placed towards the bottom edge of the carriageway in the transverse direction and towards mid-span in the longitudinal direction.

The percentage error of the standard NA loading patterns relative to the critical NA loading patterns

for the twisting moment in the obtuse corner is presented in Figure 7.1. The errors are measured as the angle of skew increases from 0° to 40° in increments of 10°. The results include the actual value at the monitored finite element node and the value of the median in the region of the monitored finite element node.

M_{11}
Obtuse Corner

	Error (%)	
Angle of Skew (°)	Actual	Median
0	-19.23%	-20.50%
10	-13.07%	-15.74%
20	-10.93%	-14.36%
30	-11.79%	-17.91%
40	-14.52%	-18.28%

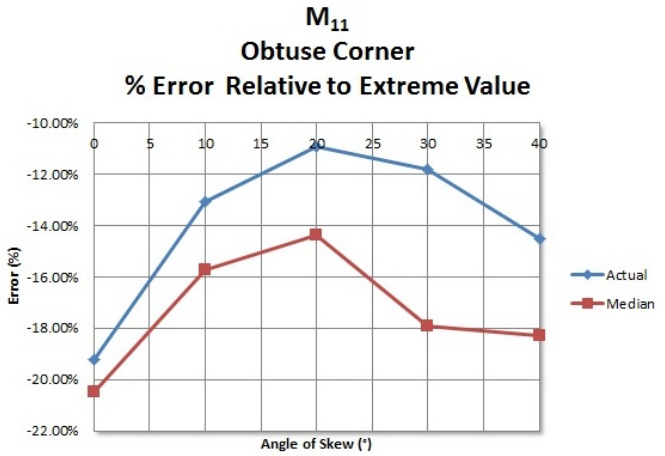

Figure 7.1: Carriageway $10\,m \times 15\,m$: Relative error for the twisting moment in the obtuse corner

The critical NA loading patterns illustrated in Table 7.1 on page 35 are not always obvious. It can be difficult to determine which loadable parts of the notional lanes should be loaded and which parts provide a relieving effect, that should not be loaded. Another difficulty, once the parts that should be loaded have been identified, is the determination of the position where the heaviest loading should be placed. It can be seen from Figure 7.1 that the standard NA loading patterns do not represent a good approximation for the critical twisting moment in the obtuse corner of the particular carriageway. Large errors occur between the standard values and the extreme values for the twisting moment in the obtuse corner.

In the case of the standard patterns all the loadable parts of the notional lanes are loaded for a single span carriageway. This can explain the large errors that occur between the standard values and the extreme values for the twisting moment in the obtuse corner, since areas that provide a relieving effect are also loaded. The largest error occurs at a 0° angle of skew, when the obtuse corner has not formed. At a 0° angle of skew, the values produced by the standard NA loading patterns are 19.23 % *smaller* than the values produced by the critical NA loading patterns. The errors decrease gradually up to an angle of skew of 20°. After 20° the errors increase again.

As the angle of skew increases the density of the twisting moment contours in the region of the obtuse corner also increases, as illustrated in Table 7.1 on page 35. This indicates a steep twisting moment gradient in the region of the obtuse corner as the angle of skew increases.

7.2 Transverse Bending Moment

The transverse bending moment is measured in the obtuse corner and at mid-span, at the centre of the carriageway. The critical NA loading patterns and a comparison with the standard NA loading patterns are presented in the following subsections in the relevant critical regions.

7.2.1 Obtuse Corner

Angle of Skew (°)	Critical NA Loading Pattern	Resulting Contour Plot (Nm)
0°	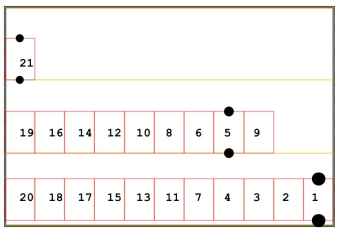 File: 10x15x00.load NA Load Pattern Number: 11	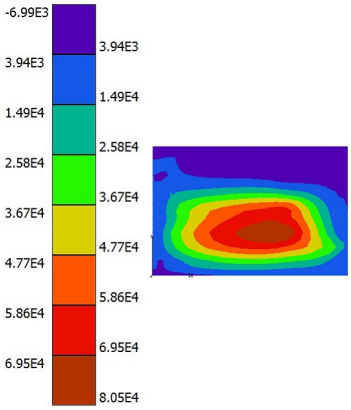
20°	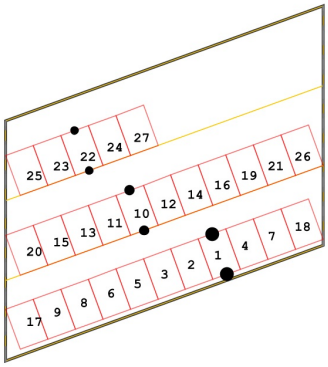 File: 10x15x20.load NA Load Pattern Number: 10	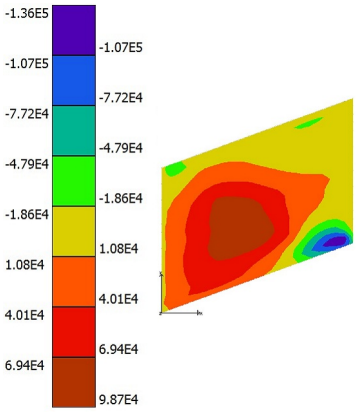
40°	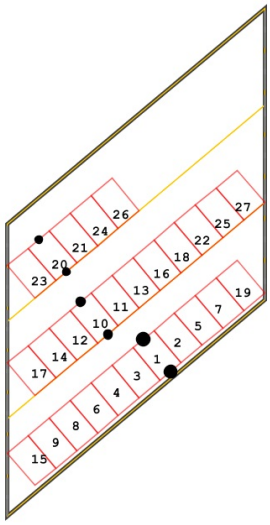 File: 10x15x40.load NA Load Pattern Number: 10	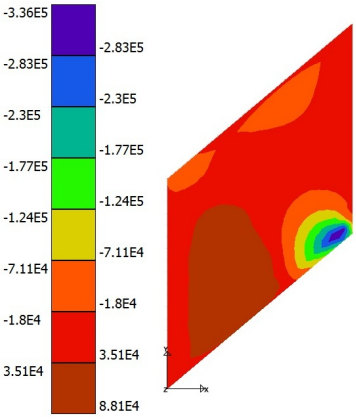

Table 7.3: Carriageway $10\,m \times 15\,m$: Critical NA loading patterns and resulting contour plots for the transverse bending moment in the obtuse corner

The critical NA loading patterns and resulting contour plots are illustrated in Table 7.3 on the preceding page for the transverse bending moment in the obtuse corner. When the carriageway is not skew and the obtuse corner has not formed, the transverse bending moment is not critical in the obtuse corner. The loading pattern at a 0˚ angle of skew is still included to illustrate the progression of the transverse bending moment in the obtuse corner as the angle of skew increases. The following can be observed from Table 7.3 on the previous page:

- To produce the critical NA loading pattern for the transverse bending moment in the bottom right obtuse corner of the carriageway, the top right acute corner of the carriageway should not be loaded.
- As illustrated by the load indices, the heaviest loading should be placed towards the bottom edge of the carriageway in the transverse direction. As the angle of skew increases, the position of the heaviest loading shifts from the obtuse corner towards mid-span in the longitudinal direction.
- A steep transverse bending moment gradient develops in the region of the obtuse corner as the angle of skew increases.

The percentage error of the standard NA loading patterns relative to the critical NA loading patterns for the transverse bending moment in the obtuse corner is presented in Figure 7.2. The errors are measured as the angle of skew increases from 0˚ to 40˚ in increments of 10˚. The results include the actual value at the monitored finite element node and the value of the median in the region of the monitored finite element node.

M_{12}
Obtuse Corner

	Error (%)	
Angle of Skew (°)	Actual	Median
0	-48.48%	-37.70%
10	-4.60%	-0.77%
20	-3.90%	-2.08%
30	-3.91%	-3.10%
40	-4.40%	-4.49%

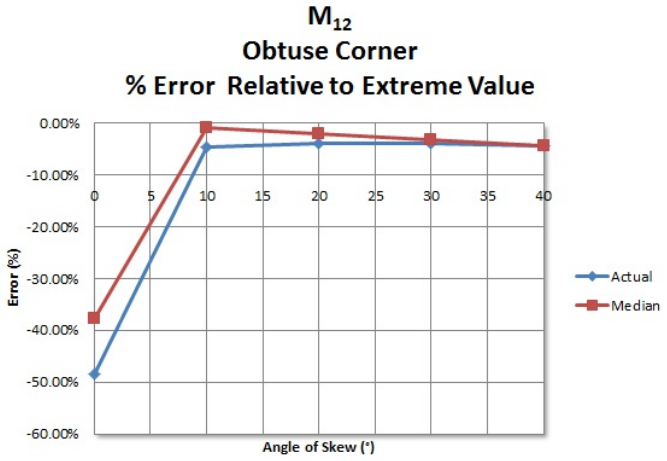

Figure 7.2: Carriageway $10\,m \times 15\,m$: Relative error for the transverse bending moment in the obtuse corner

The critical NA loading patterns for the transverse bending moment in the obtuse corner are similar to the critical NA loading patterns for the twisting moment in the obtuse corner. It can be seen from Figure 7.2 that when the angle of skew exceeds 0˚ and the obtuse corner has been formed, the standard NA loading patterns represent a good approximation for the critical transverse bending moment in the obtuse corner. When the angle of skew exceeds 0˚, the values produced by the

standard NA loading patterns are less than 5 % *smaller* than the values produced by the critical NA loading patterns for the transverse bending moment in the obtuse corner.

Angle of Skew (°)	**Critical NA Loading Pattern**	**Resulting Contour Plot (Nm)**
0°	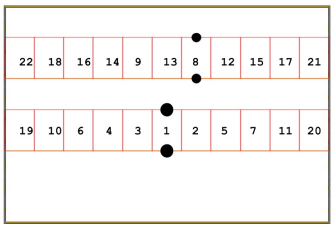 File: 10x15x00.load NA Load Pattern Number: 13	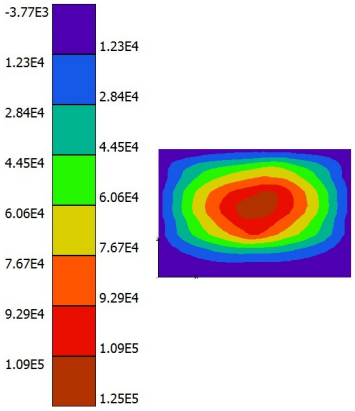
20°	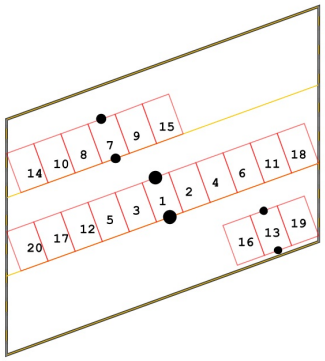 File: 10x15x20.load NA Load Pattern Number: 13	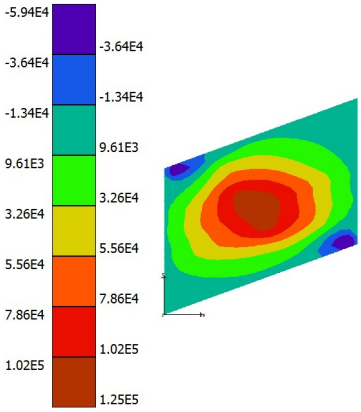
40°	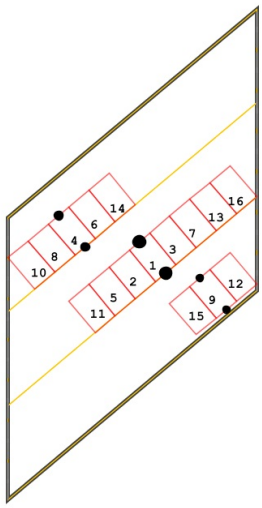 File: 10x15x40.load NA Load Pattern Number: 15	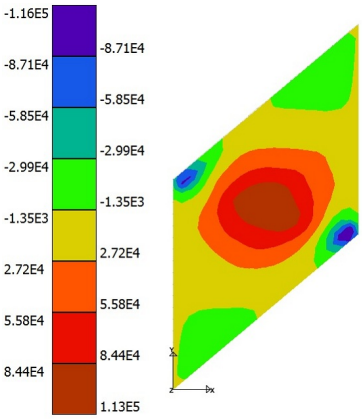

Table 7.4: Carriageway $10\,m \times 15\,m$: Critical NA loading patterns and resulting contour plots for the transverse bending moment at mid-span centre

7.2.2 Mid-span Centre

The critical NA loading patterns and resulting contour plots are presented in Table 7.4 on the preceding page for the transverse bending moment at mid-span, at the centre of the carriageway.

The following can be seen from Table 7.4 on the previous page, regarding the critical NA loading patterns for the transverse bending moment at mid-span, at the centre of the carriageway:

- To produce the critical NA loading pattern for the transverse bending moment at mid-span, at the centre of the carriageway, both the acute corners of the carriageway should not be loaded.
- The heaviest loading should be placed towards the centre of the carriageway in the longitudinal and the transverse directions.

Another observation from the contour plots in Table 7.4 on the preceding page is the concentration of the transverse bending moment in the obtuse corner, when the NA loading patterns are generated to produce critical values at mid-span, not in the obtuse corner. At a 40° angle of skew the magnitude of the value from the transverse bending moment in the obtuse corner exceeds the magnitude of the value from the transverse bending moment at mid-span, although the extreme pattern is generated for the transverse bending moment at mid-span.

The percentage error of the standard NA loading patterns relative to the critical NA loading patterns are shown in Figure 7.3 as the angle of skew increases from 0° to 40° in increments of 10°. The results include the actual value at the monitored finite element node, the value of the median in the region of the monitored finite element node as well as the Wood and Armer values for the bottom reinforcement in the transverse direction. The Wood and Armer values have been acquired with the assumption that the reinforcement will be placed parallel to the edges of the carriageway in both directions.

M_{12}
Mid-Span

	Error (%)		
Angle of Skew (°)	Actual	Median	W & A
0	-30.96%	-32.62%	-31.45%
10	-35.57%	-35.82%	-34.24%
20	-47.78%	-48.12%	-39.32%
30	-65.54%	-65.35%	-50.64%
40	-89.57%	-91.75%	-72.44%

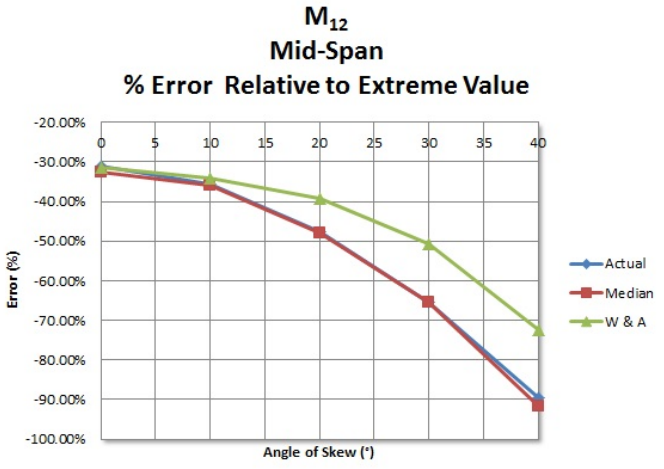

Figure 7.3: Carriageway $10\,m \times 15\,m$: Relative error for the transverse bending moment at mid-span centre

It can be seen from Figure 7.3 that the standard NA loading patterns do not represent a good approximation for the critical transverse bending moment at mid-span, at the centre of the carriageway. The standard patterns produces a value of approximately 90 % *smaller* than the value produced by

the extreme pattern at a 40° angle of skew. Large errors occur between the standard values and the extreme values since the effective area of the carriageway that should be loaded, decreases as the angle of skew increases. Partial loading of notional lanes are not provided by the standard NA patterns. As a result large areas that should not be loaded, so-called areas of relief, are loaded by the standard patterns. This results in an increased error as the angle of skew increases.

7.3 Longitudinal Bending Moment

The longitudinal bending moment corresponds to the primary bending of the carriageway and represents the dominant moment resultant. The longitudinal bending moment refers to the rotated longitudinal bending moment, rotated at the angle of skew. The longitudinal bending moment is measured in the obtuse corner and at mid-span, at the edge of the carriageway. Critical NA loading patterns for the longitudinal bending moment in these two regions are presented in the next subsections.

7.3.1 Obtuse Corner

Angle of Skew (°)	Critical NA Loading Pattern	Resulting Contour Plot (Nm)
0°	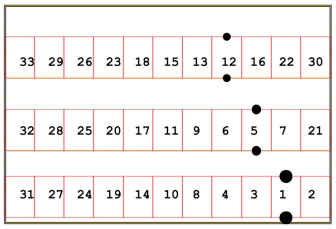 File: 10x15x00.load NA Load Pattern Number: 20	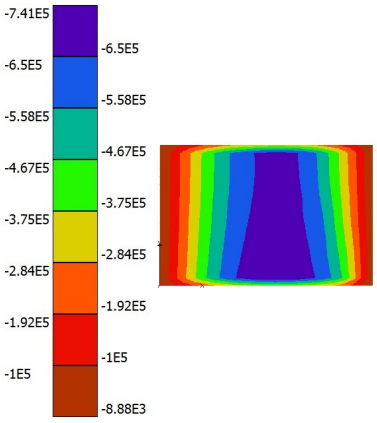
20°	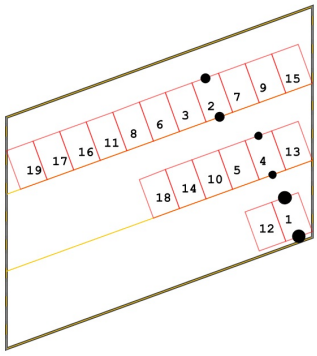 File: 10x15x20.load NA Load Pattern Number: 20	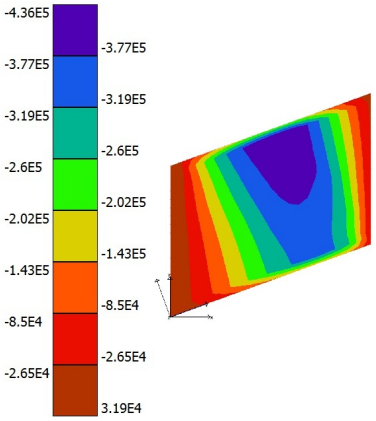

Table 7.5: Carriageway $10\,m \times 15\,m$: Critical NA loading patterns and resulting contour plots for the longitudinal bending moment in the obtuse corner (Continued on the next page)

Angle of Skew (°)	Critical NA Loading Pattern	Resulting Contour Plot (Nm)
40°	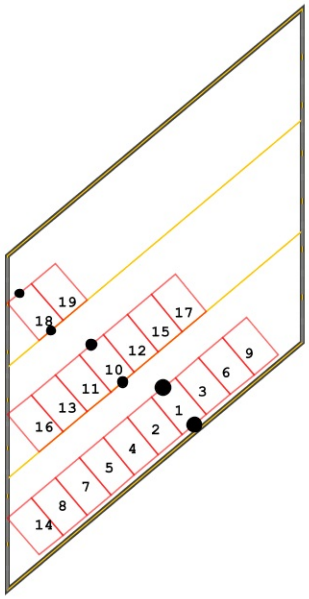 File: 10x15x40.load NA Load Pattern Number: 19	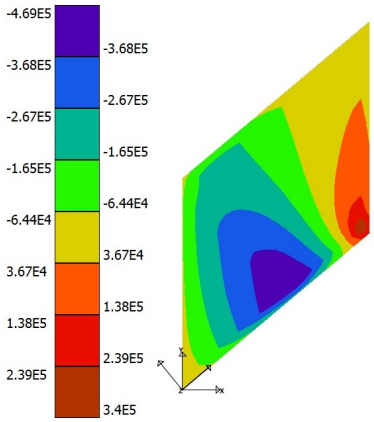

Table 7.6: Carriageway $10\,m \times 15\,m$: Critical NA loading patterns and resulting contour plots for the longitudinal bending moment in the obtuse corner (Continued from the previous page)

The critical NA loading patterns and resulting contour plots are illustrated in Table 7.5 on the previous page for the longitudinal bending moment in the obtuse corner.

The following can be seen from Table 7.5 on the preceding page, regarding the critical NA loading patterns for the longitudinal bending moment in the obtuse corner:

- The critical NA loading patterns for the longitudinal bending moment in the bottom right obtuse corner are not obvious and they do not follow a clear pattern as the angle of skew increases:
  - At a 20° angle of skew the loading is placed towards the top right acute corner of the carriageway.
  - At a 40° angle of skew the loading is placed towards the bottom left acute corner of the carriageway.
- As illustrated in the resulting contour plot, a large hogging effect develops in the obtuse corner at a 40° angle of skew.

The percentage error of the standard NA loading patterns relative to the critical NA loading patterns for the longitudinal bending moment in the obtuse corner is presented in Figure 7.4 on the next page. The errors are measured as the angle of skew increases from 0° to 40° in increments of 10°. The results include the actual value at the monitored finite element node and the value of the median in the region of the monitored finite element node.

M_{21}
Obtuse Corner

Angle of Skew (°)	Error (%)	
	Actual	Median
0	-19.74%	-21.30%
10	-28.54%	-23.73%
20	-67.63%	-42.73%
30	-35.94%	-31.20%
40	-21.69%	-39.61%

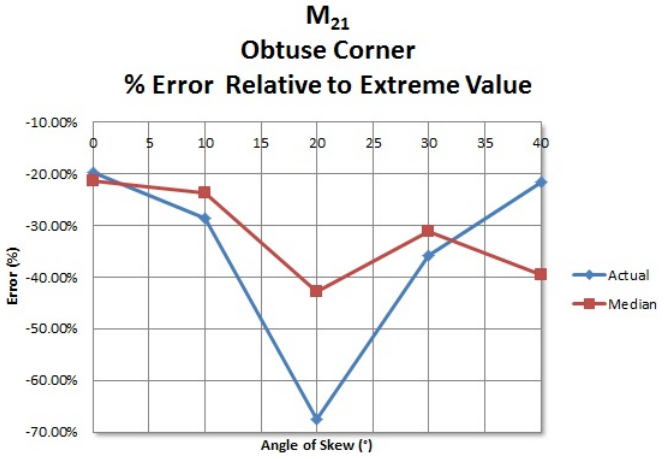

Figure 7.4: Carriageway $10\,m \times 15\,m$: Relative error for the longitudinal bending moment in the obtuse corner

Large errors occur between the standard values and the extreme values for the longitudinal bending moment in the obtuse corner, as shown in Figure 7.4. The errors decrease as the angle of skew exceeds 20°, as the critical NA loading patterns shift from the top right acute corner towards the bottom left acute corner. The critical pattern in the bottom left acute corner represents a closer approximation of one of the standard patterns, which results in a decreased error as the angle of skew exceeds 20°.

7.3.2 Mid-span Edge

The critical NA loading patterns and resulting contour plots are illustrated in Table 7.7 for the longitudinal bending moment at mid-span, at the edge of the carriageway. Extreme patterns were generated towards mid-span of the carriageway in the longitudinal direction and towards the bottom edge of the carriageway in the transverse direction.

Angle of Skew (°)	Critical NA Loading Pattern	Resulting Contour Plot (Nm)
0°	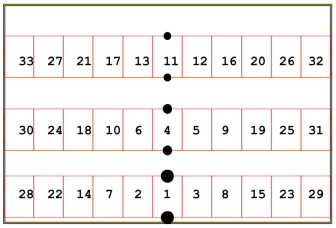 File: 10x15x00.load NA Load Pattern Number: 16	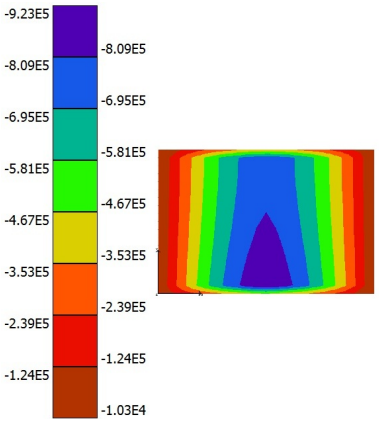

Table 7.7: Carriageway $10\,m \times 15\,m$: Critical NA loading patterns and resulting contour plots for the longitudinal bending moment at mid-span edge (Continued on the next page)

Angle of Skew (°)	Critical NA Loading Pattern	Resulting Contour Plot (Nm)
20°	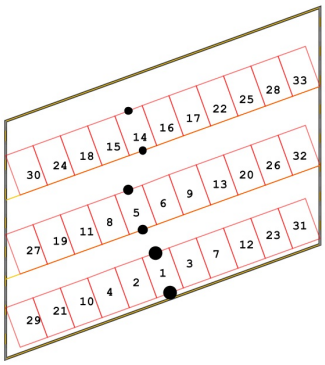 File: 10x15x20.load NA Load Pattern Number: 16	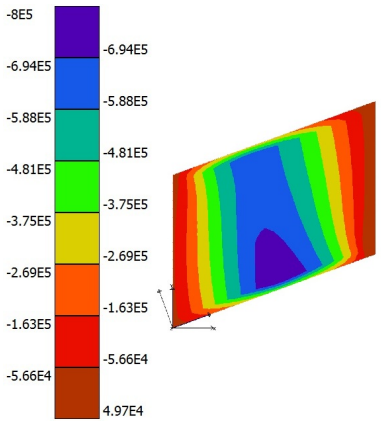
40°	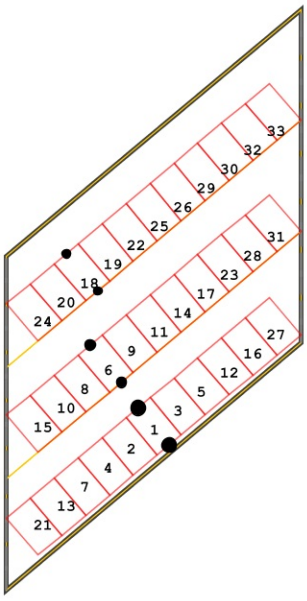 File: 10x15x40.load NA Load Pattern Number: 20	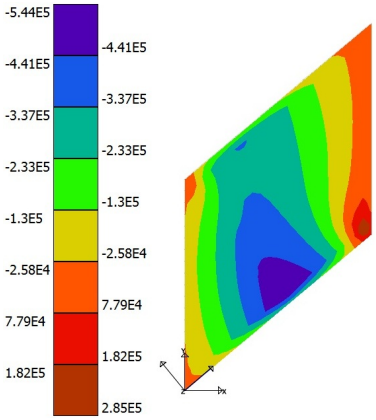

Table 7.8: Carriageway $10\,m \times 15\,m$: Critical NA loading patterns and resulting contour plots for the longitudinal bending moment at mid-span edge (Continued from the previous page)

It can be seen from Table 7.7 on the preceding page that the critical NA loading patterns for the longitudinal bending moment at mid-span, at the edge of the carriageway, are as expected for a single span carriageway:

- All the loadable parts of the notional lanes are loaded.
- The heaviest loading is placed towards mid-span in the longitudinal direction and towards the bottom edge of the carriageway in the transverse direction.
- However, as the angle of skew increases the heaviest loading on the adjacent notional lanes is placed more towards the left-edge of the carriageway. This is due to:

– The rotated nature of the longitudinal bending moment vector.

– The extreme patterns are generated for the bottom edge of the carriageway in the transverse direction, not the centre.

The percentage error of the standard NA loading patterns relative to the critical NA loading patterns for the longitudinal bending moment at mid-span, at the edge of the carriageway, is presented in Figure 7.5. The errors are measured as the angle of skew increases from 0° to 40° in increments of 10°. The results include the actual value at the monitored finite element node, the value of the median in the region of the monitored finite element node as well as the Wood and Armer values for the bottom reinforcement in the longitudinal direction. The Wood and Armer values have been acquired with the assumption that the reinforcement will be placed parallel to the edges of the carriageway in both directions.

M_{21}
Mid-Span

	Error (%)		
Angle of Skew (°)	Actual	Median	W & A
0	-3.24%	-3.29%	-3.16%
10	-2.76%	-2.98%	-2.66%
20	-2.66%	-2.45%	-2.82%
30	-2.77%	-2.49%	-3.24%
40	-4.00%	-4.68%	-4.55%

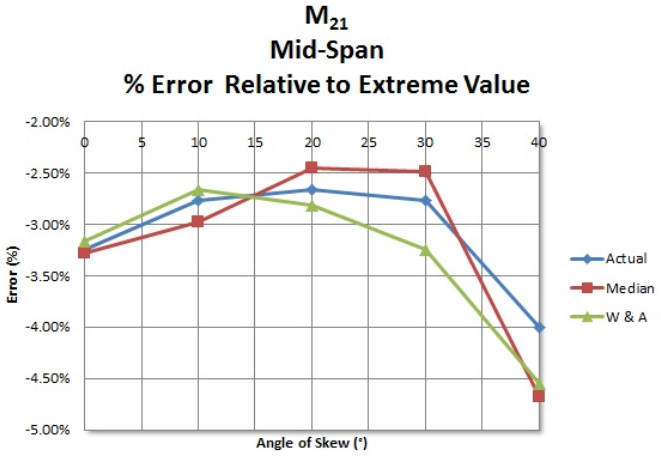

Figure 7.5: Carriageway $10\,m \times 15\,m$: Relative error for the longitudinal bending moment at mid-span edge

The standard NA loading patterns represent a good approximation for the critical longitudinal bending moment at mid-span, at the edge of the carriageway. It can be seen from Figure 7.5 that the values produced by the standard NA loading patterns are less than 5 % *smaller* than the values produced by the critical NA loading patterns for all the angles of skew. These small errors occur due to the different loading arrangement on the adjacent notional lanes as the angle of skew increases.

7.4 Normalized Maximum Moments

A carriageway with a span length of $15\,m$ and an effective width of $10\,m$ was investigated in this chapter as the angle of skew increases. The critical NA loading patterns were presented for the different moment resultants in each of the critical regions.

The flexural behaviour of the specific carriageway under the effects of normal traffic loading will be presented in this section as the angle of skew increases. The different moment resultant values are normalized and compared *relative* to the largest moment resultant in each of the critical regions. The normalized moment values are shown in Table 7.9 on the next page.

	M_{11} Twisting Moment	M_{12} Bending Moment - Transverse		M_{21} Bending Moment - Longitudinal	
Angle of Skew (°)	Obtuse Corner	Obtuse Corner	Mid-Span (Center)	Obtuse Corner	Mid-Span (Edge)
0	0.183	0.009	0.133	0.180	1.000
10	0.256	0.051	0.139	0.180	1.000
20	0.353	0.155	0.156	0.174	1.000
30	0.474	0.330	0.179	0.314	1.000
40	0.615	0.576	0.214	0.655	1.000

Table 7.9: Carriageway $10\,m \times 15\,m$: Normalized maximum moments

It can be seen from Table 7.9 that the longitudinal bending moment at mid-span, at the edge of the carriageway, remains the dominant moment resultant for all the angles of skew. The results from Table 7.9 are also presented graphically in Figure 7.6.

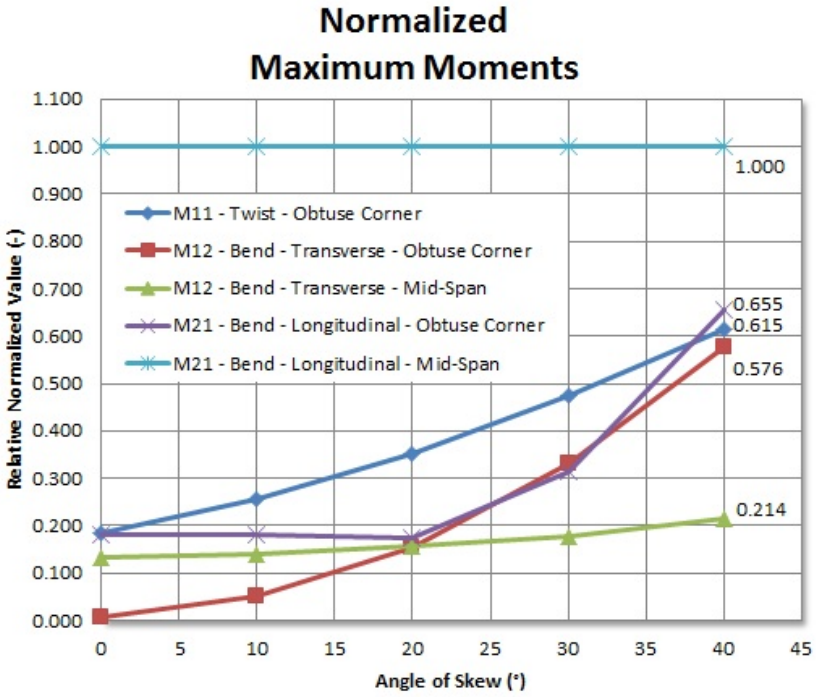

Figure 7.6: Carriageway $10\,m \times 15\,m$: Normalized maximum moments

The following can be observed regarding the normalized maximum moments for the the particular carriageway:

- The longitudinal bending moment at mid-span, at the edge of the carriageway, remains the relative dominant moment resultant for the particular carriageway, for all the angles of skew.
- The second-largest relative moment resultants are the longitudinal bending moment in the obtuse corner and the twisting moment in the obtuse corner, reaching relative values of 65.5 % and 61.5 % of the value of the longitudinal bending moment at mid-span respectively. These two moment resultants increases rapidly when the angle of skew exceeds 20°.

- The the transverse bending moment in the obtuse corner has a relative value of 0.9 % when carriageway is not skew, the value increases rapidly to 57.6 % at a 40° of skew.

The transverse bending moment at mid-span remains relatively constant as the angle of skew increases, at a relative value of approximately 20 % at a angle 40° of skew. This can be ascribed to Poisson's effect.

8 Detailed Results: Continuous

The results from a detailed analysis for a typical continuous multi-span carriageway[8] are presented in this chapter. Critical NA loading patterns are presented and compared to the standard NA loading patterns, as discussed in Chapter 5. The results are compared for each of the moment resultants in the different critical regions, as discussed in Chapter 4. The results are compared as the angle of skew of the carriageway increases. A typical continuous multi-span carriageway with the following geometry will be considered:

- two short spans with lengths of $8\,m$
- one long span with a length of $15\,m$
- effective width of $10\,m$
- angle of skew from 0° to 40°
- angle of skew increases in increments of 10°

The two short spans are on either end of the carriageway and the long span represents the centre span. Critical NA loading patterns for an additional continuous multi-span carriageway and the comparison of its results can be found in Appendix B.

8.1 Twisting Moment

The twisting moment is measured in the obtuse corner of each of the spans of the carriageway.

Short Span: The critical NA loading patterns and resulting contour plots are illustrated in Table 8.1 for the twisting moment in the obtuse corner, for the first *short span* from the left.

Angle of Skew (°)	Critical NA Loading Pattern	Resulting Contour Plot (Nm)
0°	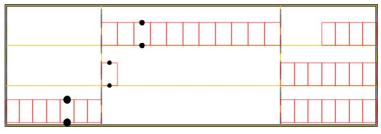 File: 10x8x15x8x00.load NA Load Pattern Number: 41	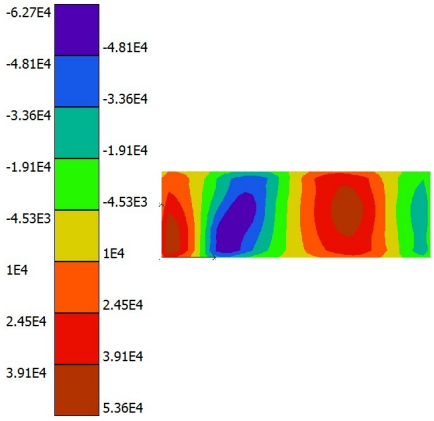

Table 8.1: Carriageway $10\,m \times (8\,m + 15\,m + 8\,m)$: Critical NA loading patterns and resulting contour plots for the twisting moment in the obtuse corner for the first short span (Continued on the next page)

[8] Detailed results for a typical single span carriageway were presented in Chapter 7.

Angle of Skew (°)	Critical NA Loading Pattern	Resulting Contour Plot (Nm)
20°	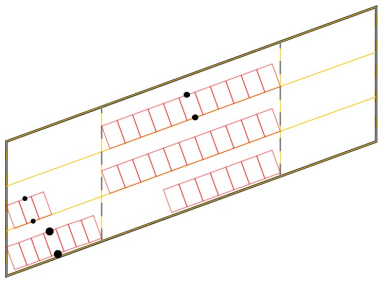 File: 10x8x15x8x20.load NA Load Pattern Number: 71	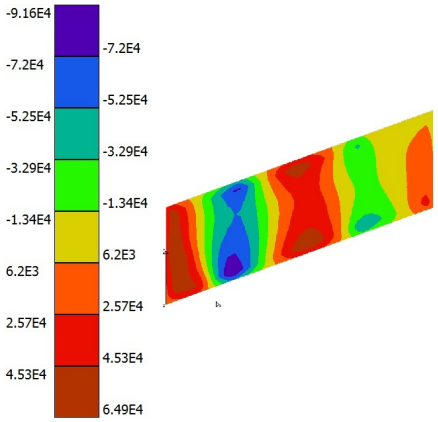
40°	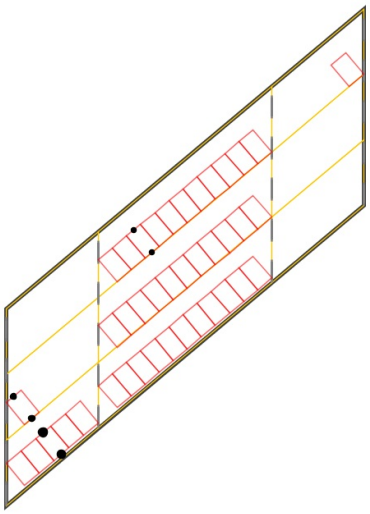 File: 10x8x15x8x40.load NA Load Pattern Number: 71	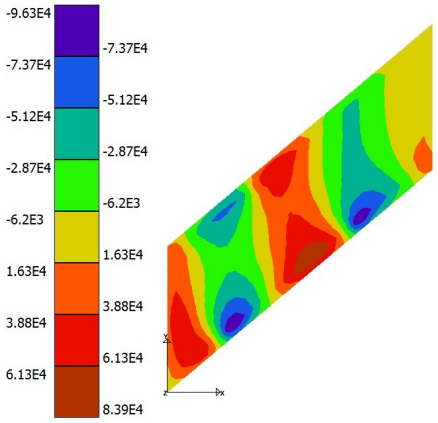

Table 8.2: Carriageway $10\,m \times (8\,m + 15\,m + 8\,m)$: Critical NA loading patterns and resulting contour plots for the twisting moment in the obtuse corner for the first short span (Continued from the previous page)

Long Span: The critical NA loading patterns and resulting contour plots are illustrated in Table 8.3 on the following page for the twisting moment in the obtuse corner, for the centre *long span* of the carriageway.

The following can be observed from Table 8.1 on the previous page and Table 8.3 on the following page regarding the twisting moment in the obtuse corner:

- To produce the critical NA loading pattern for the twisting moment in the bottom right obtuse corner of a specific span of the carriageway, the top right acute corner of that span should not be loaded.
- The critical NA loading patterns for the twisting moment in the obtuse corner do not follow a clear pattern regarding the loading arrangement on the adjacent spans.

Angle of Skew (°)	Critical NA Loading Pattern	Resulting Contour Plot (Nm)
0°	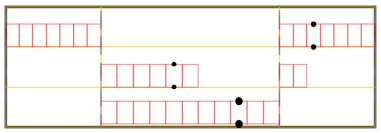 File: 10x8x15x8x00.load NA Load Pattern Number: 43	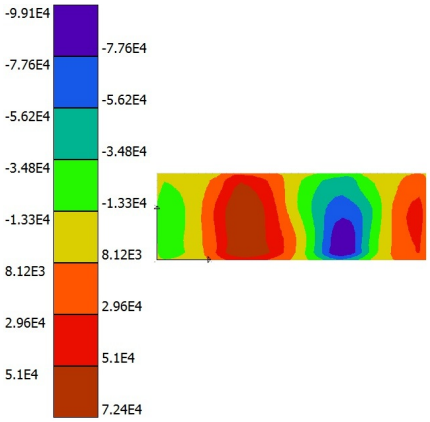
20°	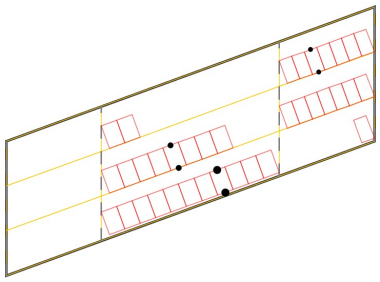 File: 10x8x15x8x20.load NA Load Pattern Number: 73	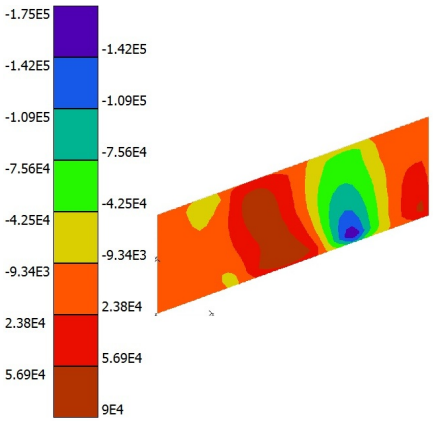
40°	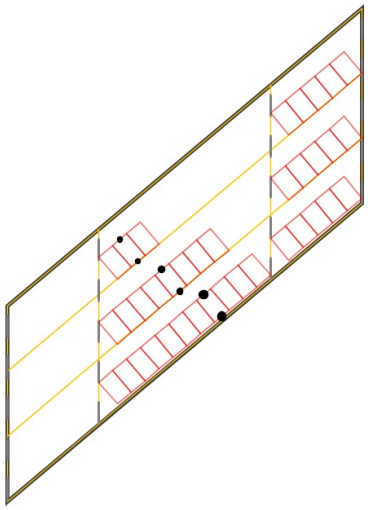 File: 10x8x15x8x40.load NA Load Pattern Number: 73	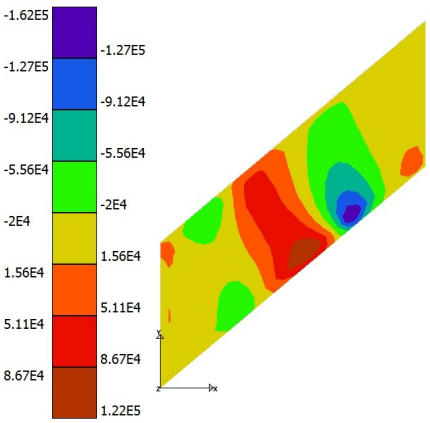

Table 8.3: Carriageway $10\,m \times (8\,m + 15\,m + 8\,m)$: Critical NA loading patterns and resulting contour plots for the twisting moment in the obtuse corner for the centre long span

The percentage errors of the standard NA loading patterns relative to the critical NA loading patterns for the twisting moment in the obtuse corner are presented for the first short span and the

centre long span of the carriageway. The errors are measured as the angle of skew increases from 0° to 40° in increments of 10°. The results include the actual value at the monitored finite element node and the value of the median in the region of the monitored finite element node.

Short Span: The percentage error of the standard NA loading patterns relative to the critical NA loading patterns for the twisting moment in the obtuse corner, for the first *short span*, is presented in Figure 8.1.

M_{11}
Obtuse Corner - Short Span

	Error (%)	
Angle of Skew (°)	Actual	Median
0	-37.68%	-41.22%
10	-28.94%	-36.27%
20	-21.46%	-30.21%
30	-14.61%	-24.22%
40	-18.64%	-28.82%

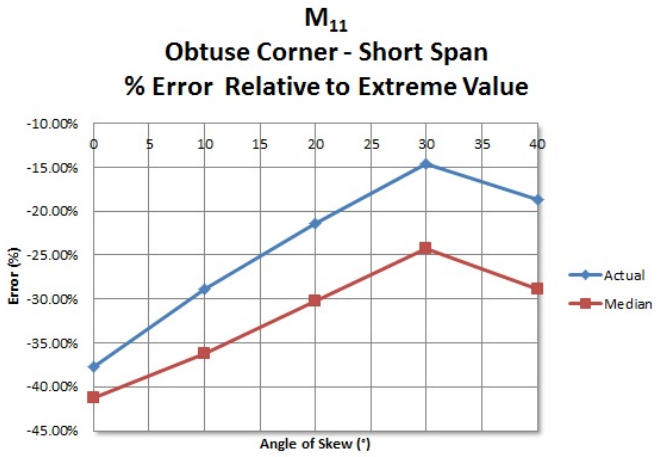

Figure 8.1: Carriageway $10\,m \times (8\,m + 15\,m + 8\,m)$: Relative error for the twisting moment in the obtuse corner for the first short span

Long Span: The percentage error of the standard NA loading patterns relative to the critical NA loading patterns for the twisting moment in the obtuse corner, for the centre *long span*, is presented in Figure 8.2.

M_{11}
Obtuse Corner - Long Span

	Error (%)	
Angle of Skew (°)	Actual	Median
0	-35.53%	-35.00%
10	-24.90%	-27.50%
20	-17.82%	-20.74%
30	-13.78%	-17.79%
40	-16.17%	-22.74%

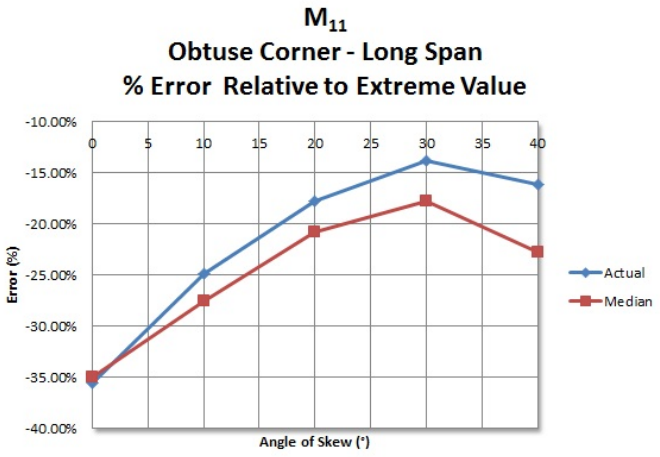

Figure 8.2: Carriageway $10\,m \times (8\,m + 15\,m + 8\,m)$: Relative error for the twisting moment in the obtuse corner for the long centre span

The standard NA loading patterns do not represent a good approximation for the critical twisting

moment in the obtuse corner for the particular carriageway. Large errors occur between the standard values and the extreme values for the twisting moment in the obtuse corner for both spans. The largest errors occur at a 0˚ angle of skew for both spans, when the obtuse corner has not formed. The values produced by the standard NA loading patterns are 37.68 % and 35.53 % *smaller* than the values produced by the critical NA loading patterns at a 0˚ angle of skew, for the short span and the long span respectively. The errors decrease gradually up to an angle of skew of 30˚. After 30˚ the errors increase again.

8.2 Transverse Bending Moment

The transverse bending moment is measured in the obtuse corner and at mid-span, at the centre of the carriageway.

8.2.1 Obtuse Corner

Critical NA loading patterns and resulting contour plots are presented for the transverse bending moment in the obtuse corner, for the first short span and the centre long span of the carriageway.

Angle of Skew (˚)	Critical NA Loading Pattern	Resulting Contour Plot (Nm)
0˚	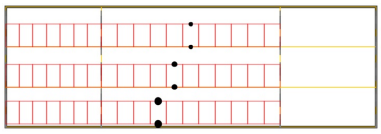 File: 10x8x15x8x00.load NA Load Pattern Number: 45	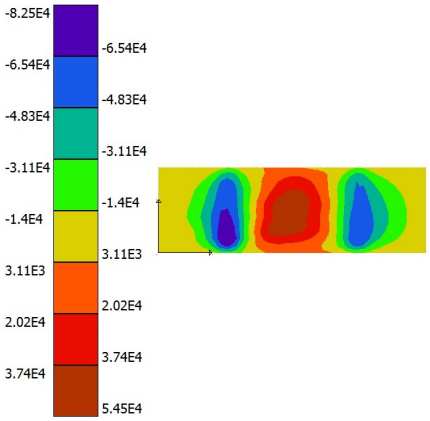
20˚	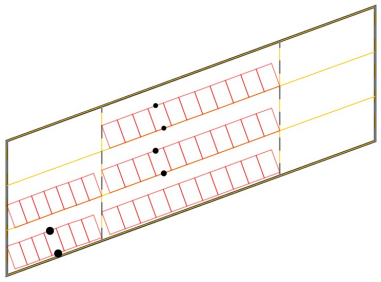 File: 10x8x15x8x20.load NA Load Pattern Number: 75	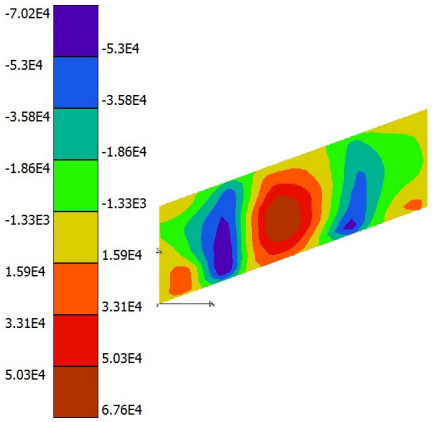

Table 8.4: Carriageway $10\,m \times (8\,m + 15\,m + 8\,m)$: Critical NA loading patterns and resulting contour plots for the transverse bending moment in the obtuse corner for the first short span (Continued on the next page)

Angle of Skew (°)	Critical NA Loading Pattern	Resulting Contour Plot (Nm)
40°	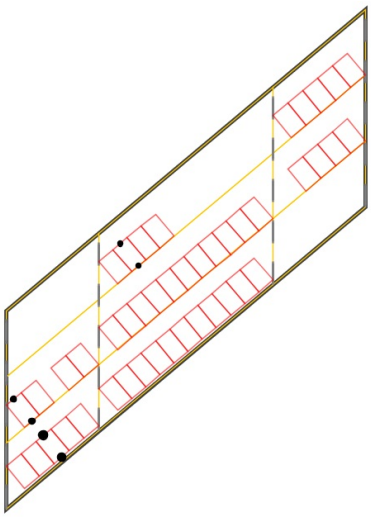 File: 10x8x15x8x40.load NA Load Pattern Number: 75	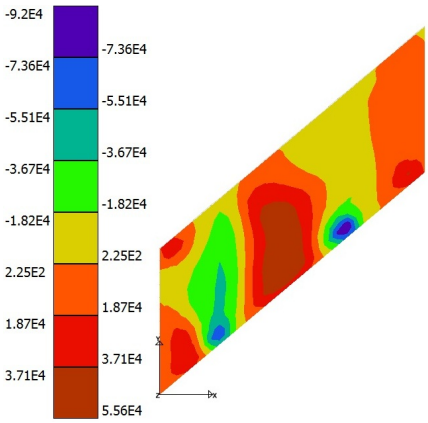

Table 8.5: Carriageway $10\,m \times (8\,m + 15\,m + 8\,m)$: Critical NA loading patterns and resulting contour plots for the transverse bending moment in the obtuse corner for the first short span (Continued from the previous page)

Short Span: The critical NA loading patterns and resulting contour plots are illustrated in Table 8.4 on the previous page for the transverse bending moment in the obtuse corner, for the first *short span* from the left.

Long Span: The critical NA loading patterns and resulting contour plots are illustrated in Table 8.6 for the transverse bending moment in the obtuse corner, for the centre *long span.*

Angle of Skew (°)	Critical NA Loading Pattern	Resulting Contour Plot (Nm)
0°	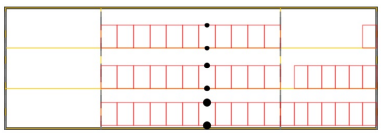 File: 10x8x15x8x00.load NA Load Pattern Number: 47	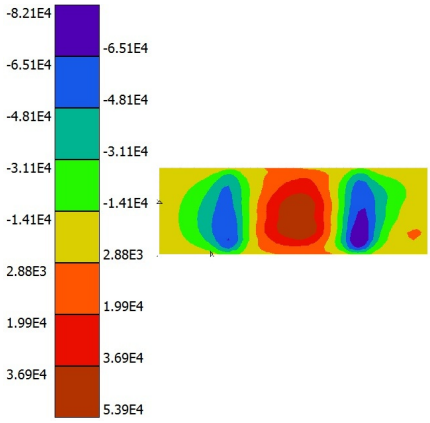

Table 8.6: Carriageway $10\,m \times (8\,m + 15\,m + 8\,m)$: Critical NA loading patterns and resulting contour plots for the transverse bending moment in the obtuse corner for the centre long span (Continued on the next page)

Angle of Skew (°)	Critical NA Loading Pattern	Resulting Contour Plot (Nm)
20°	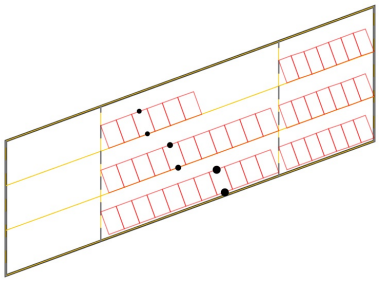 File: 10x8x15x8x20.load NA Load Pattern Number: 77	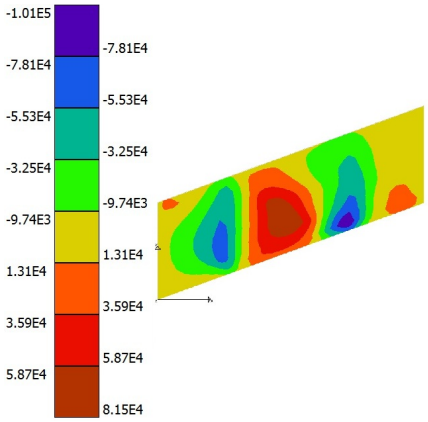
40°	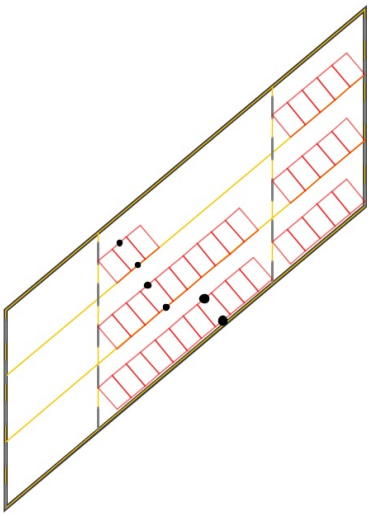 File: 10x8x15x8x40.load NA Load Pattern Number: 77	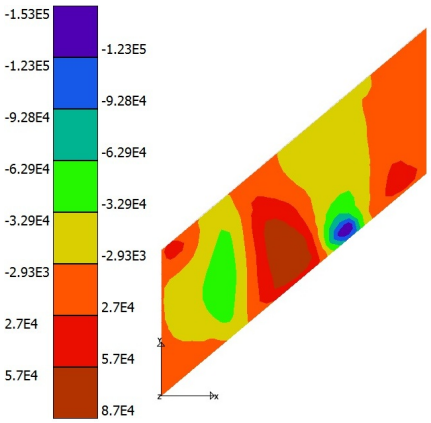

Table 8.7: Carriageway $10\,m \times (8\,m + 15\,m + 8\,m)$: Critical NA loading patterns and resulting contour plots for the transverse bending moment in the obtuse corner for the centre long span (Continued from the previous page)

The following can be seen from Table 8.4 on page 53 and Table 8.6 on the previous page regarding the transverse bending moment in the obtuse corner:

- To produce the critical NA loading pattern for the transverse bending moment in the bottom right obtuse corner of a specific span of the carriageway, the top right acute corner of that span of the carriageway should not be loaded.
- The heaviest loading should be placed towards the bottom edge of the carriageway in the transverse direction and towards mid-span in the longitudinal direction.

The percentage errors of the standard NA loading patterns relative to the critical NA loading patterns for the transverse bending moment in the obtuse corner are presented for both the first short span and the centre long span of the carriageway. The errors are measured as the angle of skew

increases from 0° to 40° in increments of 10°. The results include the actual value at the monitored finite element node and the value of the median in the region of the monitored finite element node.

Short Span: The percentage error of the standard NA loading patterns relative to the critical NA loading patterns for the transverse bending moment in the obtuse corner, for the first *short span*, is presented in Figure 8.3.

M_{12}
Obtuse Corner - Short Span

	Error (%)	
Angle of Skew (°)	Actual	Median
0	-9.17%	-0.76%
10	-7.31%	-12.36%
20	-5.52%	-7.62%
30	-2.99%	-7.10%
40	-2.94%	-5.82%

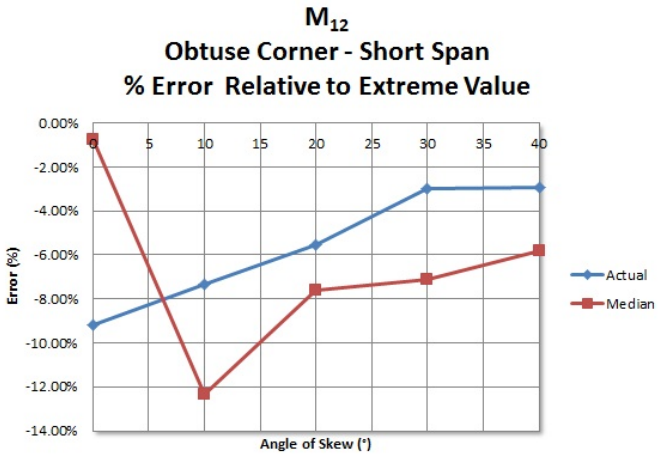

Figure 8.3: Carriageway $10\,m \times (8\,m + 15\,m + 8\,m)$: Relative error for the transverse bending moment in the obtuse corner for the first short span

Long Span: The percentage error of the standard NA loading patterns relative to the critical NA loading patterns for the transverse bending moment in the obtuse corner, for the centre *long span*, is presented in Figure 8.4.

M_{12}
Obtuse Corner - Long Span

	Error (%)	
Angle of Skew (°)	Actual	Median
0	-0.61%	-17.33%
10	-6.26%	-3.15%
20	-6.86%	-4.80%
30	-10.04%	-7.30%
40	-8.31%	-7.32%

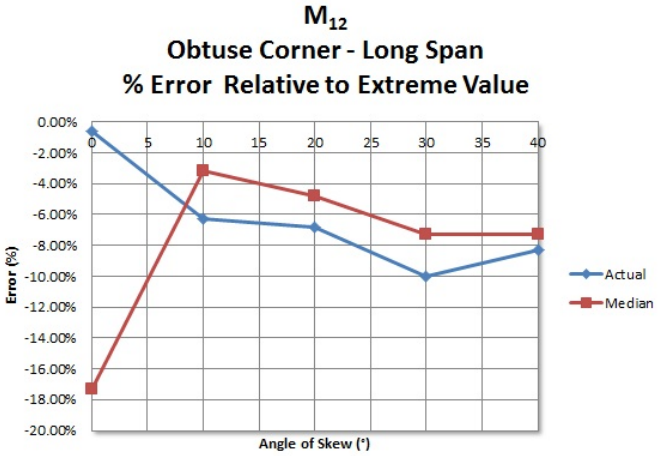

Figure 8.4: Carriageway $10\,m \times (8\,m + 15\,m + 8\,m)$: Relative error for the transverse bending moment in the obtuse corner for the centre long span

The results from the standard NA loading patterns produce a reasonable approximation for the critical transverse bending moment in the obtuse corner, especially for the longer span. The actual

results produced by the standard NA loading patterns are not more than 11 % *smaller* than the results produced by the critical NA loading patterns for the transverse bending moment in the obtuse corner for both spans and all the angles of skew.

Angle of Skew (°)	**Critical NA Loading Pattern**	**Resulting Contour Plot (Nm)**
0°	 File: 10x8x15x8x00.load NA Load Pattern Number: 50	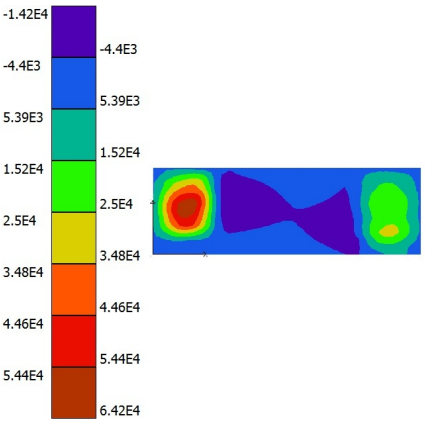
20°	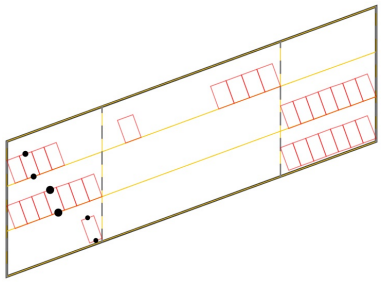 File: 10x8x15x8x20.load NA Load Pattern Number: 80	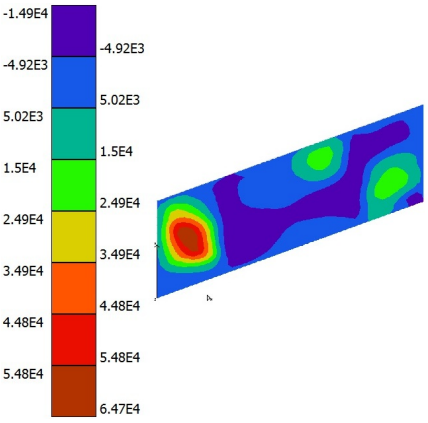
40°	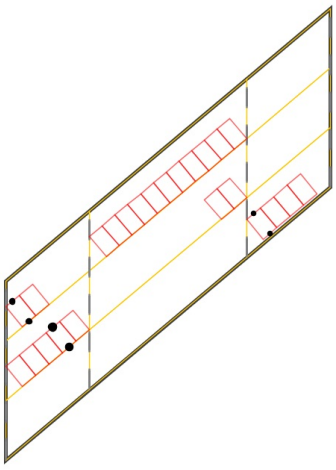 File: 10x8x15x8x40.load NA Load Pattern Number: 80	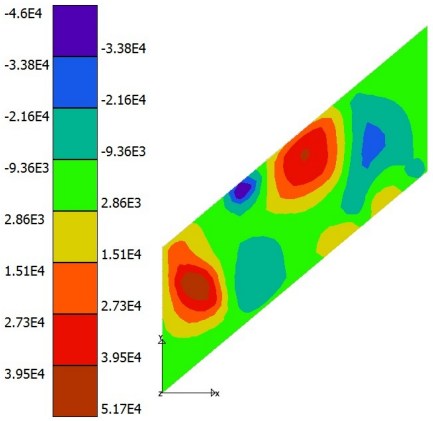

Table 8.8: Carriageway $10\,m \times (8\,m + 15\,m + 8\,m)$: Critical NA loading patterns and resulting contour plots for the transverse bending moment at mid-span centre, for the first short span

8.2.2 Mid-span Centre

The critical NA loading patterns and resulting contour plots are presented for the transverse bending moment at mid-span, at the centre of the carriageway.

Angle of Skew (°)	Critical NA Loading Pattern	Resulting Contour Plot (Nm)
0°	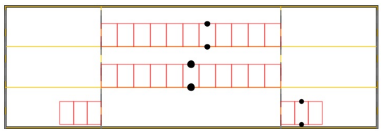 File: 10x8x15x8x00.load NA Load Pattern Number: 52	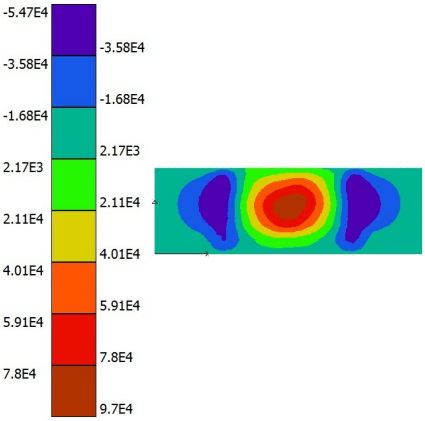
20°	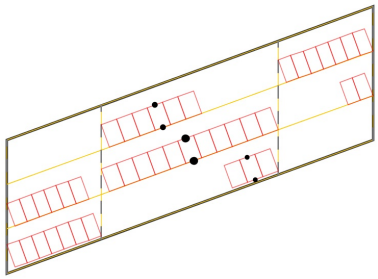 File: 10x8x15x8x20.load NA Load Pattern Number: 82	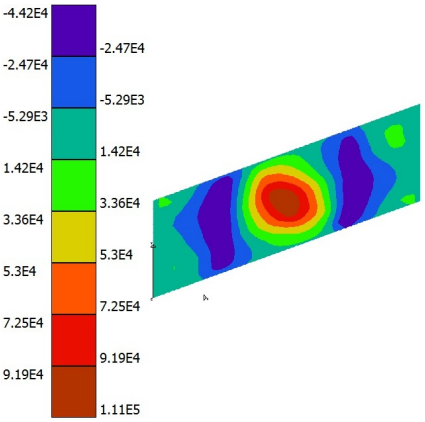
40°	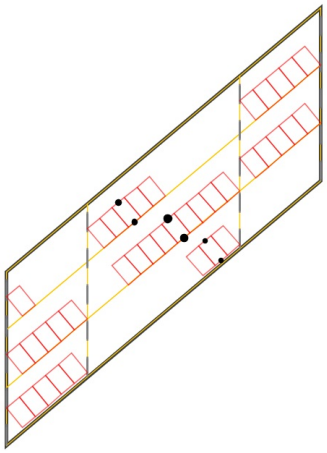 File: 10x8x15x8x40.load NA Load Pattern Number: 82	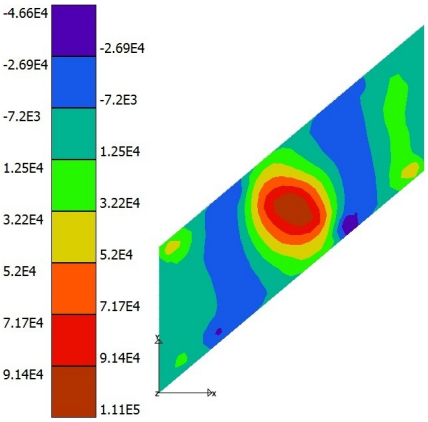

Table 8.9: Carriageway $10\,m \times (8\,m + 15\,m + 8\,m)$: Critical NA loading patterns and resulting contour plots for the transverse bending moment at mid-span centre, for the centre long span

Short Span: The critical NA loading patterns and resulting contour plots are illustrated in Table 8.8 on page 57 for the transverse bending moment at mid-span centre, for the first *short span* from the left.

Long Span: The critical NA loading patterns and resulting contour plots are illustrated in Table 8.9 on the previous page for the transverse bending moment at mid-span centre, for the centre *long span.*

The following can be seen from the Table 8.8 on page 57 and Table 8.9 on the previous page regarding the transverse bending moment at mid-span, at the centre of the carriageway:

- To produce the critical NA loading pattern for the transverse bending moment at mid-span centre, for a specific span of the carriageway, both the acute corners of that span should not be loaded.
- The heaviest loading should be placed towards the centre of the carriageway in the longitudinal and transverse directions.
- The critical NA loading patterns for the transverse bending moment at mid-span centre, do not follow a clear pattern regarding the loading arrangement on the adjacent spans.

The percentage error of the standard NA loading patterns relative to the critical NA loading patterns are presented as the angle of skew increases from 0° to 40° in increments of 10°. The results include the actual value at the monitored finite element node, the value of the median in the region of the monitored finite element node as well as the Wood and Armer values for the bottom reinforcement in the transverse direction. The Wood and Armer values have been acquired with the assumption that the reinforcement will be placed parallel to the edges of the carriageway in both directions.

Short Span: The percentage error of the standard NA loading patterns relative to the critical NA loading patterns for the transverse bending moment at mid-span centre, for the first *short span*, is presented in Figure 8.5.

M_{12}
Mid-Span - Short Span

	Error (%)		
Angle of Skew (°)	Actual	Median	W & A
0	-38.33%	-37.19%	-37.30%
10	-41.96%	-37.84%	-46.66%
20	-47.34%	-45.29%	-50.80%
30	-53.54%	-56.68%	-55.42%
40	-57.29%	-58.77%	-58.08%

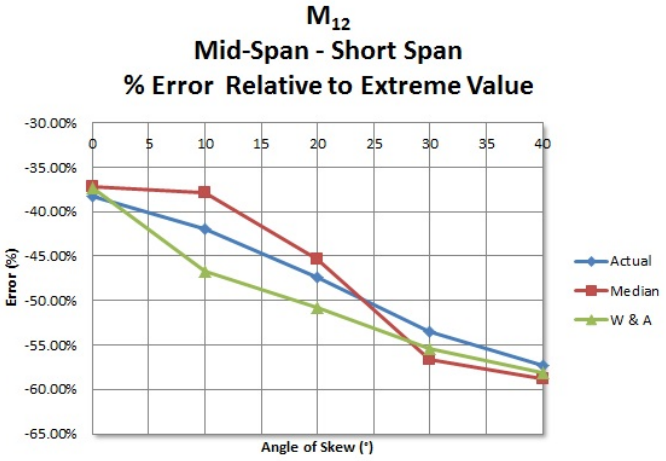

Figure 8.5: Carriageway $10\,m \times (8\,m + 15\,m + 8\,m)$: Relative error for the transverse bending moment at mid-span centre, for the first short span

Long Span: The percentage error of the standard NA loading patterns relative to the critical NA loading patterns for the transverse bending moment at mid-span centre, for the centre *long span*, is presented in Figure 8.6.

M_{12}
Mid-Span - Long Span

	Error (%)		
Angle of Skew (°)	Actual	Median	W & A
0	-44.91%	-44.27%	-43.74%
10	-47.69%	-47.42%	-42.99%
20	-53.29%	-50.73%	-44.50%
30	-60.07%	-60.73%	-48.57%
40	-69.76%	-67.48%	-57.55%

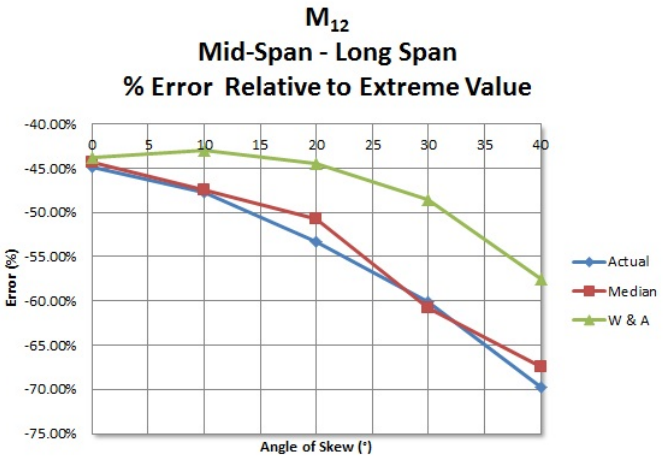

Figure 8.6: Carriageway $10\,m \times (8\,m + 15\,m + 8\,m)$: Relative error for the transverse bending moment at mid-span centre, for the centre long span

The standard NA loading patterns do not represent a good approximation for the critical NA loading patterns for the transverse bending moment at mid-span, at the centre of the carriageway. Large errors occur between the standard values and the extreme values for both spans. The largest errors occur at a 40° angle of skew, for both spans. The values produced by the standard NA loading patterns are 57.29 % and 69.76 % *smaller* than the values produced by the critical NA loading patterns at a 40° angle of skew, for the short span and the long span respectively. Large errors occur between the standard values and the extreme values since the effective area of the carriageway that should be loaded, decreases as the angle of skew increases. The standard NA patterns either loads an entire span of the carriageway, or the span is not loaded at all, i.e. partial loading of a span is not provided by the standard NA patterns. As a result large areas that should not be loaded, so-called areas of relief, are loaded by the standard patterns. This results in an increased error as the angle of skew increases.

8.3 Longitudinal Bending Moment

The longitudinal bending moment is measured at mid-span and over the supports, at the edge of the carriageway. The sagging, hogging and support moments are presented in the next subsections.

8.3.1 Sagging Moment at Mid-span Edge

The critical NA loading patterns and resulting contour plots are presented for the sagging longitudinal bending moment at mid-span, at the edge of the carriageway. The results are presented for the first short span and the centre long span of the particular carriageway.

Short Span: The critical NA loading patterns and resulting contour plots are illustrated in Table 8.10 on the next page for the sagging longitudinal bending moment at mid-span edge, for the

first *short span* from the left.

Angle of Skew (°)	Critical NA Loading Pattern	Resulting Contour Plot (Nm)
0°	 File: 10x8x15x8x00.load NA Load Pattern Number: 53	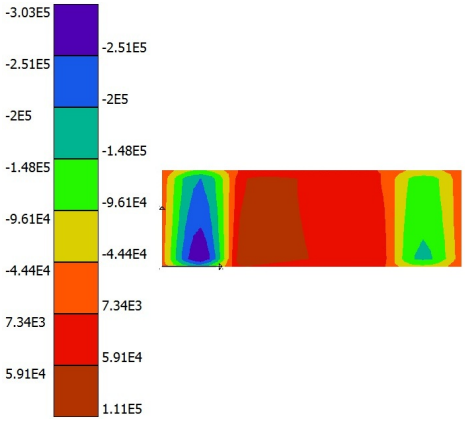
20°	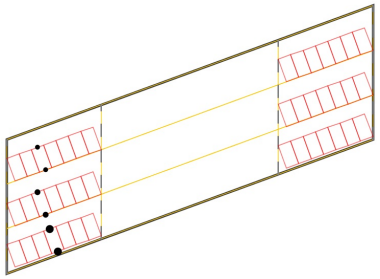 File: 10x8x15x8x20.load NA Load Pattern Number: 83	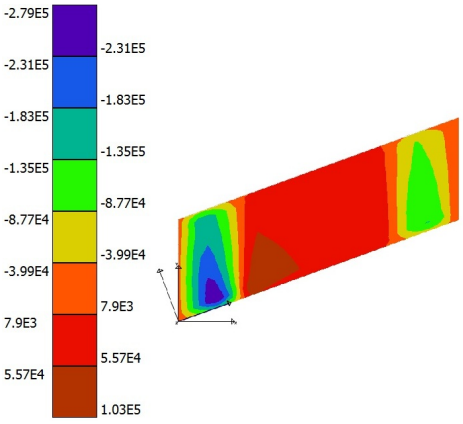
40°	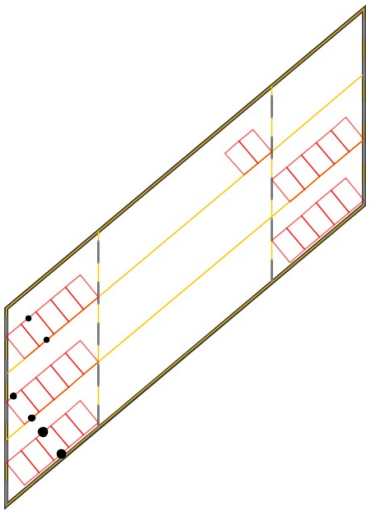 File: 10x8x15x8x40.load NA Load Pattern Number: 83	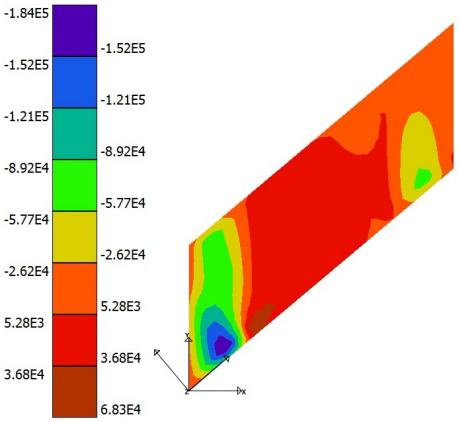

Table 8.10: Carriageway $10\,m \times (8\,m + 15\,m + 8\,m)$: Critical NA loading patterns and resulting contour plots for the sagging longitudinal bending moment at mid-span edge, for the first short span

Long Span: The critical NA loading patterns and resulting contour plots are illustrated in Table 8.11 for the sagging longitudinal bending moment at mid-span edge, for the centre *long span*.

Angle of Skew (°)	Critical NA Loading Pattern	Resulting Contour Plot (Nm)
0°	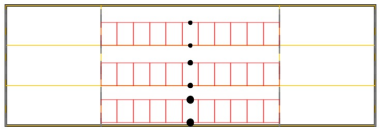 File: 10x8x15x8x00.load NA Load Pattern Number: 57	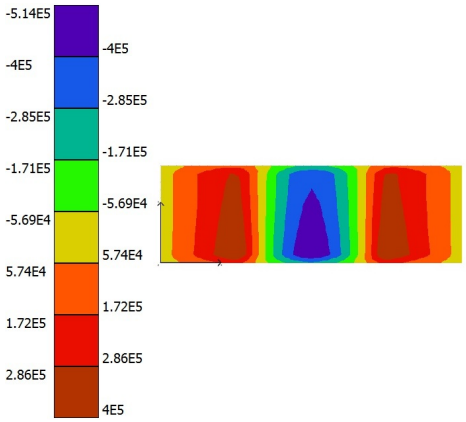
20°	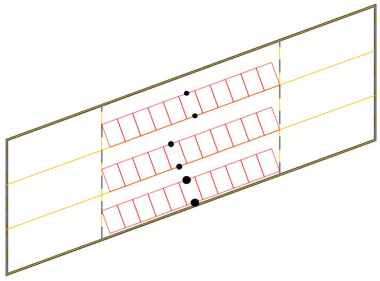 File: 10x8x15x8x20.load NA Load Pattern Number: 87	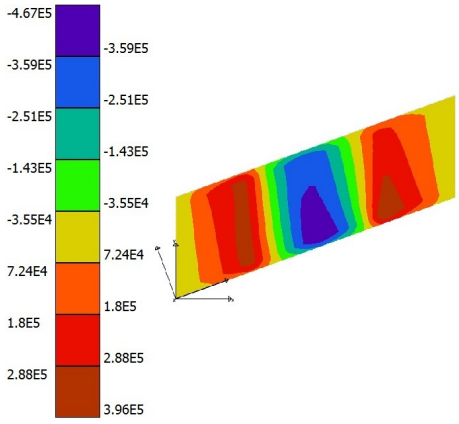
40°	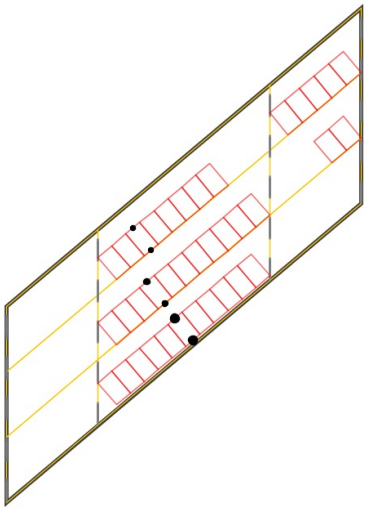 File: 10x8x15x8x40.load NA Load Pattern Number: 87	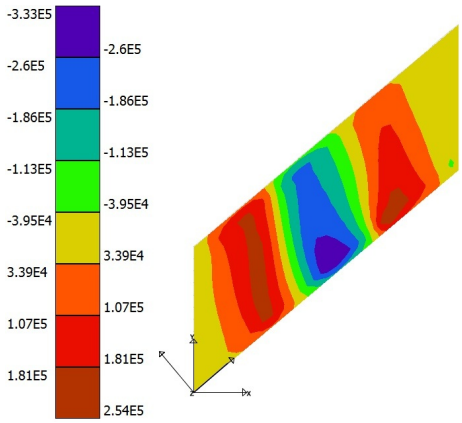

Table 8.11: Carriageway $10\,m \times (8\,m + 15\,m + 8\,m)$: Critical NA loading patterns and resulting contour plots for the sagging longitudinal bending moment at mid-span edge, for the centre long span

It can be seen from Table 8.10 on page 61 and Table 8.11 on the previous page regarding the critical NA loading patterns for the sagging longitudinal bending moment at mid-span, at the edge of the carriageway:

- The critical NA loading patterns are as expected, similar to continuous beam patterns, for angles of skew up to 20°, for the short span and the centre long span.
- The critical NA loading patterns become less predictable at a 40° angle of skew regarding the loading arrangement on the adjacent spans and the alternate spans.

The percentage error of the standard NA loading patterns relative to the critical NA loading patterns is presented as the angle of skew increases from 0° to 40° in increments of 10°. The results include the actual value at the monitored finite element node, the value of the median in the region of the monitored finite element node as well as the Wood and Armer values for the bottom reinforcement in the longitudinal direction. The Wood and Armer values have been acquired with the assumption that the reinforcement will be placed parallel to the edges of the carriageway in both directions.

Short Span: The percentage error of the standard NA loading patterns relative to the critical NA loading patterns for the sagging longitudinal bending moment at mid-span edge, for the first *short span*, is presented in Figure 8.7.

M_{21}
Sagging - Short Span

	Error (%)		
Angle of Skew (°)	Actual	Median	W & A
0	-1.30%	-1.34%	-1.20%
10	-0.73%	-0.85%	-0.69%
20	-1.30%	-5.52%	-1.79%
30	-2.00%	-2.38%	-2.33%
40	-2.91%	-4.45%	-3.70%

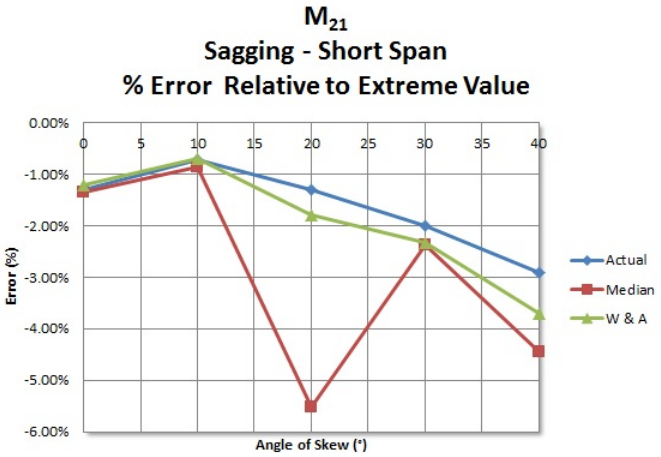

Figure 8.7: Carriageway $10\,m \times (8\,m + 15\,m + 8\,m)$: Relative error for the sagging longitudinal bending moment at mid-span edge, for the first short span

Long Span: The percentage error of the standard NA loading patterns relative to the critical NA loading patterns for the sagging longitudinal bending moment at mid-span edge, for the centre *long span*, is presented in Figure 8.8 on the next page.

The standard NA loading patterns produce a good approximation for the critical sagging longitudinal bending moment at mid-span, at the edge of the carriageway. The actual results produced by the standard NA loading patterns are less than 6 % *smaller* than the results produced by the critical NA loading patterns, for both spans and all the angles of skew. The errors tend to increase from a 10° angle of skew, since the loading arrangement becomes less predictable on the adjacent and alternate spans for larger angles of skew.

M_{21}
Sagging - Long Span

	Error (%)		
Angle of Skew (°)	Actual	Median	W & A
0	-2.49%	-2.86%	-2.35%
10	-2.18%	-2.27%	-2.19%
20	-2.72%	-4.10%	-2.94%
30	-4.43%	-5.02%	-4.44%
40	-5.09%	-7.01%	-5.83%

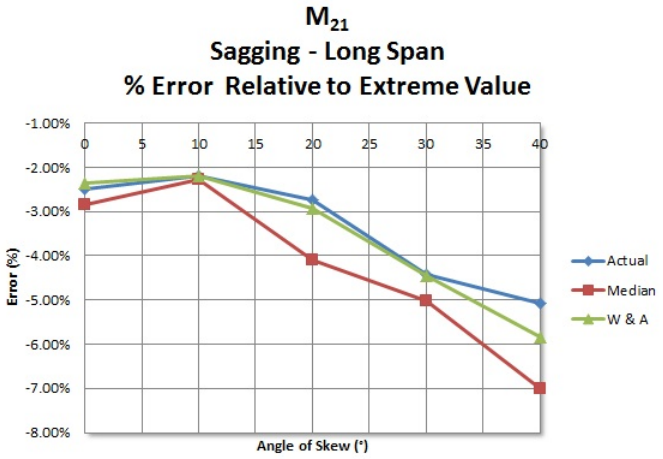

Figure 8.8: Carriageway $10\,m \times (8\,m + 15\,m + 8\,m)$: Relative error for the sagging longitudinal bending moment at mid-span edge, for the centre long span

8.3.2 Hogging Moment at Mid-span Edge

The critical NA loading patterns and resulting contour plots are presented for the hogging longitudinal bending moment at mid-span, at the edge of the carriageway. The hogging longitudinal bending moment refers to the moment to be resisted by the top reinforcement of the carriageway at mid-span, in the longitudinal direction. The results are presented for the first short span and the centre long span of the particular carriageway.

Short Span: The critical NA loading patterns and resulting contour plots are illustrated in Table 8.12 for the hogging longitudinal bending moment at mid-span edge, for the first *short span* from the left.

Angle of Skew (°)	Critical NA Loading Pattern	Resulting Contour Plot (Nm)
0°	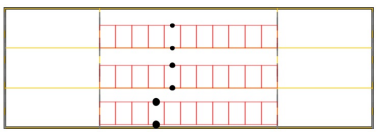 File: 10x8x15x8x00.load NA Load Pattern Number: 54	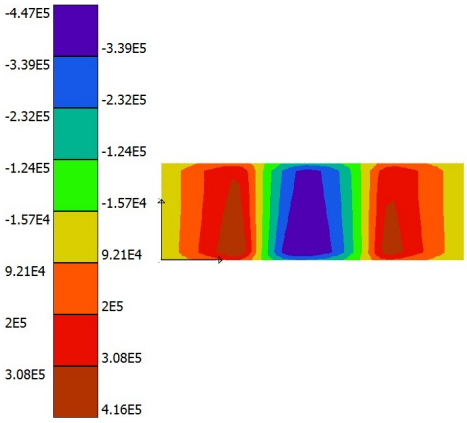

Table 8.12: Carriageway $10\,m \times (8\,m + 15\,m + 8\,m)$: Critical NA loading patterns and resulting contour plots for the hogging longitudinal bending moment at mid-span edge, for the first short span
(Continued on the next page)

Angle of Skew (°)	Critical NA Loading Pattern	Resulting Contour Plot (Nm)
20°	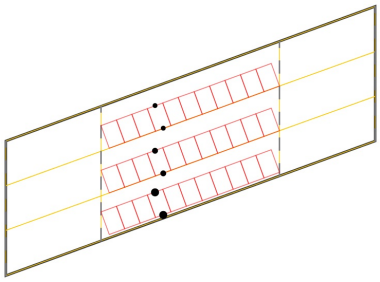 File: 10x8x15x8x20.load NA Load Pattern Number: 84	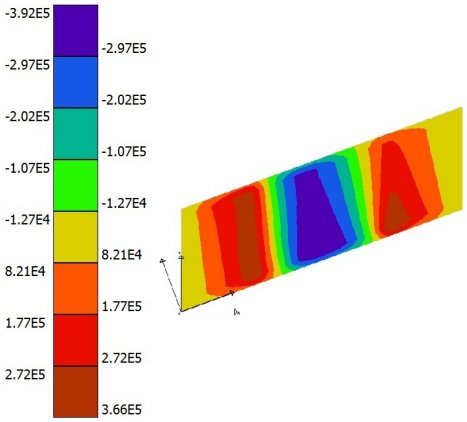
40°	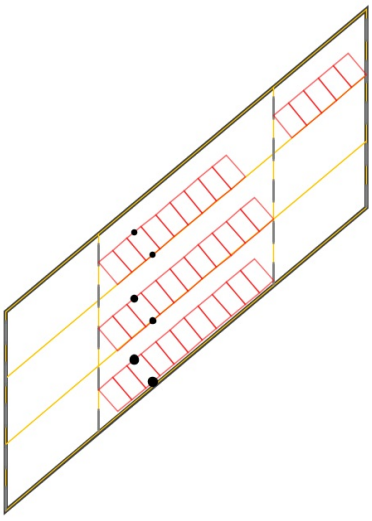 File: 10x8x15x8x40.load NA Load Pattern Number: 84	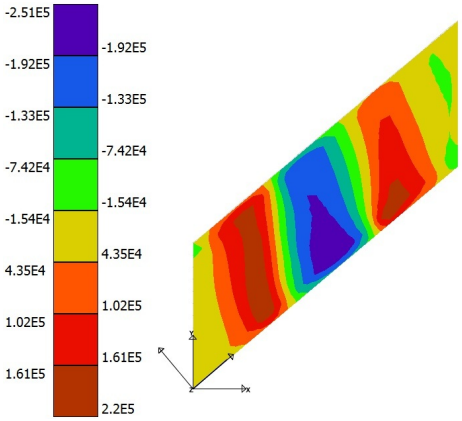

Table 8.13: Carriageway $10\,m \times (8\,m + 15\,m + 8\,m)$: Critical NA loading patterns and resulting contour plots for the hogging longitudinal bending moment at mid-span edge, for the first short span (Continued from the previous page)

Long Span: The critical NA loading patterns and resulting contour plots are illustrated in Table 8.14 on the next page for the hogging longitudinal bending moment at mid-span edge, for the centre *long span*.

It can be seen from Table 8.12 on the preceding page and Table 8.14 on the next page regarding the critical NA loading patterns for the hogging longitudinal bending moment at mid-span, at the edge of the carriageway:

- The critical NA loading patterns are as expected, similar to continuous beam patterns, for angles of skew up to 20°, for the short span and the centre long span.
- The critical NA loading patterns become less predictable at a 40° angle of skew regarding the loading arrangement on the adjacent spans and the alternate spans.

Angle of Skew (°)	Critical NA Loading Pattern	Resulting Contour Plot (Nm)
0°	 File: 10x8x15x8x00.load NA Load Pattern Number: 58	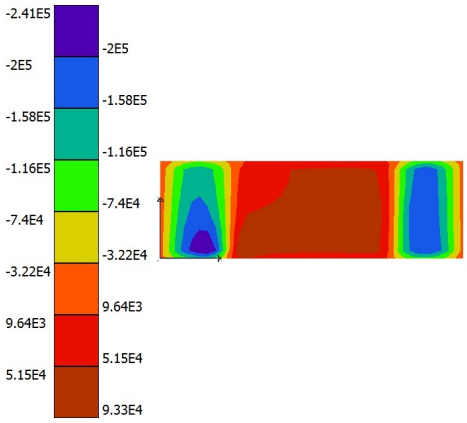
20°	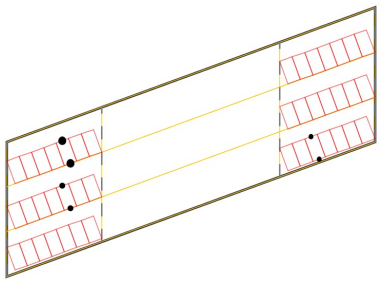 File: 10x8x15x8x20.load NA Load Pattern Number: 88	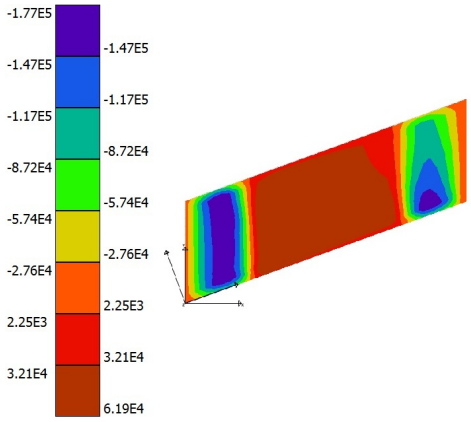
40°	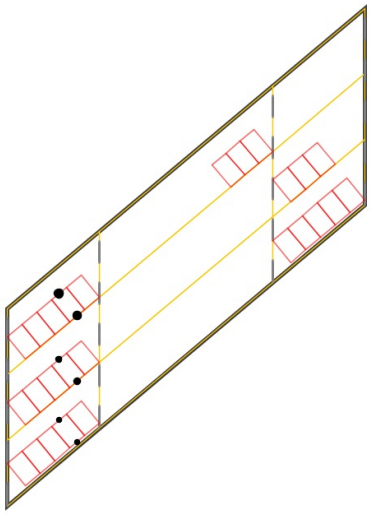 File: 10x8x15x8x40.load NA Load Pattern Number: 88	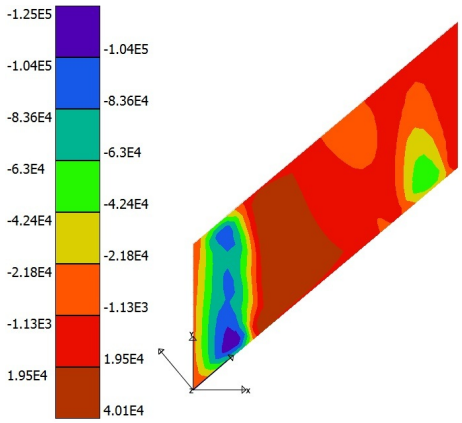

Table 8.14: Carriageway $10\,m \times (8\,m + 15\,m + 8\,m)$: Critical NA loading patterns and resulting contour plots for the hogging longitudinal bending moment at mid-span edge, for the centre long span

The percentage error of the standard NA loading patterns relative to the critical NA loading patterns

is presented as the angle of skew increases from 0° to 40° in increments of 10°. The results include the actual value at the monitored finite element node, the value of the median in the region of the monitored finite element node as well as the Wood and Armer values for the top reinforcement in the longitudinal direction. The Wood and Armer values have been acquired with the assumption that the reinforcement will be placed parallel to the edges of the carriageway in both directions.

Short Span: The percentage error of the standard NA loading patterns relative to the critical NA loading patterns for the hogging longitudinal bending moment at mid-span edge, for the first *short span*, is presented in Figure 8.9.

M_{21}
Hogging - Short Span

Angle of Skew (°)	Error (%) Actual	Median	W & A
0	-5.76%	-5.89%	-5.66%
10	-5.13%	-5.18%	-5.12%
20	-5.54%	-5.52%	-5.62%
30	-6.68%	-6.68%	-6.83%
40	-7.90%	-8.15%	-7.94%

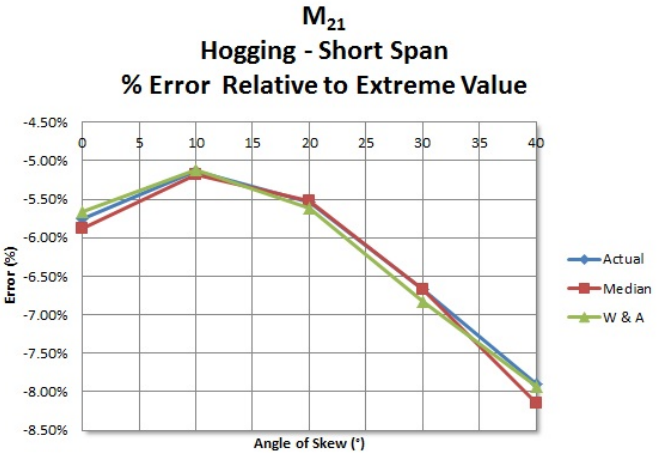

Figure 8.9: Carriageway $10\,m \times (8\,m + 15\,m + 8\,m)$: Relative error for the hogging longitudinal bending moment at mid-span edge, for the first short span

Long Span: The percentage error of the standard NA loading patterns relative to the critical NA loading patterns for the hogging longitudinal bending moment at mid-span edge, for the centre *long span*, is presented in Figure 8.10.

M_{21}
Hogging - Long Span

Angle of Skew (°)	Error (%) Actual	Median	W & A
0	-4.59%	-7.98%	-4.50%
10	-3.28%	-6.79%	-5.81%
20	-3.92%	-6.95%	-10.73%
30	-5.73%	-5.83%	-10.97%
40	-11.92%	-11.92%	-24.23%

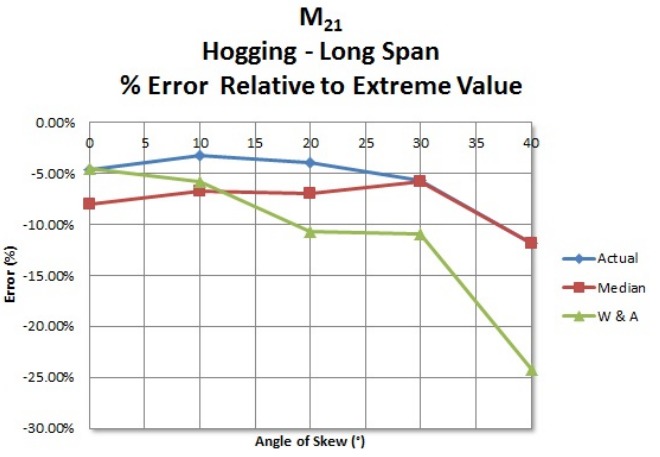

Figure 8.10: Carriageway $10\,m \times (8\,m + 15\,m + 8\,m)$: Relative error for the hogging longitudinal bending moment at mid-span edge, for the centre long span

The standard NA loading patterns produce a good approximation for the critical hogging longitudinal bending moment at mid-span, at the edge of the carriageway, especially for the short span. The actual results produced by the standard NA loading patterns are less than 12 % *smaller* than the results produced by the critical NA loading patterns, for both spans and all the angles of skew. The errors tend to increase from a 10° angle of skew, since the loading arrangement becomes less predictable on the adjacent and alternate spans for larger angles of skew.

8.3.3 Support Moment at the Edge

The critical NA loading patterns and resulting contour plots are presented for the longitudinal bending moment over the supports, at the edge of the carriageway. The longitudinal bending moment over the supports refers to the moment to be resisted by the top reinforcement of the carriageway. The results are presented for the interior support at the first short span and the support after the centre long span of the particular carriageway.

Short Span: The critical NA loading patterns and resulting contour plots are illustrated in Table 8.15 for the longitudinal bending moment at the first interior support, for the first *short span* from the left.

Angle of Skew (°)	Critical NA Loading Pattern	Resulting Contour Plot (Nm)
0°	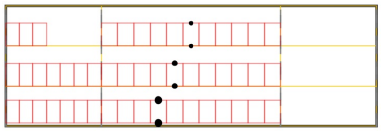 File: 10x8x15x8x00.load NA Load Pattern Number: 56	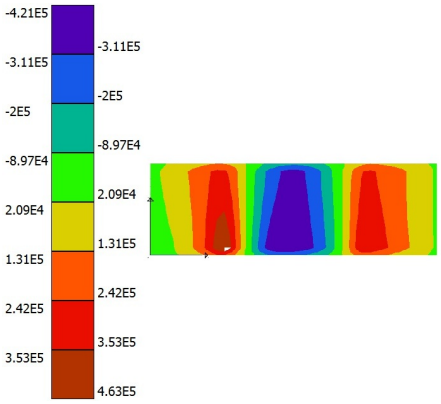
20°	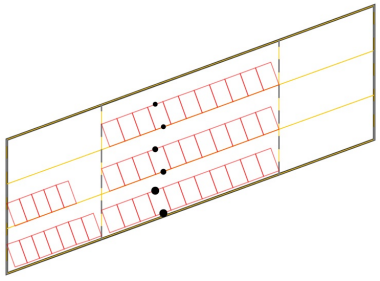 File: 10x8x15x8x20.load NA Load Pattern Number: 86	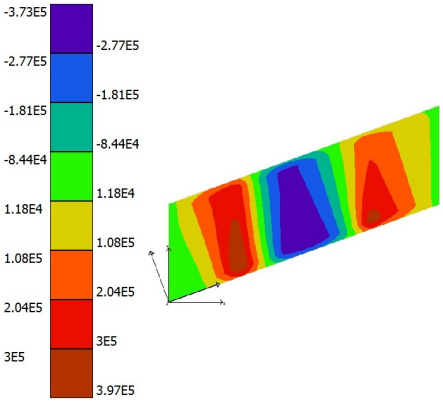

Table 8.15: Carriageway $10\,m \times (8\,m + 15\,m + 8\,m)$: Critical NA loading patterns and resulting contour plots for the longitudinal bending moment at the first interior support, at the edge of the carriageway (Continued on the next page)

Angle of Skew (°)	Critical NA Loading Pattern	Resulting Contour Plot (Nm)
40°	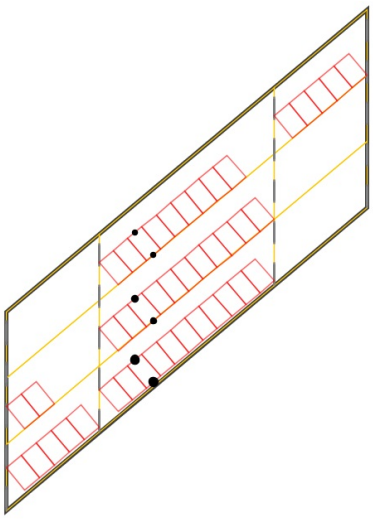	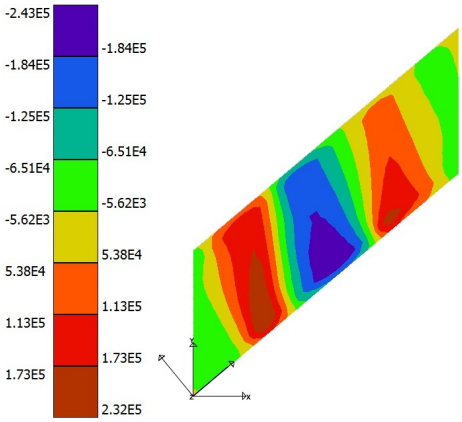

File: 10x8x15x8x40.load
NA Load Pattern Number: 86

Table 8.16: Carriageway $10\,m \times (8\,m + 15\,m + 8\,m)$: Critical NA loading patterns and resulting contour plots for the longitudinal bending moment at the first interior support, at the edge of the carriageway (Continued from the previous page)

Long Span: The critical NA loading patterns and resulting contour plots are illustrated in Table 8.17 on the next page for the longitudinal bending moment at the second interior support, for the centre *long span*.

It can be seen from Table 8.15 on the preceding page and Table 8.17 on the next page regarding the critical NA loading patterns for the longitudinal bending moment over the supports, at the edge of the carriageway:

- The critical NA loading patterns are as expected, for the loading arrangement on the bottom notional lane in the transverse direction, similar to continuous beam patterns, at the bottom edge of the carriageway.
- At larger angles of skew, the loading arrangement changes in the transverse direction for the span to the left of the support for which the critical NA loading pattern was generated. The top right acute corner of the span to the left of the support should not be loaded.
- The critical NA loading patterns become less predictable at a 40° angle of skew regarding the loading arrangement on the adjacent spans and the alternate spans.

The percentage error of the standard NA loading patterns relative to the critical NA loading patterns is presented as the angle of skew increases from 0° to 40° in increments of 10°. The results include the actual value at the monitored finite element node, the value of the median in the region of the monitored finite element node as well as the Wood and Armer values for the top reinforcement, over the supports, in the longitudinal direction. The Wood and Armer values have been acquired with the assumption that the reinforcement will be placed parallel to the edges of the carriageway in both directions.

Angle of Skew (°)	Critical NA Loading Pattern	Resulting Contour Plot (Nm)
0°	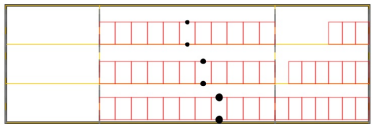 File: 10x8x15x8x00.load NA Load Pattern Number: 60	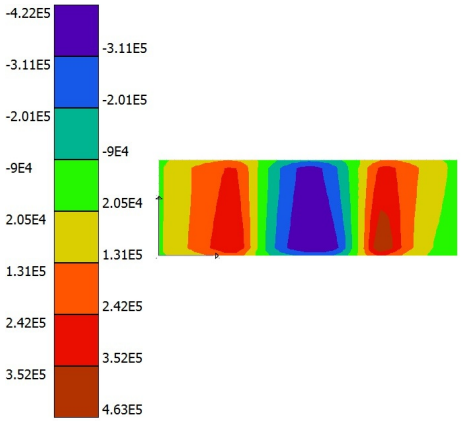
20°	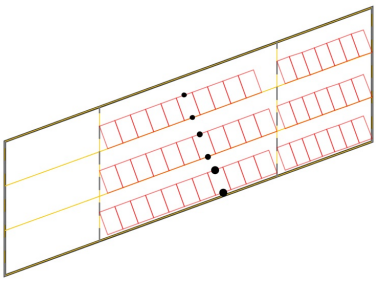 File: 10x8x15x8x20.load NA Load Pattern Number: 90	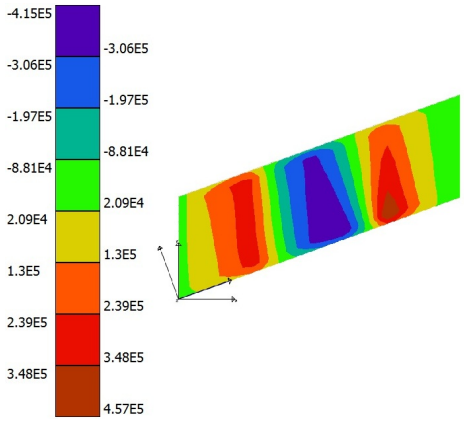
40°	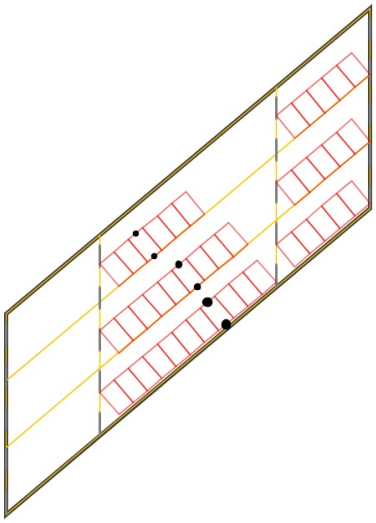 File: 10x8x15x8x40.load NA Load Pattern Number: 90	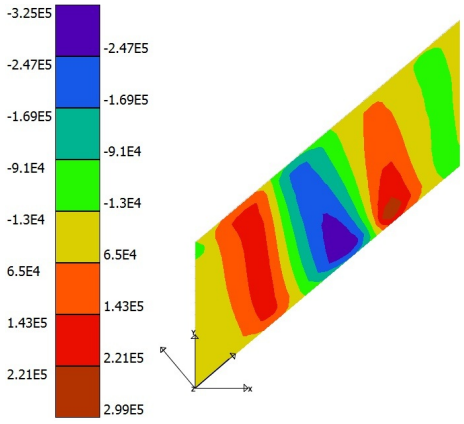

Table 8.17: Carriageway $10\,m \times (8\,m + 15\,m + 8\,m)$: Critical NA loading patterns and resulting contour plots for the longitudinal bending moment at the second interior support, at the edge of the carriageway

Short Span: The percentage error of the standard NA loading patterns relative to the critical NA loading patterns for the longitudinal bending moment at the first interior support, for the first *short span*, is presented in Figure 8.11.

M_{21}
Support - Short Span

	Error (%)		
Angle of Skew (°)	Actual	Median	W & A
0	-8.65%	-9.14%	-6.88%
10	-8.42%	-8.61%	-8.78%
20	-8.89%	-8.67%	-9.05%
30	-10.40%	-10.40%	-9.28%
40	-11.34%	-10.45%	-11.03%

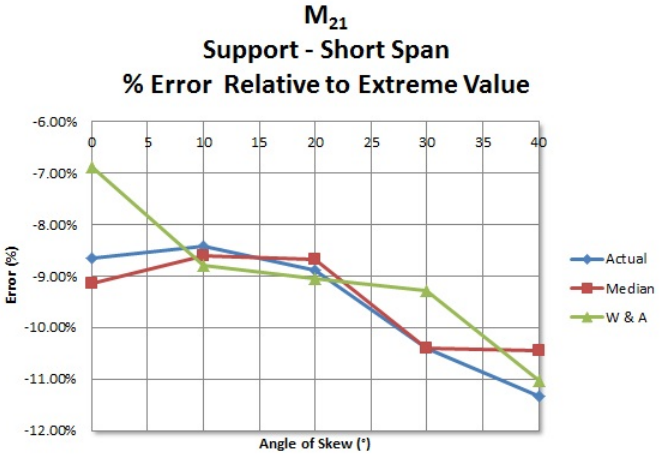

Figure 8.11: Carriageway $10\,m \times (8\,m + 15\,m + 8\,m)$: Relative error for the longitudinal bending moment at the first interior support, at the edge of the carriageway

Long Span: The percentage error of the standard NA loading patterns relative to the critical NA loading patterns for the longitudinal bending moment at the second interior support, for the centre *long span*, is presented in Figure 8.12.

M_{21}
Support - Long Span

	Error (%)		
Angle of Skew (°)	Actual	Median	W & A
0	-13.81%	-11.77%	-10.97%
10	-7.97%	-8.34%	-7.57%
20	-7.75%	-8.66%	-7.22%
30	-8.49%	-8.14%	-8.71%
40	-8.81%	-7.25%	-9.15%

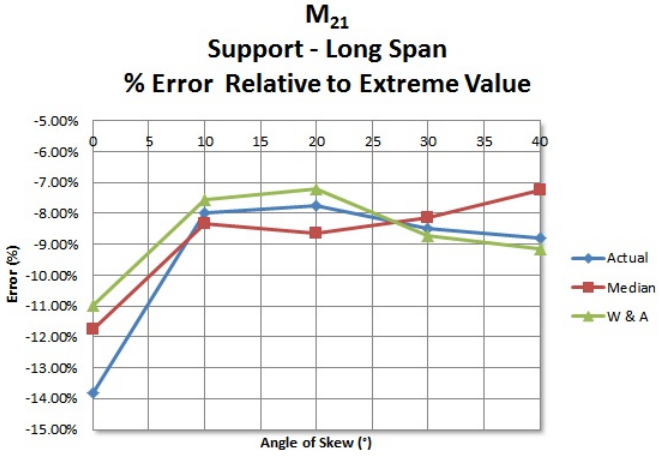

Figure 8.12: Carriageway $10\,m \times (8\,m + 15\,m + 8\,m)$: Relative error for the longitudinal bending moment at the second interior support, at the edge of the carriageway

The standard NA loading patterns produce a good approximation for the critical longitudinal bending moment over the supports, at the edge of the carriageway. The actual results produced by the standard NA loading patterns are less than 14 % *smaller* than the results produced by the critical NA loading patterns, for both spans and all the angles of skew. The errors tend to increase at the first interior support as the angle of skew increases. The errors remain relatively constant at

the second interior support, after 10° at approximately 8 %.

8.4 Normalized Maximum Moments

A multi-span continuous carriageway with an effective width of 10 m, two short spans of 8 m and a long centre span of 15 m was investigated in this chapter as the angle of skew increases. The two short spans are on either end of the carriageway and the long span represents the centre span. The critical NA loading patterns were presented for the different moment resultants in each of the critical regions.

The flexural behaviour of the specific carriageway under the effects of normal traffic loading will be presented in this section as the angle of skew increases. The different moment resultant values are normalized and compared *relative* to the largest moment resultant in each of the critical regions for the first short span and the centre long span of the particular carriageway.

Short Span: The normalized moment values are shown in Table 8.18 for the first *short span* from the left.

	M_{11}	M_{12}		M_{21}		
	Twisting Moment	Bending Moment - Transverse		Bending Moment - Longitudinal		
Angle of Skew (°)	Obtuse Corner	Obtuse Corner	Mid-Span (Center)	Sagging (Edge)	Hogging (Edge)	Support (Edge)
0	0.125	0.133	0.137	0.654	0.464	1.000
10	0.165	0.130	0.147	0.677	0.406	1.000
20	0.225	0.159	0.163	0.703	0.330	1.000
30	0.324	0.245	0.197	0.746	0.233	1.000
40	0.370	0.318	0.219	0.793	0.155	1.000

Table 8.18: Carriageway 10 $m \times (8\,m + 15\,m + 8\,m)$: Normalized maximum moments for the first short span

It can be seen from Table 8.18 that the longitudinal bending moment over the supports, at the edge of the carriageway, remains the dominant moment resultant for all the angles of skew for the first short span of the particular carriageway. The results from Table 8.18 are also presented graphically in Figure 8.13 on the next page.

The following can be observed regarding the normalized maximum moments for the first short span of the particular carriageway:

- The longitudinal bending moment over the supports, at the edge of the carriageway, remains the relative dominant moment resultant for the first short span, for all the angles of skew.
- The second-largest relative moment resultant for the first short span of the carriageway is the sagging longitudinal bending moment at mid-span, at the edge of the carriageway, for all the angles of skew. The sagging longitudinal bending moment reaches a value of approximately 80 % of the value of the dominant longitudinal bending moment at the first interior support.
- The twisting and transverse bending moment resultants are not dominant for the short span of the particular carriageway, although they increase relative to the dominant moment resultant as the angle of skew increases. The largest secondary moment resultant is the twisting moment in the obtuse corner of the first short span, with a relative value of 37 %.

- The hogging longitudinal bending moment decreases relative to the dominant moment resultant as the angle of skew increases, with a relative value of 15.5 % at a 40° angle of skew.

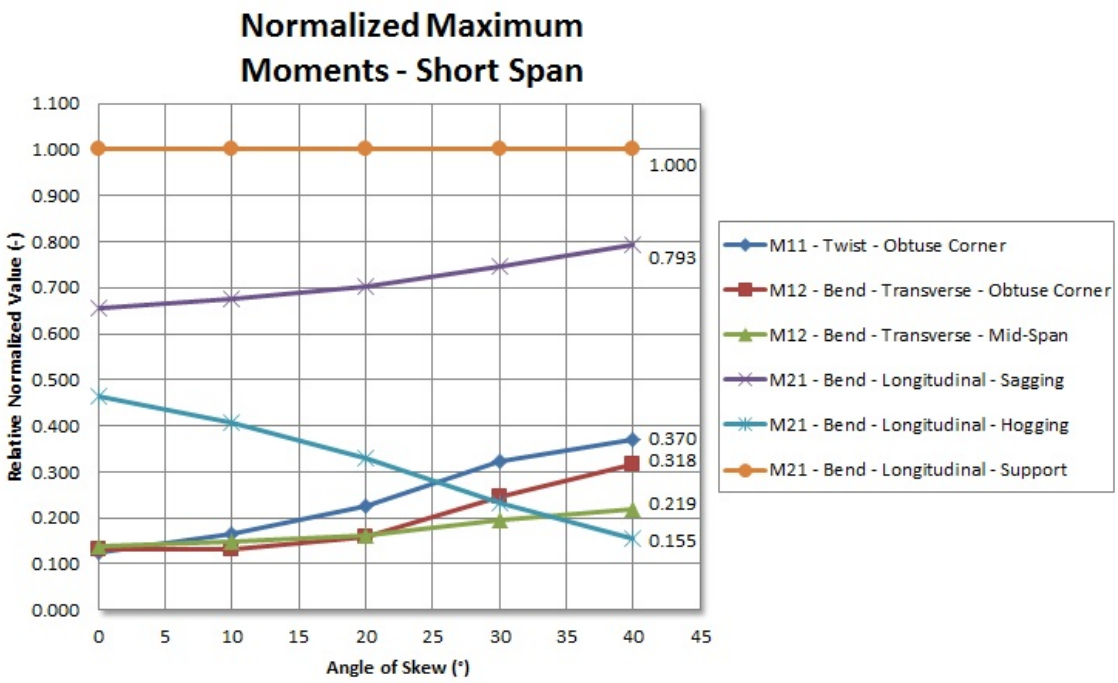

Figure 8.13: Carriageway $10\,m \times (8\,m + 15\,m + 8\,m)$: Normalized maximum moments for the first short span

Long Span: The normalized moment values are shown in Table 8.19 for the centre *long span*.

	M_{11} Twisting Moment	M_{12} Bending Moment - Transverse		M_{21} Bending Moment - Longitudinal		
Angle of Skew (°)	Obtuse Corner	Obtuse Corner	Mid-Span (Center)	Sagging (Edge)	Hogging (Edge)	Support (Edge)
0	0.179	0.096	0.186	1.000	0.115	0.901
10	0.270	0.149	0.202	1.000	0.113	0.944
20	0.375	0.216	0.238	1.000	0.107	0.979
30	0.484	0.367	0.278	0.936	0.090	1.000
40	0.516	0.487	0.354	1.000	0.086	0.952

Table 8.19: Carriageway $10\,m \times (8\,m + 15\,m + 8\,m)$: Normalized maximum moments for the centre long span

The following can be observed from Table 8.19 regarding the normalized maximum moments for the centre long span of the particular carriageway:

- The dominant moment resultants for the centre long span of the particular carriageway varies between the sagging longitudinal bending moment at mid-span and the longitudinal bending moment at the second interior support, at the edge of the carriageway, for all the angles of skew.

- The twisting and transverse bending moment resultants are not dominant for the centre long span of the particular carriageway, although they increase relative to the dominant moment resultants as the angle of skew increases. The largest secondary moment resultant is the twisting moment in the obtuse corner of the centre span, with a relative value of 51.6 %. The twisting moment in the obtuse corner is also the largest secondary moment for the first short span of the particular carriageway.
- The hogging longitudinal bending moment decreases slightly relative to the dominant moment resultant as the angle of skew increases, with a relative value of 8.6 % at a 40° angle of skew.

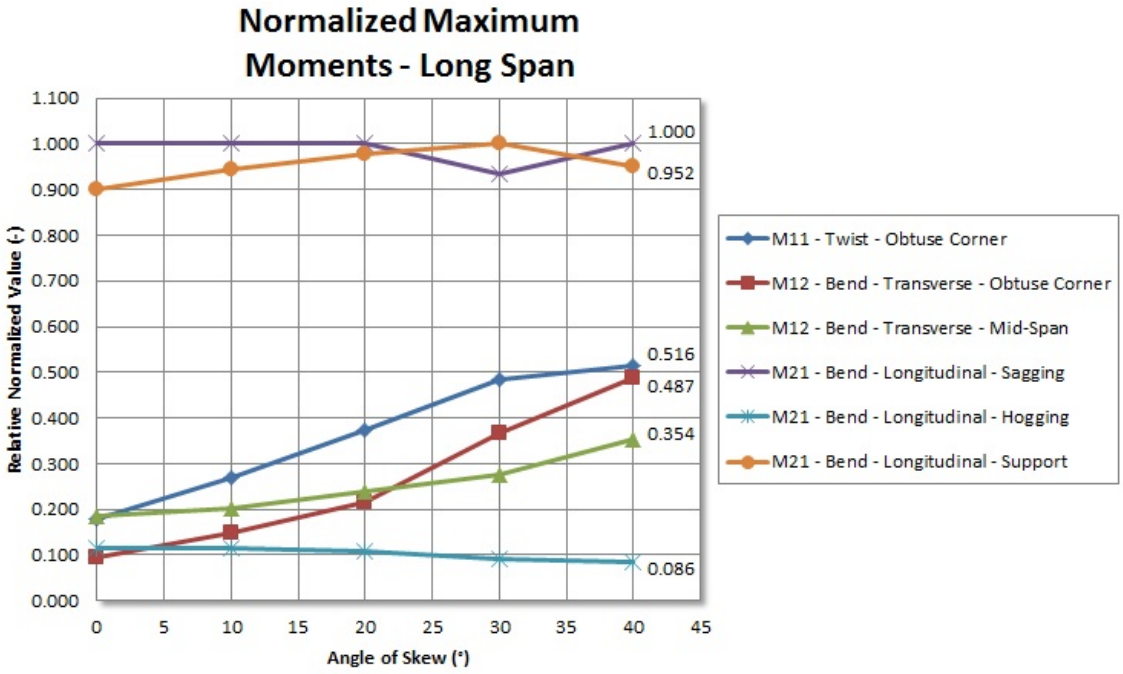

Figure 8.14: Carriageway $10\,m \times (8\,m + 15\,m + 8\,m)$: Normalized maximum moments for the centre long span

The results from Table 8.19 on the preceding page are also presented graphically in Figure 8.14.

9 Conclusions and Recommendations

The conclusions and recommendations are presented in this chapter. Certain proposals for future work are also described. As an introduction to this chapter, a quote from Hambly [7] is presented:

> "Finally the design loading for live load, temperature, creep, settlement and so on are idealizations based on statistical studies. It is unlikely that the critical design load will ever act on the structure, even though it might be exceeded. For these reasons, large errors are likely whatever method of analysis is used. It is suggested that the greater emphasis should be given to considering the physical behaviour of the structure and anticipating consequences of calculations being in error by more than 10 %, than to refining calculations in pursuit of the last 1 % of apparent accuracy."

In summary, the final concluding remarks are presented at the end of this chapter.

9.1 Conclusions

The aim of the study was to provide an insight into the flexural analysis of skew bridges, under the effects of normal traffic loading. Critical normal traffic loading patterns were presented and compared to the standard NA loading patterns for specific moment resultants in certain regions of the carriageway. A number of carriageways were analyzed and investigated under the effects of normal traffic loading as the angle of skew increased. Single span carriageways were presented in Chapter 7 and Appendix A. The results for continuous multi-span carriageways were presented in Chapter 8 and Appendix B. Conclusions regarding the study of flexure for skew bridges, under the effects of normal traffic loading are presented in the following subsections.

9.1.1 Critical Regions

When starting with the investigation of the flexural analysis of skew bridges, it is not always clear in which region of the bridge deck each of the moment resultants should be measured. Reinforcement is designed and placed differently for each *type* of moment resultant. For example, even though the transverse bending moment may not be the overall critical moment resultant, it is still important to know where the largest transverse bending moment occurs, in order to provide appropriate reinforcement. The critical regions and the corresponding moment resultants were discussed in Chapter 4 and they are summarized, in conclusion in Table 9.1. The corresponding critical region in which each of the moment resultants should be measured is indicated with a tick-mark.

	Moment Resultant		
	M_{11}	M_{12}	M_{21}
Critical Region	**Twisting Moment**	**Transverse Bending Moment**	**Longitudinal Bending Moment**
Obtuse Corner	✓	✓	✓
Mid-span Center		✓	
Mid-span Edge			✓

Table 9.1: Critical regions and corresponding moment resultants

The critical regions and corresponding moment resultants in Table 9.1 also apply to continuous multi-span carriageways. For continuous multi-span carriageways, the moment resultants should

be measured in the critical regions for each of the spans of the carriageway. Furthermore, the longitudinal bending moment should also be measured at the internal supports, at the edge of the carriageway, not just at mid-span.

9.1.2 Critical Normal Traffic Loading

The South African specification of TMH7 for bridge loading does not specify application patterns for normal traffic loading. The intensity of normal traffic loading is specified and it should be applied to yield the most adverse effect in a specific region for a selected mode of failure.

Critical NA Loading Area	Description
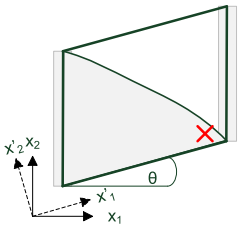	Twisting moment in the bottom-right obtuse corner.
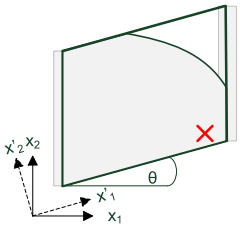	Transverse bending moment in the bottom-right obtuse corner.
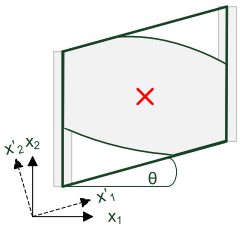	Transverse bending moment at mid-span, at the centre of the carriageway.
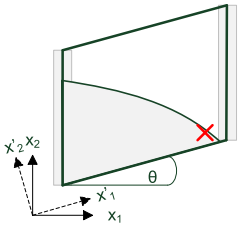	Longitudinal bending moment in the bottom-right obtuse corner.
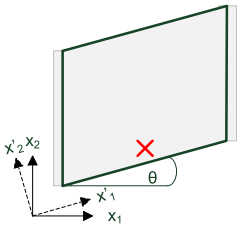	Longitudinal bending moment at mid-span, at the bottom-edge of the carriageway.

Table 9.2: Critical NA loading areas

It was shown that for the carriageways presented in this study, the critical NA loading patterns are not always obvious as the angle of skew increases, especially for the twisting and transverse bending moments. It can be difficult to determine which loadable parts of the notional lanes should be loaded and which parts provide a relieving effect, that should not be loaded. Another difficulty, once the parts that should be loaded have been identified, is the determination of the position where the highest intensity loading should be placed.

Certain guidelines, regarding the area that should be loaded to provide a critical effect in a specific region, can however be provided. These areas are summarized in Table 9.2 on the preceding page. The shaded area represents the area that should be loaded to provide a critical effect in the region marked with an "x". Although these guidelines do not apply in all cases, they represent a starting point for finding the appropriate area to load for critical flexural effects in a specific region. In general, the areas that should be loaded to provide the critical moment resultants for type NA loading, also apply to continuous multi-span carriageways in a *specific* span. For continuous multi-span carriageways, the areas indicated in Table 9.2 should be considered in each of the spans of the carriageway. However, the loading arrangement on the adjacent and alternate spans for continuous carriageways do not always follow a clear pattern as the angle of skew increases.

Even though certain areas that should be loaded can been identified, it can be difficult to predict the position where the highest intensity loading should be placed for each of the moment resultants in the various critical regions, without the aid of specialist software.

9.1.3 Standard Patterns and Critical Patterns

A comparison between the so-called standard NA loading patterns and the critical NA loading patterns was performed for each of the moment resultants in the corresponding critical regions, for a number of carriageways considered in this study. The results from the standard patterns were compared to the results from the critical patterns as the angle of skew increased.

For most of the cases, the standard NA loading patterns did not represent a good approximation for the critical moment resultants in the corresponding critical regions. Large errors occurred between the values produced by the standard patterns and the values produced by the critical patterns. The only moment resultant for which the envelope of the standard NA loading patterns produced a good approximation is the longitudinal bending moment at the edge of the carriageway.

It can be concluded that the standard NA loading patterns can only be used as a preliminary approximation for the critical longitudinal bending moment at the edge of the carriageway. It most cases, the standard NA loading patterns will not provide a good approximation for the critical moment resultants in the various critical regions, especially for the twisting and transverse bending moments as the angle of skew increases.

9.1.4 Flexural Bridge Deck Behaviour

A number of numerical experiments were performed for typical single span and multi-span continuous carriageways. Each of the moment resultants were measured and documented *relative* to each other in the various critical regions as the angle of skew increased. For all of the cases considered in this study, the longitudinal bending moment at the edge of the carriageway remained the dominant moment resultant relative to the other moment resultants, in each of the critical regions. For

example, the carriageway considered in Appendix A, where the twisting moment in the obtuse corner reached a relative value of 76 % of the value of the dominant longitudinal bending moment.

In the finite element modeling of the bridge structure, the supports of the bridge deck were represented by rigid supports. For this reason, the concentration of secondary moments in the obtuse corner may have been exaggerated, since non-rigid spring-type supports can be used to reduce these effects in practice. However, the use of rigid supports, even though the secondary effects may have been exaggerated, provides insight into the bridge deck behaviour as the angle of skew increases. When the carriageway is not skew, the twisting and transverse bending moment resultants are not large relative to the primary longitudinal bending moment. However, as the angle of skew of the carriageway increases, the twisting and transverse bending moment resultants increase (not necessarily in each of the critical regions) *relative* to the dominant longitudinal bending moment. Even though the design is not necessarily done directly for the secondary moment resultants, e.g. the incorporation of the twisting moment in the Wood and Armer design values, this means that the secondary moment resultants reach large relative values. Consequently, the secondary moment resultants deserves a larger design consideration as the angle of skew increases.

9.1.5 Developed Software

Through the course of this study a large number of analyses were performed and a large number of load-cases compared to each other. The development of effective, specialized software was a prerequisite for the conduction of this study. The software was developed specifically for the South African specification of TMH7, for the generation of extreme NA loading patterns for a selected mode of failure in any selected region of the carriageway. The procedure used does not simply use an influence surface approach to generate extreme NA loading patterns, but rather small increments of type NA loading.

Further complications that arise from partial loading of parts of influence lines and the corresponding correction factor (k-factor) specified by TMH7 was described in Chapter 5. Where the k-factor represents a correction factor used to compensate for the effects of partial loading of parts of influence lines. The value of the k-factor depends on the tails of the influence lines and is difficult to implement in software. The procedure adopted in this study, with the incremental generation of extreme patterns, effectively eliminates the need for the k-factor.

The software techniques implemented in this study provide technically correct loading application procedures, by making use of consistent line and point loads. Although the software can be used to generate extreme NA loading patterns for a selected mode of failure in any selected region of the carriageway, the software remains a tool to aid the designer. The responsibility rests with the engineer to understand when an extreme pattern is also the critical pattern, to understand the bridge deck behaviour and critically interpret the results.

9.2 Future Work

In order to keep the study detailed and focused, the scope of the study was limited to critical normal traffic loading for flexure of bridges. Possible proposals for future work are presented in the paragraphs below:

Additional Modes of Failure: Critical normal traffic loading for flexure of bridges was presented and discussed in this study. Similar studies can be conducted for critical reaction patterns and critical shear patterns. The current DKT (Discrete Kirchoff Triangle) plate bending element used in this study behaves well in bending. The DKT plate element does not behave well in shear, since the shear stresses cannot be derived from the shear strains, due to the Kirchoff hypothesis. Instead the shear stresses are derived from the equilibrium equations. A Mindlin-type plate element, suitable for thick plates, can be implemented and used for critical reaction and critical shear analysis. Furthermore, decks with void formers can be analyzed with anisotropic plate finite elements, a topic which falls outside the scope of this study.

Additional types of Traffic Loading: A proposal for future work includes the investigation of critical loading for additional types of traffic. Normal (NA) traffic loading was investigated in this study. Similar studies can be conducted for Abnormal (NB) and Super (NC) traffic loads. The current software framework can easily be extended to accommodate type NB and type NC loadings.

Eurocode Considerations: The current South African specification of TMH7 was written in 1981 and has last been revised in 1988. In contrast, the Eurocode experienced more recent upgrades since 2002. A comparative calibration analysis can be performed between the Eurocode and TMH7, similar to the comparative analysis performed in this study, between the standard patterns and the extreme patterns.

Straddling Lanes: Normal traffic loading patterns were investigated in this study, without the incorporation of straddling lanes. The case of straddling lanes will in some cases provide the critical longitudinal bending moment at mid-span, at the edge of the carriageway. More adverse effects will be obtained for the longitudinal bending moment, since the loading that is normally placed on two or three notional lanes, may now be confined towards the edge of the carriageway in the transverse direction. Generation of extreme NA loading patterns should be extended to include a case where the placement of extreme loads are confined to the geometry of the straddling lanes.

Grillage Analysis Extension: The approximate representation of bridge decks by a grillage of interconnected beams is a convenient way of determining the general behaviour of the bridge deck under loads [4]. The method of grillage analysis involves the idealization of the bridge deck through its representation as a plane grillage of discrete interconnected beams. A large number of bridge decks are analyzed and designed according to a grillage approximation. The current study can be extended to incorporate a grillage analysis. The number of interconnected beams in the longitudinal and transverse directions can be specified and incorporated in the software. Loads applied to the bridge deck can be transferred to the grillage of interconnected beams. Results from the grillage analysis can be compared to the results acquired in this study for slab decks.

9.3 Concluding Remarks

It can be concluded that for the typical carriageways presented in this study, with primary bending in the longitudinal direction, the standard NA loading patterns can be used as a preliminary approximation for the critical longitudinal bending moment at mid-span, at the edge of the carriageway.

For wide short-span carriageways, where the width exceeds the length, this generalization may not apply, especially as the angle of skew increases. To obtain the critical transverse bending and twisting moment resultants more effort, rigorous distribution analysis and specialist software are required. In most cases partial loading of notional lanes will have to be applied, in order to avoid loading areas that provide a relieving effect and results in less adverse values. Without the aid of specialist software, finding the critical loading patterns for all the moment resultants in each of the critical regions will be a difficult task, especially for continuous multi-span carriageways.

References

[1] D. Bell. UML basics: The class diagram. An introduction to structure diagrams in UML 2. `http://www.ibm.com/developerworks/rational/library/content/RationalEdge/sep04/bell/`, 2004. Accessed: February 2012.

[2] G. Bracha. Generics in the Java Programming Language. `http://www8.cs.umu.se/kurser/tdbb24/HT05/jem/download/generics-tutorial.pdf`, 2004. Accessed: February 2012.

[3] P. Coad, M. Mayfield, and J. Kern. *Java Design: Building Better Apps and Applets*. Prentice Hall PTR, New Jersey, 1998. Second Edition.

[4] A.R. Cusens and R.P. Pama. *Bridge Deck Analysis*. John Wiley & Sons, Ltd., Great Britain, 1975. Pages 201–203.

[5] B. Firmenich. *System Design of an Open Engineering Platform*. Bauhaus-Universität Weimar, Fakultät Bauingenieurwesen, Weimar, 2006. English translation by Gert van Rooyen.

[6] J. Gosling, B. Joy, G. Steele, G. Bracha, and A. Buckley. The Java Language Specification. `http://docs.oracle.com/javase/specs/#237601`, 2001. Accessed: October 2012.

[7] E.C. Hambly. *Bridge Deck Behaviour*. Chapman and Hall, London, 1976.

[8] J. Koehler and J. Vanhatalo. Process anti-patterns: How to avoid the common traps of business process modeling. `http://www.ibm.com/developerworks/websphere/techjournal/0702_koehler/0702_koehler.html`, 2007. Accessed: February 2012.

[9] Y.T. Lee. Information modeling: From design to implementation. *National Institute of Standards and Technology*, 1999. Gaithersburg, MD, USA.

[10] J. Li. Reinforced Plate Design for M_{xy} Twisting Moment. *Solutions Research Centre*, 2002. Hong Kong.

[11] A.D. Malan. Die Implementering en Verifikasie van 'n Plat, Driehoekige Dopelement in 'n Java-gebaseerde Eindige Element Raamwerk, 2010. University of Stellenbosch, Stellenbosch, South Africa. Final Year Project: F-05.

[12] F.A. Markram. Extracting Appropriate Design Information from a Finite Element Analysis for a Large Number of Load Cases, 2011. University of Stellenbosch, Stellenbosch, South Africa. Final Year Project: F-06.

[13] K. Mason. Finite Element Pre-Processing for Plane Structures in 3D, 2010. University of Stellenbosch, Stellenbosch, South Africa. Final Year Project: F-02.

[14] Committee of State Road Authorities. *Code of Practice for the Design of Highway Bridges and Culverts in South Africa*. Department of Transport, Pretoria, 1981. Revised 1988.

[15] P.J. Pahl and R. Damrath. *Mathematical Foundations of Computational Engineering*. Springer, Berlin Heidelberg, 2001.

[16] A. Pucher. *Einflussfelder Elastischer Platten: Influence Surfaces of Elastic Plates*. Springer-Verlag, 1964. http://books.google.co.za/books?id=eSeJQgAACAAJ. Englische Übersetzung durch Heinz Juhl.

[17] G.C. van Rooyen, G.P.A.G. van Zijl, and J.A.v.B. Strasheim. *Finite Element Method*. Institute of Structural Engineering, University of Stellenbosch, Stellenbosch, South Africa, 2008. Class Notes: Theory of Structures 354.

[18] Wikipedia. Median. http://en.wikipedia.org/w/index.php?title=Median&oldid=514203841, 2012. Accessed: September 2012.

[19] R.H. Wood. The Reinforcement of Slabs in accordance with a Pre-determined Field of Moments. *Concrete*, Volume 2, 1968.

A Additional Single Span Results

A typical simply supported single span carriageway with the following geometry will be considered:

- span length of $20\,m$
- effective width of $20\,m$
- angle of skew from 0° to 40°
- angle of skew increases in increments of 10°

Critical NA loading patterns are presented for the particular carriageway in this appendix. The critical NA loading patterns are generated for each of the moment resultants in each of the critical regions.

A.1 Twisting Moment

The twisting moment is measured in the obtuse corner of the carriageway. The critical NA loading patterns and resulting contour plots are illustrated in Table A.1 for the twisting moment in the obtuse corner.

Angle of Skew (°)	Critical NA Loading Pattern	Resulting Contour Plot (Nm)
0°	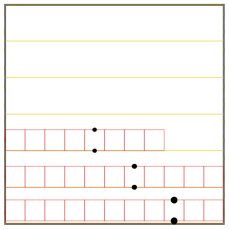 File: 20x20x00.load NA Load Pattern Number: 11	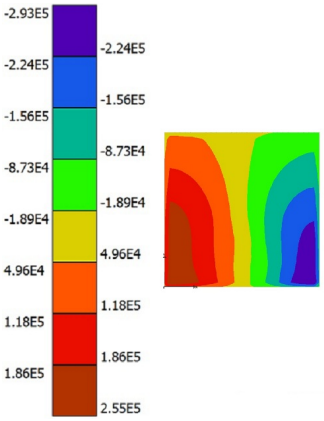
20°	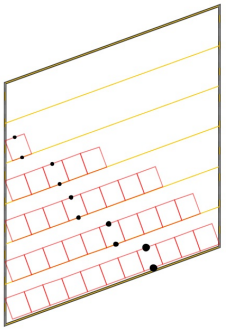 File: 20x20x20.load NA Load Pattern Number: 11	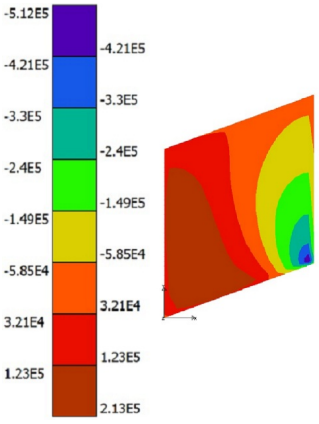

Table A.1: Carriageway $20\,m \times 20\,m$: Critical NA loading patterns and resulting contour plots for the twisting moment in the obtuse corner (Continued on the next page)

Angle of Skew (°)	Critical NA Loading Pattern	Resulting Contour Plot (Nm)
40°	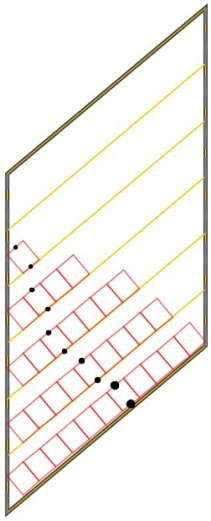 File: 20x20x40.load NA Load Pattern Number: 11	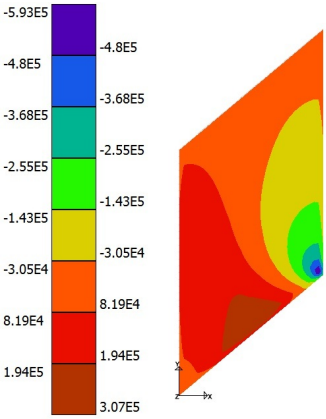

Table A.2: Carriageway $20\,m \times 20\,m$: Critical NA loading patterns and resulting contour plots for the twisting moment in the obtuse corner (Continued from the previous page)

The percentage error of the standard NA loading patterns relative to the critical NA loading patterns for the twisting moment in the obtuse corner is presented in Figure A.1. The errors are measured as the angle of skew increases from 0° to 40° in increments of 10°. The results include the actual value at the monitored finite element node and the value of the median in the region of the monitored finite element node.

M_{11}
Obtuse Corner

	Error (%)	
Angle of Skew (°)	Actual	Median
0	-17.14%	-17.90%
10	-12.74%	-14.22%
20	-10.72%	-12.69%
30	-10.27%	-13.34%
40	-9.95%	-13.78%

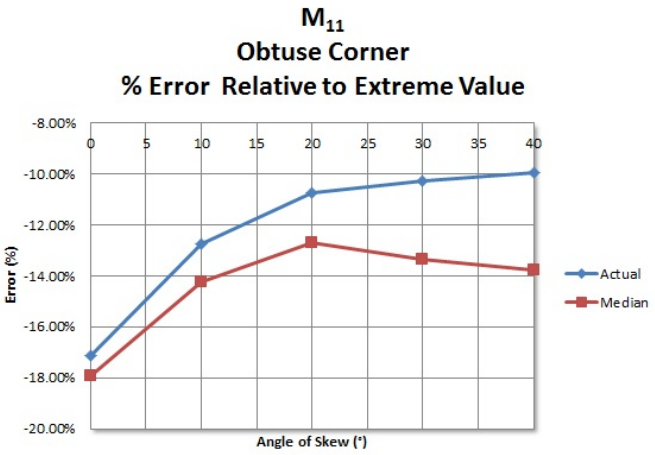

Figure A.1: Carriageway $20\,m \times 20\,m$: Relative error for the twisting moment in the obtuse corner

A.2 Transverse Bending Moment

The transverse bending moment is measured in the obtuse corner and at mid-span of the carriageway.

A.2.1 Obtuse Corner

Angle of Skew (°)	Critical NA Loading Pattern	Resulting Contour Plot (Nm)
0°	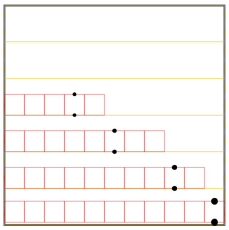 File: 20x20x00.load NA Load Pattern Number: 14	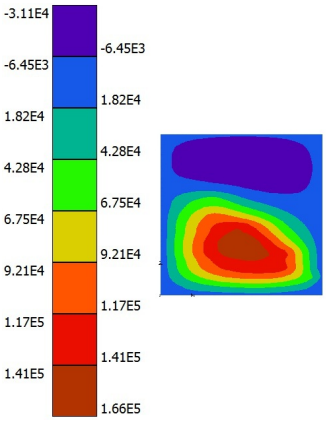
20°	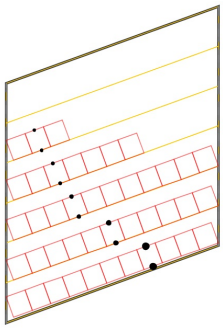 File: 20x20x20.load NA Load Pattern Number: 13	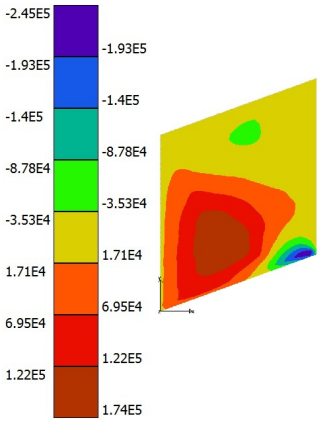
40°	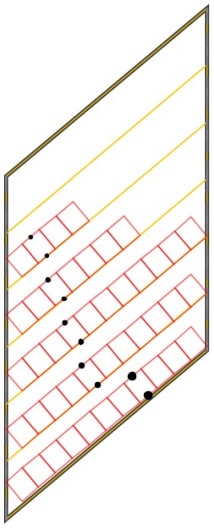 File: 20x20x40.load NA Load Pattern Number: 13	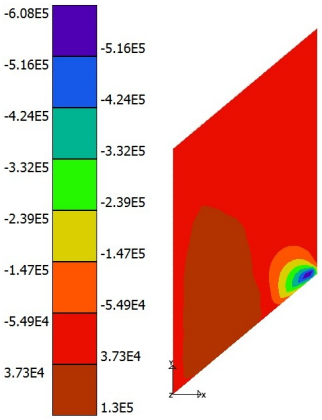

Table A.3: Carriageway $20\,m \times 20\,m$: Critical NA loading patterns and resulting contour plots for the transverse bending moment in the obtuse corner

The critical NA loading patterns and resulting contour plots are illustrated in Table A.3 on page A-3 for the transverse bending moment in the obtuse corner. The percentage error of the standard NA loading patterns relative to the critical NA loading patterns for the transverse bending moment in the obtuse corner is presented in Figure A.2. The errors are measured as the angle of skew increases from 0° to 40° in increments of 10°. The results include the actual value at the monitored finite element node and the value of the median in the region of the monitored finite element node.

M_{12}
Obtuse Corner

Angle of Skew (°)	Error (%) Actual	Median
0	-42.54%	-39.58%
10	-7.54%	-5.10%
20	-6.05%	-4.83%
30	-5.52%	-4.67%
40	-4.43%	-4.54%

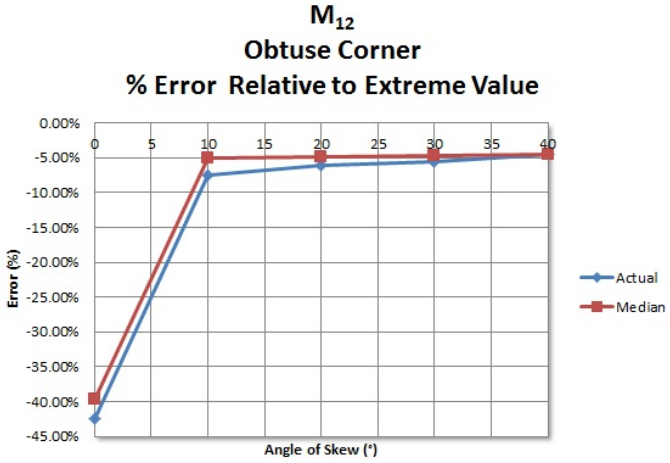

Figure A.2: Carriageway $20\,m \times 20\,m$: Relative error for the transverse bending moment in the obtuse corner

A.2.2 Mid-span Centre

The critical NA loading patterns and resulting contour plots are illustrated in Table A.4 for the transverse bending moment at mid-span centre.

Angle of Skew (°)	Critical NA Loading Pattern	Resulting Contour Plot (Nm)
0°	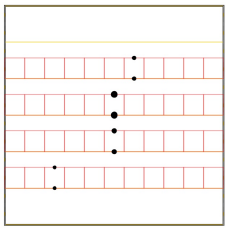 File: 20x20x00.load NA Load Pattern Number: 16	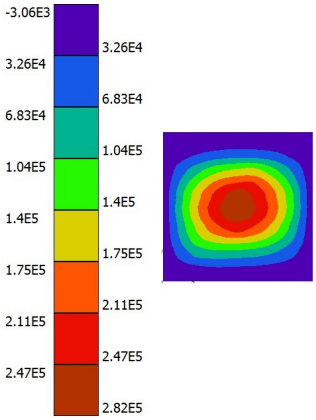

Table A.4: Carriageway $20\,m \times 20\,m$: Critical NA loading patterns and resulting contour plots for the transverse bending moment at mid-span centre (Continued on the next page)

Angle of Skew (°)	Critical NA Loading Pattern	Resulting Contour Plot (Nm)
20°	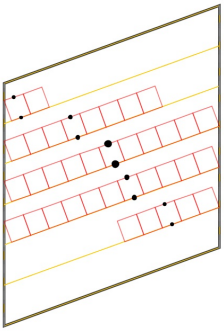 File: 20x20x20.load NA Load Pattern Number: 16	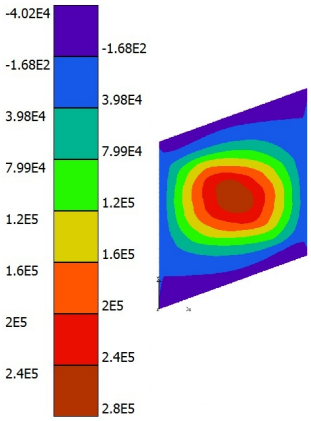
40°	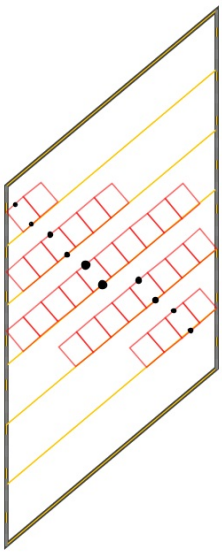 File: 20x20x40.load NA Load Pattern Number: 16	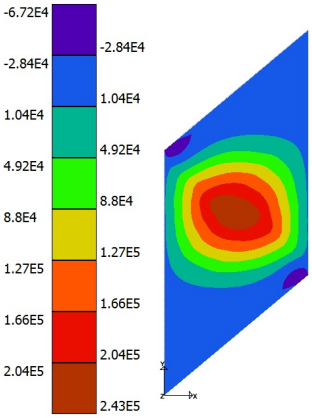

Table A.5: Carriageway $20\,m \times 20\,m$: Critical NA loading patterns and resulting contour plots for the transverse bending moment at mid-span centre (Continued from the previous page)

The percentage error of the standard NA loading patterns relative to the critical NA loading patterns are shown in Figure A.3 on page A-6 as the angle of skew increases from 0° to 40° in increments of 10°. The results include the actual value at the monitored finite element node, the value of the median in the region of the monitored finite element node as well as the Wood and Armer values for the bottom reinforcement in the transverse direction. The Wood and Armer values have been acquired with the assumption that the reinforcement will be placed parallel to the edges of the carriageway in both directions.

A.3 Longitudinal Bending Moment

The longitudinal bending moment is measured in the obtuse corner and at mid-span of the edge of the carriageway.

M_{12}
Mid-Span

	Error (%)		
Angle of Skew (°)	Actual	Median	W & A
0	-66.09%	-65.63%	-64.84%
10	-68.40%	-67.84%	-66.91%
20	-73.75%	-73.49%	-70.44%
30	-81.59%	-82.05%	-77.99%
40	-88.58%	-88.89%	-86.40%

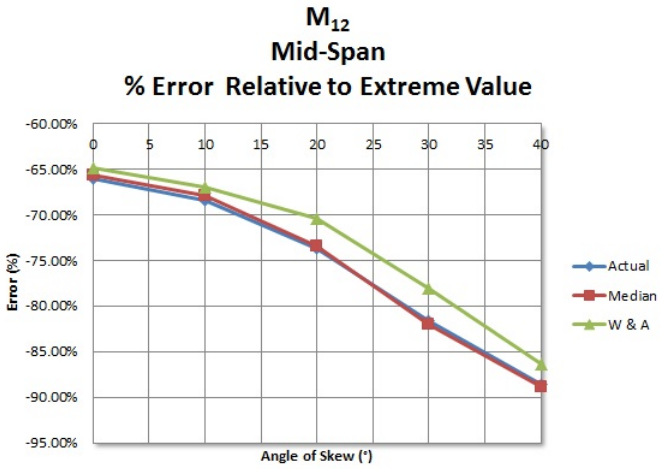

Figure A.3: Carriageway $20\,m \times 20\,m$: Relative error for the transverse bending moment at mid-span centre

A.3.1 Obtuse Corner

Angle of Skew (°)	Critical NA Loading Pattern	Resulting Contour Plot (Nm)
0°	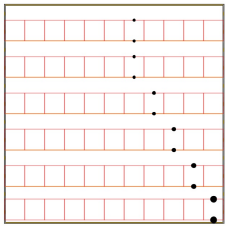 File: 20x20x00.load NA Load Pattern Number: 17	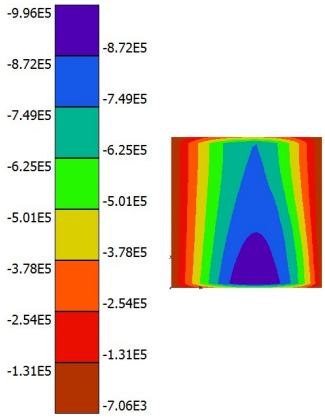
20°	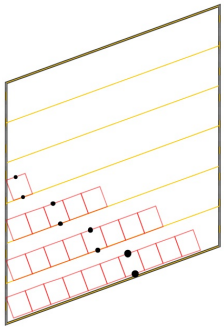 File: 20x20x20.load NA Load Pattern Number: 18	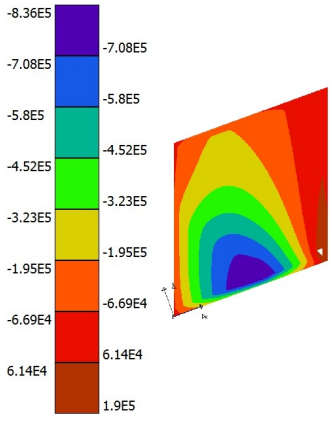

Table A.6: Carriageway $20\,m \times 20\,m$: Critical NA loading patterns and resulting contour plots for the longitudinal bending moment in the obtuse corner (Continued on the next page)

Angle of Skew (°)	Critical NA Loading Pattern	Resulting Contour Plot (Nm)
40°	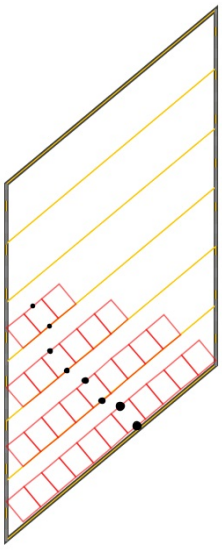	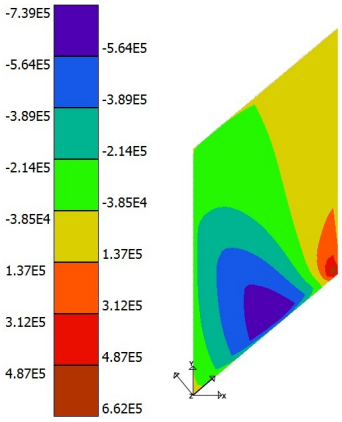

File: 20x20x40.load
NA Load Pattern Number: 22

Table A.7: Carriageway $20\,m \times 20\,m$: Critical NA loading patterns and resulting contour plots for the longitudinal bending moment in the obtuse corner (Continued from the previous page)

The critical NA loading patterns and resulting contour plots are illustrated in Table A.6 on page A-6 for the longitudinal bending moment in the obtuse corner. The percentage error of the standard NA loading patterns relative to the critical NA loading patterns for the longitudinal bending moment in the obtuse corner is presented in Figure A.4. The errors are measured as the angle of skew increases from 0° to 40° in increments of 10°. The results include the actual value at the monitored finite element node and the value of the median in the region of the monitored finite element node.

M_{21}
Obtuse Corner

	Error (%)	
Angle of Skew (°)	Actual	Median
0	-22.81%	-23.31%
10	-44.95%	-34.73%
20	-48.40%	-25.40%
30	-21.12%	-35.43%
40	-13.24%	-21.28%

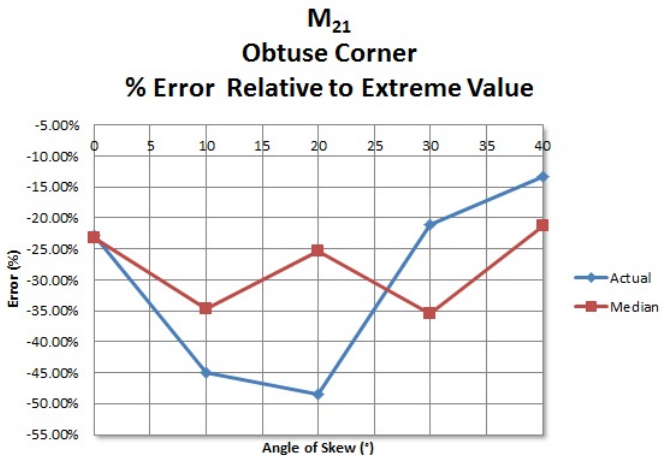

Figure A.4: Carriageway $20\,m \times 20\,m$: Relative error for the longitudinal bending moment in the obtuse corner

A.3.2 Mid-span Edge

Angle of Skew (°)	Critical NA Loading Pattern	Resulting Contour Plot (Nm)
0°	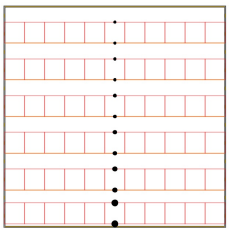 File: 20x20x00.load NA Load Pattern Number: 19	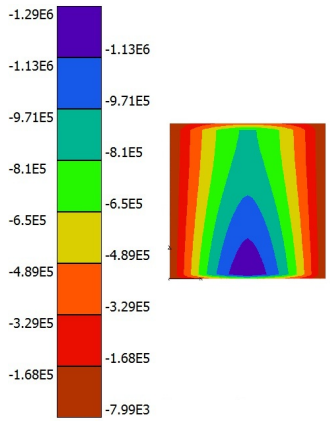
20°	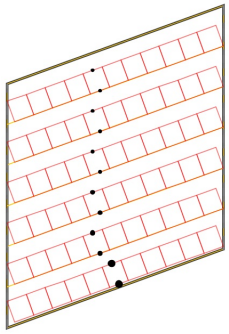 File: 20x20x20.load NA Load Pattern Number: 19	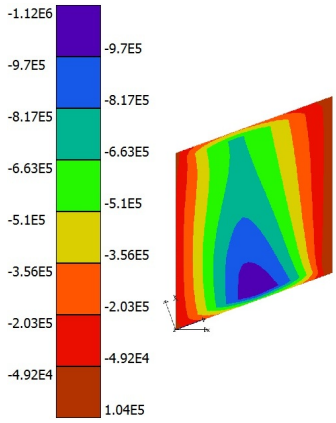
40°	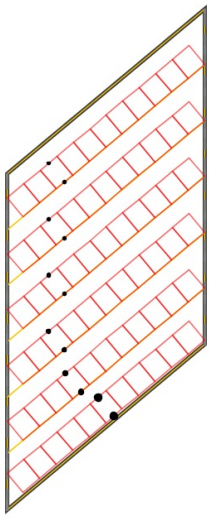 File: 20x20x40.load NA Load Pattern Number: 19	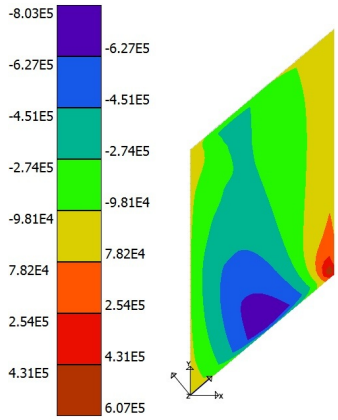

Table A.8: Carriageway $20\,m \times 20\,m$: Critical NA loading patterns and resulting contour plots for the longitudinal bending moment at mid-span edge

The critical NA loading patterns and resulting contour plots are illustrated in Table A.8 on page A-8 for the longitudinal bending moment at mid-span, at the edge of the carriageway. The percentage error of the standard NA loading patterns relative to the critical NA loading patterns for the longitudinal bending moment at mid-span, at the edge of the carriageway, is presented in Figure A.5. The errors are measured as the angle of skew increases from 0° to 40° in increments of 10°. The results include the actual value at the monitored finite element node, the value of the median in the region of the monitored finite element node as well as the Wood and Armer values for the bottom reinforcement in the longitudinal direction. The Wood and Armer values have been acquired with the assumption that the reinforcement will be placed parallel to the edges of the carriageway in both directions.

M_{21}
Mid-Span
Error (%)

Angle of Skew (°)	Actual	Median	W & A
0	-5.89%	-6.01%	-5.81%
10	-5.40%	-5.58%	-5.52%
20	-5.52%	-5.72%	-5.88%
30	-6.30%	-6.81%	-6.30%
40	-6.12%	-6.82%	-6.69%

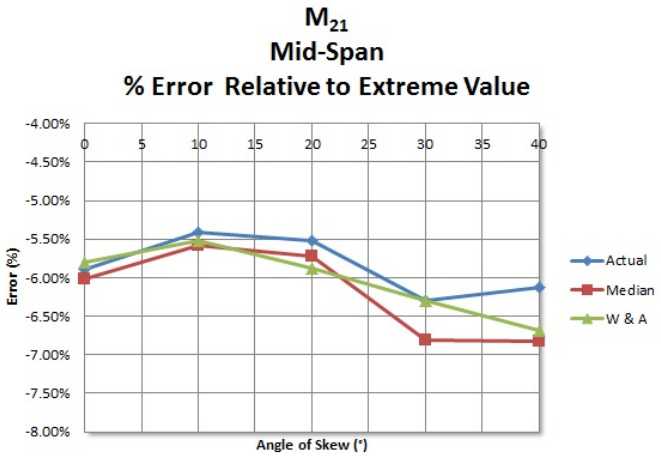

Figure A.5: Carriageway $20\,m \times 20\,m$: Relative error for the longitudinal bending moment at mid-span edge

A.4 Normalized Maximum Moments

A carriageway with a span length of $20\,m$ and an effective width of $20\,m$ was investigated in this appendix as the angle of skew increases. The critical NA loading patterns were presented for the different moment resultants in each of the critical regions. The flexural behaviour of the specific carriageway under the effects of normal traffic loading will be presented in this section as the angle of skew increases.

	M_{11} Twisting Moment	M_{12} Bending Moment - Transverse		M_{21} Bending Moment - Longitudinal	
Angle of Skew (°)	Obtuse Corner	Obtuse Corner	Mid-Span (Center)	Obtuse Corner	Mid-Span (Edge)
0	0.227	0.008	0.219	0.153	1.000
10	0.322	0.064	0.228	0.155	1.000
20	0.457	0.190	0.250	0.170	1.000
30	0.598	0.391	0.274	0.446	1.000
40	0.760	0.667	0.306	0.849	1.000

Table A.9: Carriageway $20\,m \times 20\,m$: Normalized maximum moments

The different moment resultant values are normalized and compared *relative* to the largest moment resultant in each of the critical regions. The normalized moment values are shown in Table A.9 on page A-9.

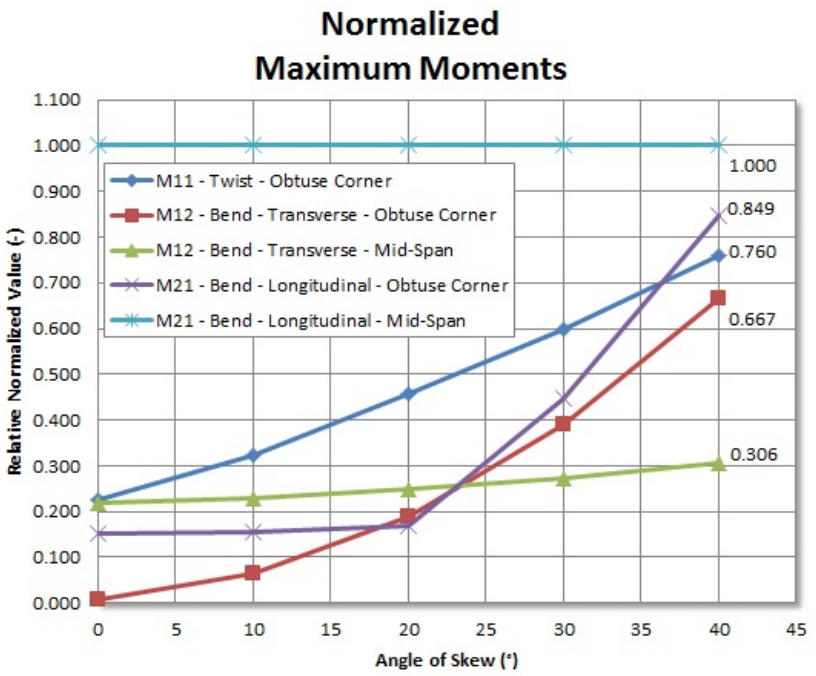

Figure A.6: Carriageway $20\,m \times 20\,m$: Normalized maximum moments

It can be seen from Table A.9 on page A-9 that the longitudinal bending moment at mid-span, at the edge of the carriageway, remains the dominant moment resultant for all the angles of skew. The results from Table A.9 are also presented graphically in Figure A.6.

B Additional Continuous Results

A typical continuous multi-span carriageway with the following geometry will be considered:

- two short spans with lengths of $8\,m$
- two long spans with lengths of $15\,m$
- effective width of $10\,m$
- angle of skew from 0° to 40°
- angle of skew increases in increments of 10°

The two short spans are on either end of the carriageway and the two long spans represent the two centre spans. Critical NA loading patterns are presented for the particular carriageway in this appendix. The critical NA loading patterns are generated for each of the moment resultants in each of the critical regions. The results are presented for both a short span and a long span of the particular carriageway.

Angle of Skew ($^{\circ}$)	Critical NA Loading Pattern	Resulting Contour Plot (Nm)
0°	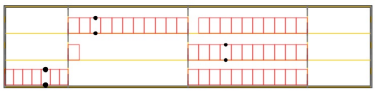 File: 10x8x15x15x8x00.load NA Load Pattern Number: 65	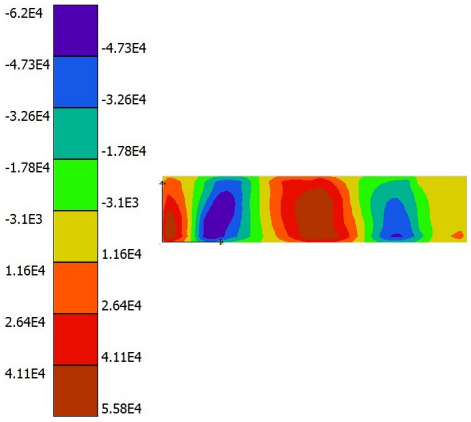
20°	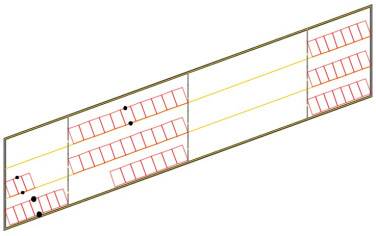 File: 10x8x15x15x8x20.load NA Load Pattern Number: 116	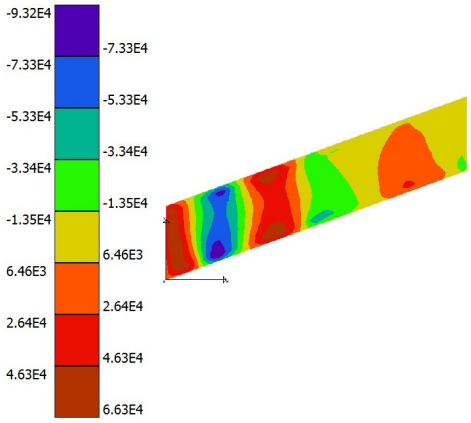

Table B.1: Carriageway $10\,m \times (8\,m + 15\,m + 15\,m + 8\,m)$: Critical NA loading patterns and resulting contour plots for the twisting moment in the obtuse corner for the first short span (Continued on the next page)

Angle of Skew (°)	Critical NA Loading Pattern	Resulting Contour Plot (Nm)
40°	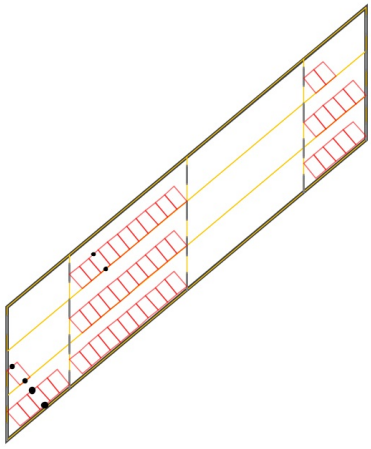 File: 10x8x15x15x8x40.load NA Load Pattern Number: 116	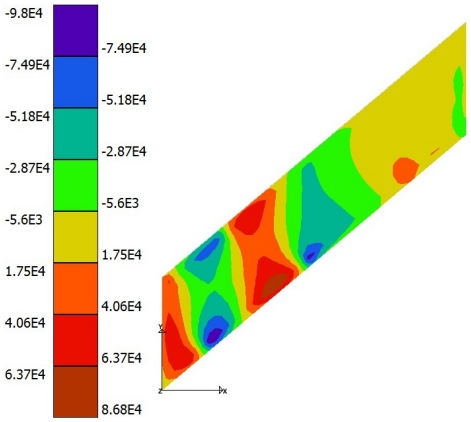

Table B.2: Carriageway $10\,m \times (8\,m + 15\,m + 15\,m + 8\,m)$: Critical NA loading patterns and resulting contour plots for the twisting moment in the obtuse corner for the first short span (Continued from the previous page)

B.1 Twisting Moment

The twisting moment is measured in the obtuse corner of each of the spans of the carriageway.

Short Span: The critical NA loading patterns and resulting contour plots are illustrated in Table B.1 on page B-1 for the twisting moment in the obtuse corner, for the first *short span* from the left.

Angle of Skew (°)	Critical NA Loading Pattern	Resulting Contour Plot (Nm)
0°	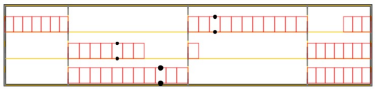 File: 10x8x15x15x8x00.load NA Load Pattern Number: 67	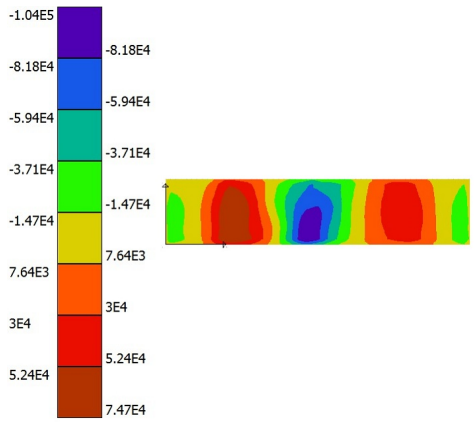

Table B.3: Carriageway $10\,m \times (8\,m + 15\,m + 15\,m + 8\,m)$: Critical NA loading patterns and resulting contour plots for the twisting moment in the obtuse corner for the first long span (Continued on the next page)

Long Span: The critical NA loading patterns and resulting contour plots are illustrated in Table B.3 on page B-2 for the twisting moment in the obtuse corner, for the first *long span* from the left.

Angle of Skew (°)	Critical NA Loading Pattern	Resulting Contour Plot (Nm)
20°	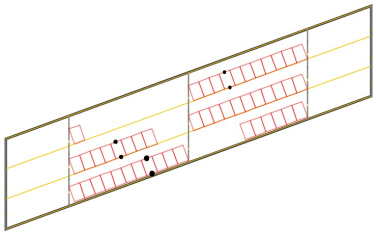 File: 10x8x15x15x8x20.load NA Load Pattern Number: 118	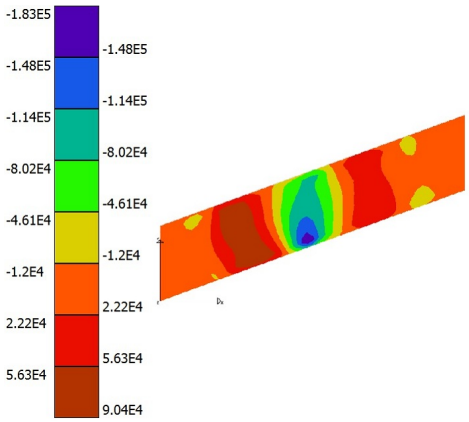
40°	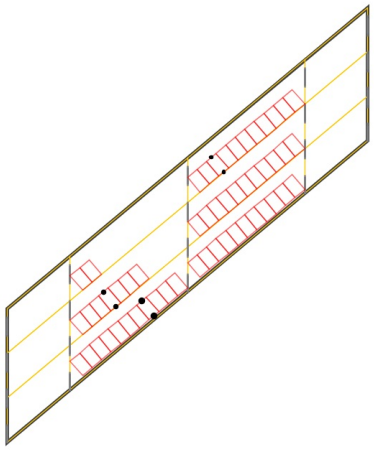 File: 10x8x15x15x8x40.load NA Load Pattern Number: 118	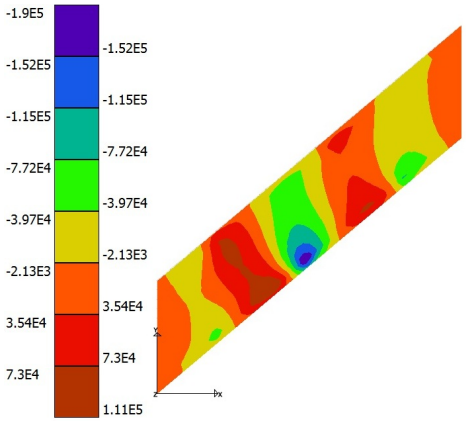

Table B.4: Carriageway $10\,m \times (8\,m + 15\,m + 15\,m + 8\,m)$: Critical NA loading patterns and resulting contour plots for the twisting moment in the obtuse corner for the first long span (Continued from the previous page)

The percentage errors of the standard NA loading patterns relative to the critical NA loading patterns for the twisting moment in the obtuse corner are presented for both the first short span and the first long span of the carriageway. The errors are measured as the angle of skew increases from 0° to 40° in increments of 10°. The results include the actual value at the monitored finite element node and the value of the median in the region of the monitored finite element node.

Short Span: The percentage error of the standard NA loading patterns relative to the critical NA loading patterns for the twisting moment in the obtuse corner, for the first *short span*, is presented in Figure B.1 on page B-4.

M_{11}
Obtuse Corner - Short Span

Angle of Skew (°)	Error (%)	
	Actual	Median
0	-33.28%	-41.26%
10	-28.16%	-34.79%
20	-21.41%	-27.08%
30	-17.21%	-21.20%
40	-19.34%	-19.63%

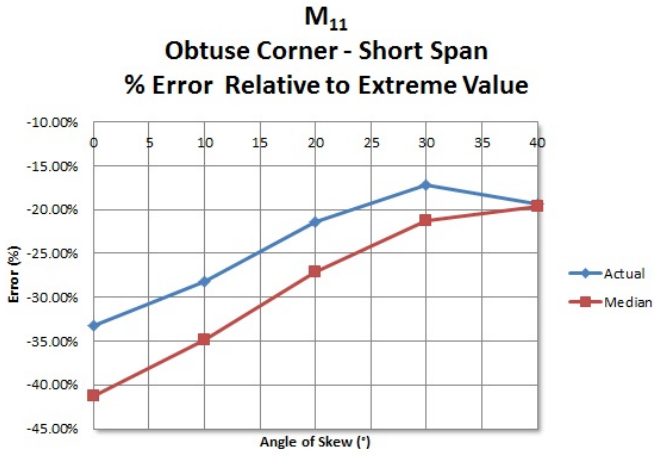

Figure B.1: Carriageway $10\,m \times (8\,m + 15\,m + 15\,m + 8\,m)$: Relative error for the twisting moment in the obtuse corner of the first short span

Long Span: The percentage error of the standard NA loading patterns relative to the critical NA loading patterns for the twisting moment in the obtuse corner, for the first *long span*, is presented in Figure B.2.

M_{11}
Obtuse Corner - Long Span

Angle of Skew (°)	Error (%)	
	Actual	Median
0	-33.04%	-35.51%
10	-24.74%	-30.65%
20	-23.17%	-27.94%
30	-19.58%	-24.09%
40	-20.67%	-26.47%

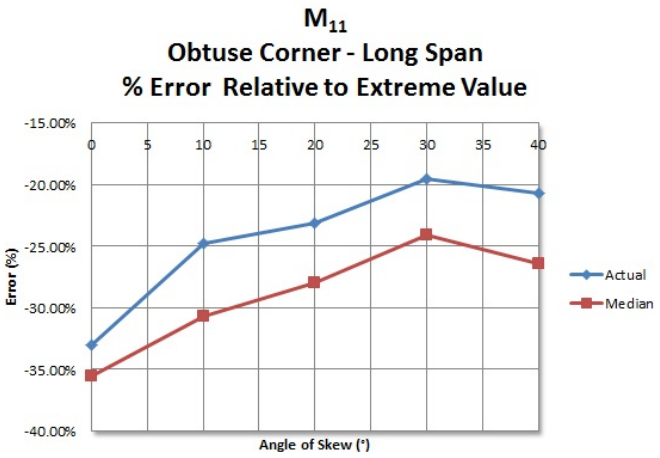

Figure B.2: Carriageway $10\,m \times (8\,m + 15\,m + 15\,m + 8\,m)$: Relative error for the twisting moment in the obtuse corner of the first long span

B.2 Transverse Bending Moment

The transverse bending moment is measured in the obtuse corner and at mid-span of the carriageway.

B.2.1 Obtuse Corner

The critical NA loading patterns and resulting contour plots are presented for the transverse bending moment in the obtuse corner, for the first short span and the first long span of the particular carriageway.

Short Span: The critical NA loading patterns and resulting contour plots are illustrated in Table B.5 for the transverse bending moment in the obtuse corner, for the first *short span* from the left.

Angle of Skew (°)	Critical NA Loading Pattern	Resulting Contour Plot (Nm)
0°	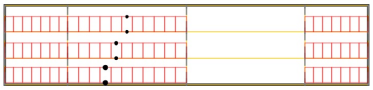 File: 10x8x15x15x8x00.load NA Load Pattern Number: 69	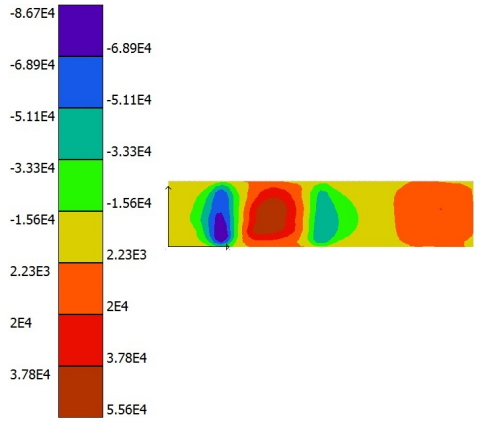
20°	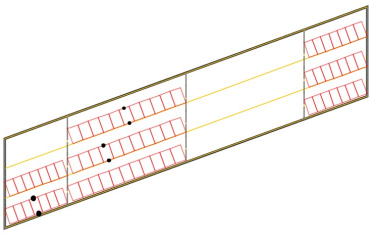 File: 10x8x15x15x8x20.load NA Load Pattern Number: 120	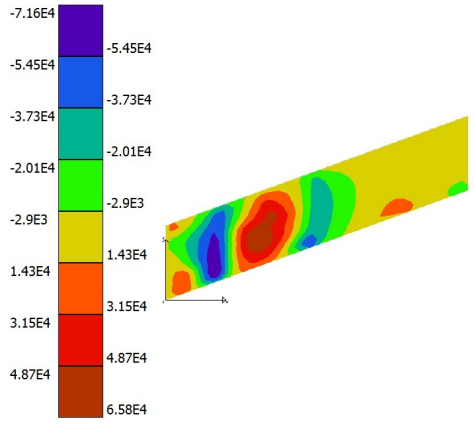
40°	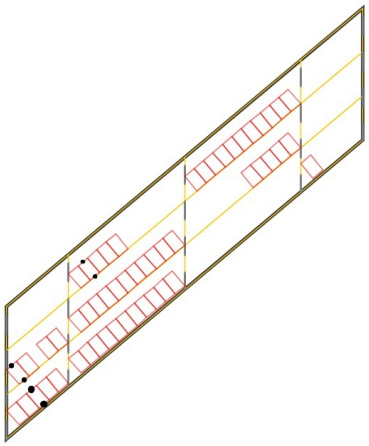 File: 10x8x15x15x8x40.load NA Load Pattern Number: 120	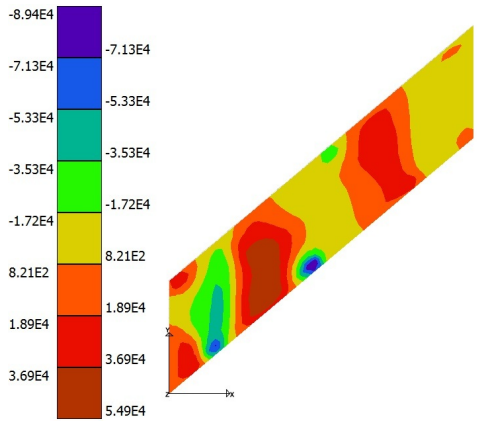

Table B.5: Carriageway $10\,m \times (8\,m + 15\,m + 15\,m + 8\,m)$: Critical NA loading patterns and resulting contour plots for the transverse bending moment in the obtuse corner for the first short span

Long Span: The critical NA loading patterns and resulting contour plots are illustrated in Table B.6 for the transverse bending moment in the obtuse corner, for the first *long span* from the left.

Angle of Skew (°)	Critical NA Loading Pattern	Resulting Contour Plot (Nm)
0°	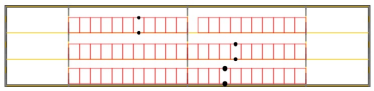 File: 10x8x15x15x8x00.load NA Load Pattern Number: 71	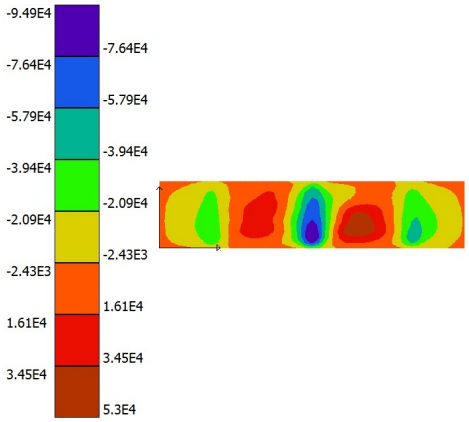
20°	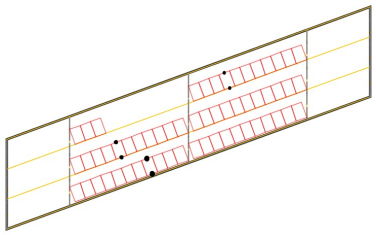 File: 10x8x15x15x8x20.load NA Load Pattern Number: 122	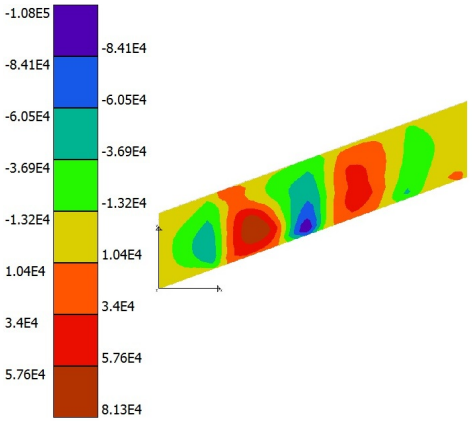
40°	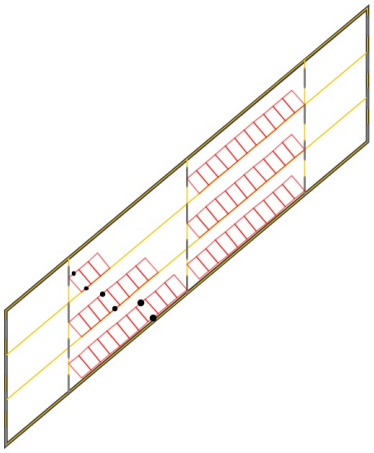 File: 10x8x15x15x8x40.load NA Load Pattern Number: 122	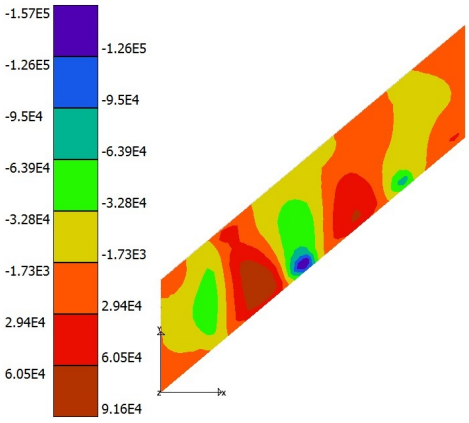

Table B.6: Carriageway $10\,m \times (8\,m + 15\,m + 15\,m + 8\,m)$: Critical NA loading patterns and resulting contour plots for the transverse bending moment in the obtuse corner for the first long span

The percentage errors of the standard NA loading patterns relative to the critical NA loading patterns for the transverse bending moment in the obtuse corner are presented for both the first short span and the first long span of the carriageway. The errors are measured as the angle of skew increases from 0° to 40° in increments of 10°. The results include the actual value at the monitored finite element node and the value of the median in the region of the monitored finite element node.

Short Span: The percentage error of the standard NA loading patterns relative to the critical NA loading patterns for the transverse bending moment in the obtuse corner, for the first *short span*, is presented in Figure B.3.

M_{12}
Obtuse Corner - Short Span

	Error (%)	
Angle of Skew (°)	Actual	Median
0	-9.73%	-6.94%
10	-7.62%	-9.93%
20	-5.72%	-6.85%
30	-3.64%	-3.87%
40	-2.93%	-6.87%

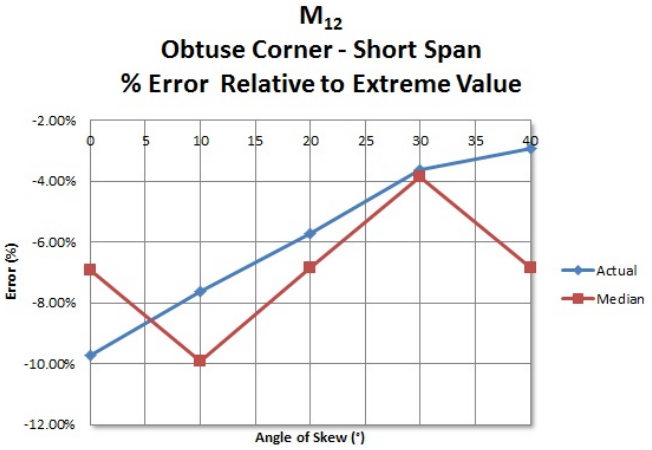

Figure B.3: Carriageway $10\,m \times (8\,m + 15\,m + 15\,m + 8\,m)$: Relative error for the transverse bending moment in the obtuse corner of the first short span

Long Span: The percentage error of the standard NA loading patterns relative to the critical NA loading patterns for the transverse bending moment in the obtuse corner, for the first *long span*, is presented in Figure B.4.

M_{12}
Obtuse Corner - Long Span

	Error (%)	
Angle of Skew (°)	Actual	Median
0	-15.24%	-16.69%
10	-11.16%	-9.33%
20	-11.16%	-10.77%
30	-12.29%	-12.72%
40	-13.35%	-11.82%

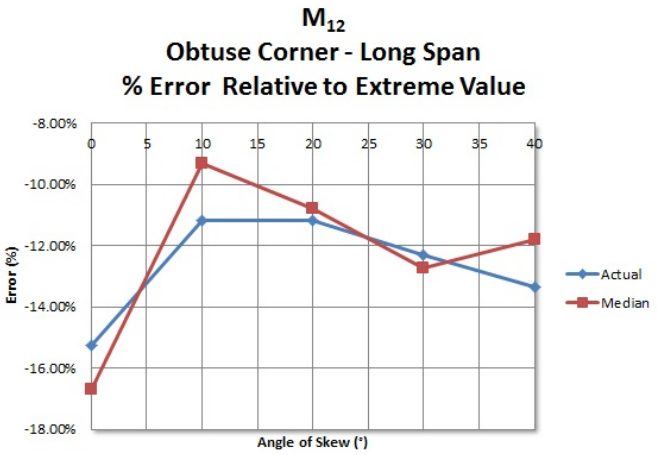

Figure B.4: Carriageway $10\,m \times (8\,m + 15\,m + 15\,m + 8\,m)$: Relative error for the transverse bending moment in the obtuse corner of the first long span

B.2.2 Mid-span Centre

The critical NA loading patterns and resulting contour plots are presented for the transverse bending moment at mid-span, at the centre of the carriageway.

Angle of Skew (°)	Critical NA Loading Pattern	Resulting Contour Plot (Nm)
0°	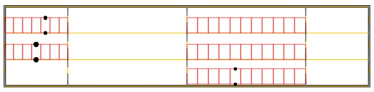 File: 10x8x15x15x8x00.load NA Load Pattern Number: 74	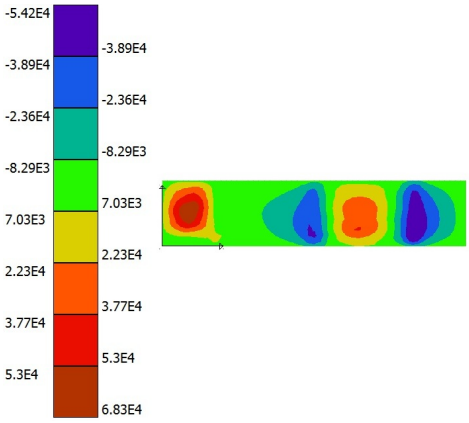
20°	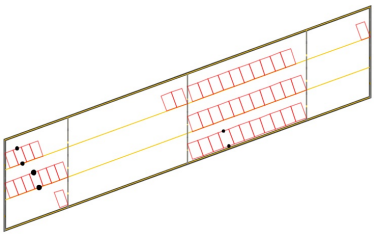 File: 10x8x15x15x8x20.load NA Load Pattern Number: 125	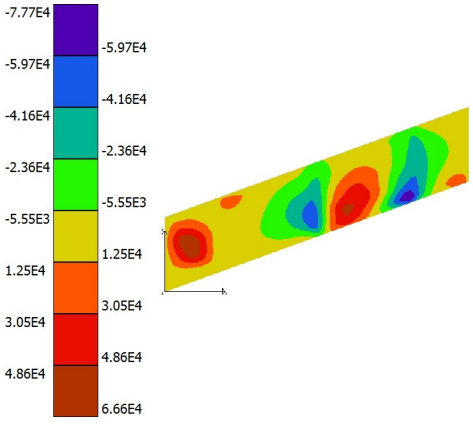
40°	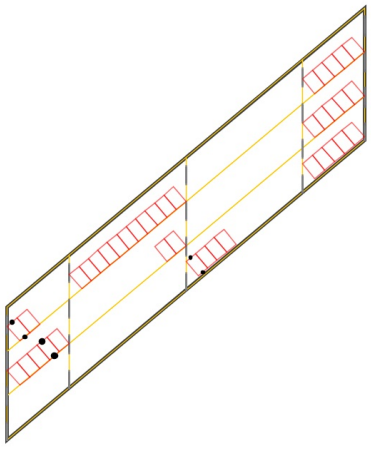 File: 10x8x15x15x8x40.load NA Load Pattern Number: 125	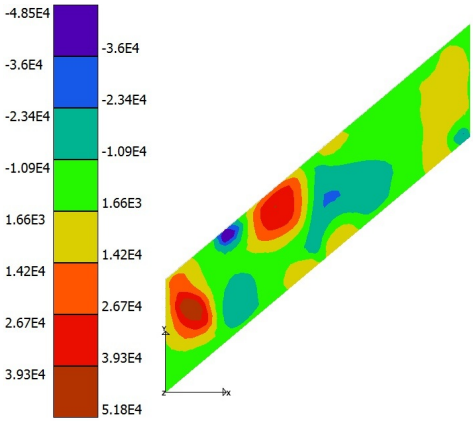

Table B.7: Carriageway $10\,m \times (8\,m + 15\,m + 15\,m + 8\,m)$: Critical NA loading patterns and resulting contour plots for the transverse bending moment at mid-span centre, for the first short span

Short Span: The critical NA loading patterns and resulting contour plots are illustrated in Table B.7 on page B-8 for the transverse bending moment at mid-span, for the first *short span* from the left.

Angle of Skew (°)	Critical NA Loading Pattern	Resulting Contour Plot (Nm)
0°	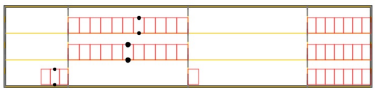 File: 10x8x15x15x8x00.load NA Load Pattern Number: 76	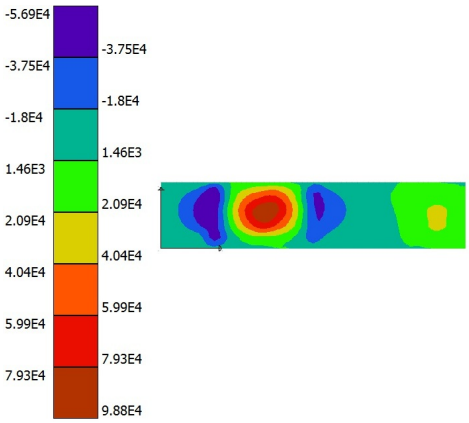
20°	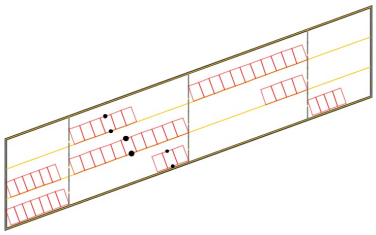 File: 10x8x15x15x8x20.load NA Load Pattern Number: 127	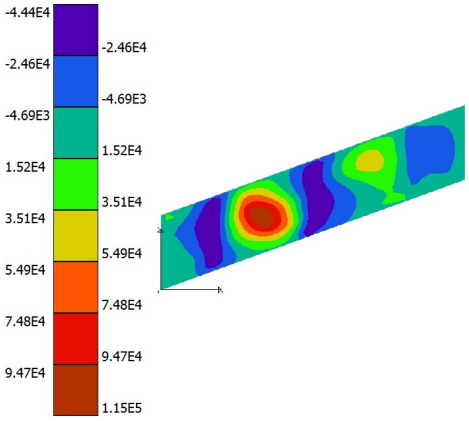
40°	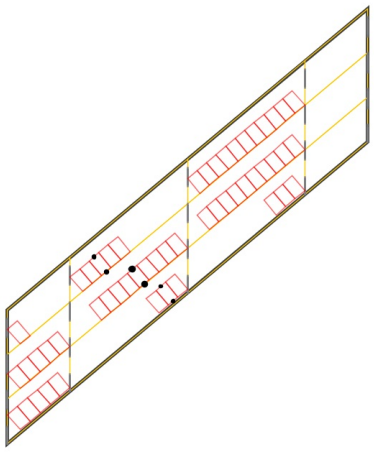 File: 10x8x15x15x8x40.load NA Load Pattern Number: 127	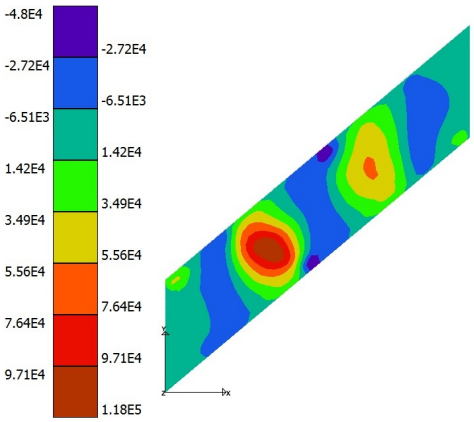

Table B.8: Carriageway $10\,m \times (8\,m + 15\,m + 15\,m + 8\,m)$: Critical NA loading patterns and resulting contour plots for the transverse bending moment at mid-span centre, for the first long span

Long Span: The critical NA loading patterns and resulting contour plots are illustrated in Table B.8 on page B-9 for the transverse bending moment at mid-span, for the first *long span* from the left.

The percentage error of the standard NA loading patterns relative to the critical NA loading patterns are presented as the angle of skew increases from 0° to 40° in increments of 10°. The results include the actual value at the monitored finite element node, the value of the median in the region of the monitored finite element node as well as the Wood and Armer values for the bottom reinforcement in the transverse direction. The Wood and Armer values have been acquired with the assumption that the reinforcement will be placed parallel to the edges of the carriageway in both directions.

Short Span: The percentage error of the standard NA loading patterns relative to the critical NA loading patterns for the transverse bending moment at mid-span centre, for the first *short span*, is presented in Figure B.5.

M_{12}
Mid-Span - Short Span

	Error (%)		
Angle of Skew (°)	Actual	Median	W & A
0	-38.48%	-36.17%	-36.28%
10	-42.47%	-40.66%	-42.47%
20	-48.51%	-46.87%	-51.47%
30	-54.33%	-55.83%	-55.74%
40	-57.36%	-58.84%	-58.15%

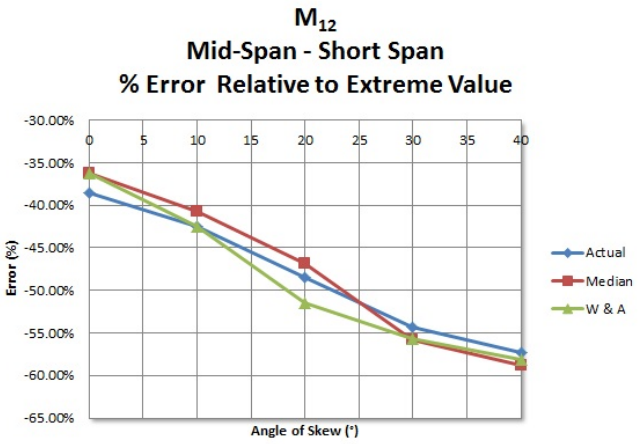

Figure B.5: Carriageway $10\,m \times (8\,m + 15\,m + 15\,m + 8\,m)$: Relative error for the transverse bending moment at mid-span centre, for the first short span

M_{12}
Mid-Span - Long Span

	Error (%)		
Angle of Skew (°)	Actual	Median	W & A
0	-43.88%	-43.73%	-42.06%
10	-37.42%	-33.94%	-38.61%
20	-51.97%	-51.22%	-43.41%
30	-58.88%	-59.12%	-47.23%
40	-68.82%	-68.93%	-57.22%

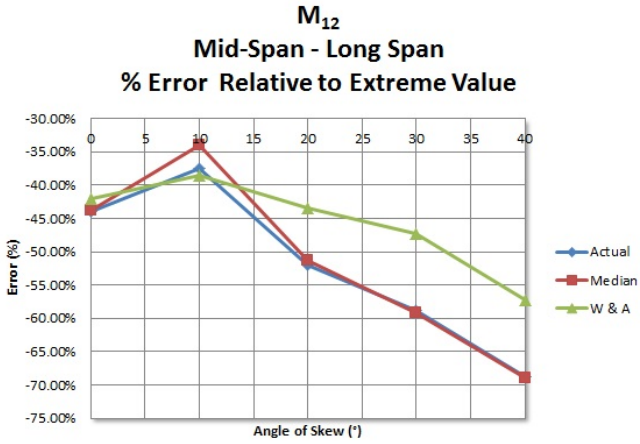

Figure B.6: Carriageway $10\,m \times (8\,m + 15\,m + 15\,m + 8\,m)$: Relative error for the transverse bending moment at mid-span centre, for the first long span

Long Span: The percentage error of the standard NA loading patterns relative to the critical NA loading patterns for the transverse bending moment at mid-span centre, for the first *long span*, is presented in Figure B.6 on page B-10.

B.3 Longitudinal Bending Moment

The longitudinal bending moment is measured at mid-span and over the supports, at the edge of the carriageway. The sagging, hogging and support moments are presented in the next subsections.

B.3.1 Sagging Moment at Mid-span Edge

The critical NA loading patterns and resulting contour plots are presented for the sagging longitudinal bending moment at mid-span, at the edge of the carriageway. The results are presented for both the first short span and the first long span of the particular carriageway.

Short Span: The critical NA loading patterns and resulting contour plots are illustrated in Table B.9 for the sagging longitudinal bending moment at mid-span edge, for the first *short span* from the left.

Angle of Skew (°)	Critical NA Loading Pattern	Resulting Contour Plot (Nm)
0°	 File: 10x8x15x15x8x00.load NA Load Pattern Number: 77	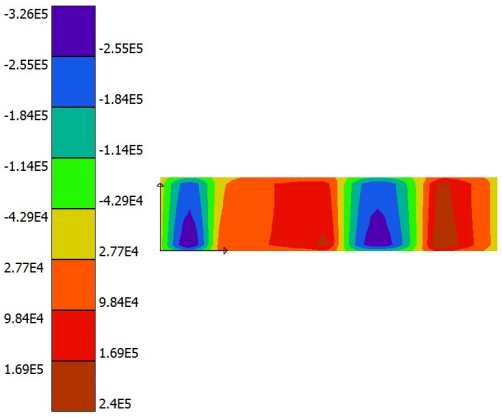
20°	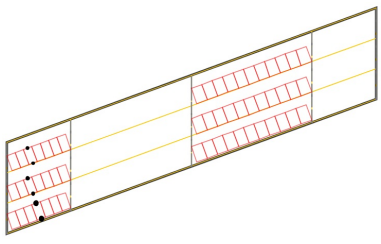 File: 10x8x15x15x8x20.load NA Load Pattern Number: 128	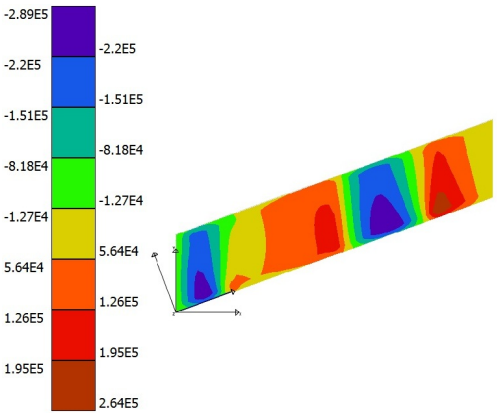

Table B.9: Carriageway $10\,m \times (8\,m + 15\,m + 15\,m + 8\,m)$: Critical NA loading patterns and resulting contour plots for the sagging longitudinal bending moment at mid-span edge, for the first short span (Continued on the next page)

Angle of Skew (°)	Critical NA Loading Pattern	Resulting Contour Plot (Nm)
40°	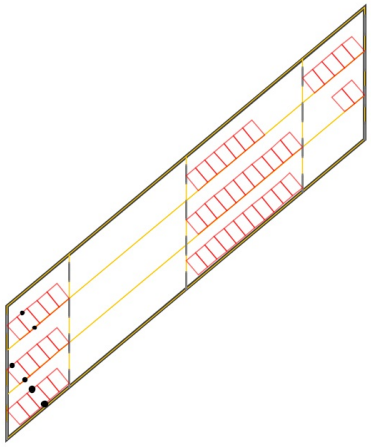 File: 10x8x15x15x8x40.load NA Load Pattern Number: 128	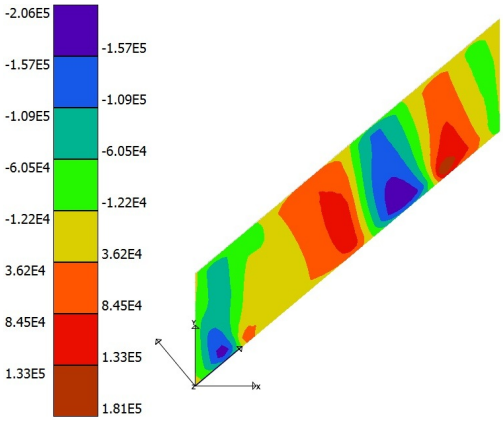

Table B.10: Carriageway $10\,m \times (8\,m + 15\,m + 15\,m + 8\,m)$: Critical NA loading patterns and resulting contour plots for the sagging longitudinal bending moment at mid-span edge, for the first short span (Continued from the previous page)

Long Span: The critical NA loading patterns and resulting contour plots are illustrated in Table B.11 for the sagging longitudinal bending moment at mid-span edge, for the first *long span* from the left.

Angle of Skew (°)	Critical NA Loading Pattern	Resulting Contour Plot (Nm)
0°	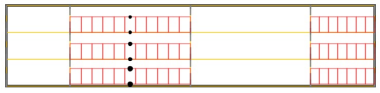 File: 10x8x15x15x8x00.load NA Load Pattern Number: 81	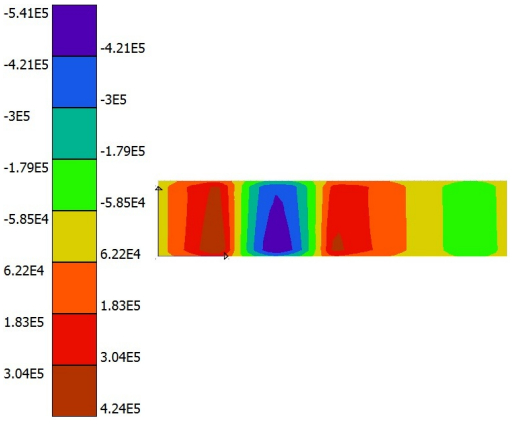

Table B.11: Carriageway $10\,m \times (8\,m + 15\,m + 15\,m + 8\,m)$: Critical NA loading patterns and resulting contour plots for the sagging longitudinal bending moment at mid-span edge, for the first long span (Continued on the next page)

The percentage error of the standard NA loading patterns relative to the critical NA loading patterns is presented as the angle of skew increases from 0° to 40° in increments of 10°. The results include the actual value at the monitored finite element node, the value of the median in the region of the monitored finite element node as well as the Wood and Armer values for the bottom reinforcement

in the longitudinal direction. The Wood and Armer values have been acquired with the assumption that the reinforcement will be placed parallel to the edges of the carriageway in both directions.

Angle of Skew (°)	Critical NA Loading Pattern	Resulting Contour Plot (Nm)
20°	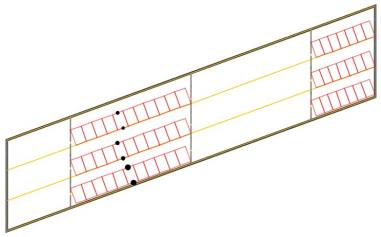 File: 10x8x15x15x8x20.load NA Load Pattern Number: 132	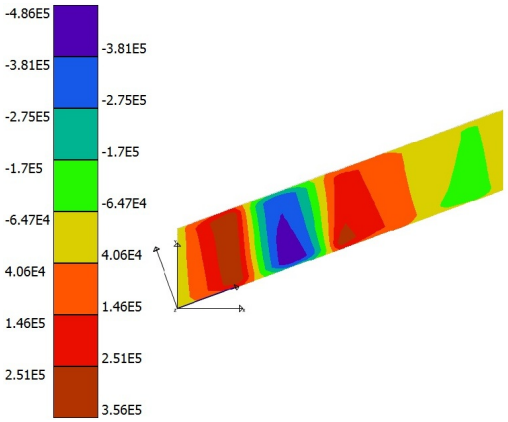
40°	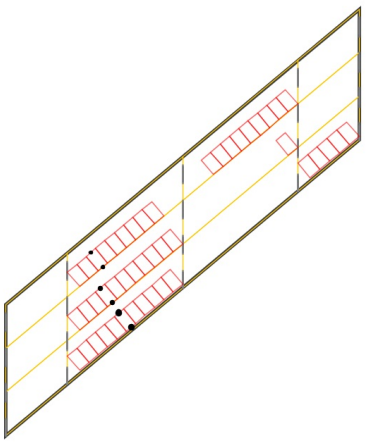 File: 10x8x15x15x8x40.load NA Load Pattern Number: 132	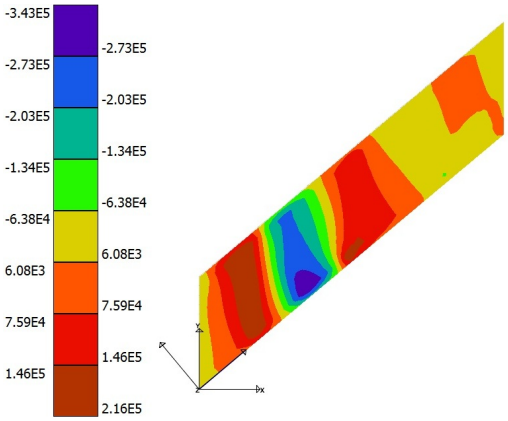

Table B.12: Carriageway $10\,m \times (8\,m + 15\,m + 15\,m + 8\,m)$: Critical NA loading patterns and resulting contour plots for the sagging longitudinal bending moment at mid-span edge, for the first long span (Continued from the previous page)

It can be seen from Table B.9 on page B-11 and Table B.11 on page B-12 that the sagging longitudinal bending moment for a specific span, refers to the moment to be resisted by the bottom reinforcement of the carriageway in that span.

Short Span: The percentage error of the standard NA loading patterns relative to the critical NA loading patterns for the sagging longitudinal bending moment at mid-span edge, for the first *short span*, is presented in Figure B.7 on page B-14.

Long Span: The percentage error of the standard NA loading patterns relative to the critical NA loading patterns for the sagging longitudinal bending moment at mid-span edge, for the first *long span*, is presented in Figure B.8 on page B-14.

M_{21}
Sagging - Short Span

	Error (%)		
Angle of Skew (°)	Actual	Median	W & A
0	-2.74%	-3.37%	-2.55%
10	-2.37%	-2.81%	-2.28%
20	-3.09%	-4.59%	-3.34%
30	-3.41%	-3.56%	-3.62%
40	-3.56%	-6.50%	-4.09%

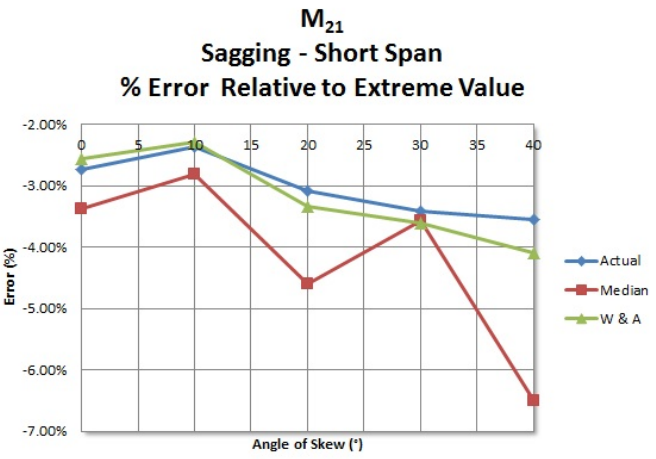

Figure B.7: Carriageway $10\,m \times (8\,m + 15\,m + 15\,m + 8\,m)$: Relative error for the sagging longitudinal bending moment at mid-span edge, for the first short span

M_{21}
Sagging - Long Span

	Error (%)		
Angle of Skew (°)	Actual	Median	W & A
0	-3.16%	-3.76%	-3.03%
10	-2.67%	-2.67%	-2.66%
20	-3.03%	-4.47%	-3.32%
30	-3.36%	-4.57%	-3.69%
40	-4.93%	-6.84%	-5.72%

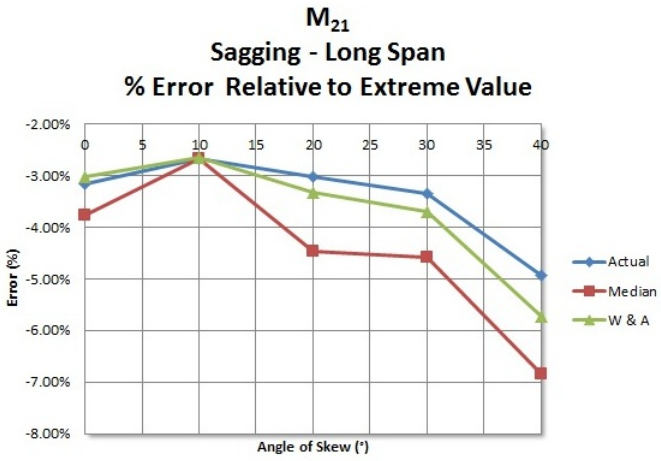

Figure B.8: Carriageway $10\,m \times (8\,m + 15\,m + 15\,m + 8\,m)$: Relative error for the sagging longitudinal bending moment at mid-span edge, the first long span

B.3.2 Hogging Moment at Mid-span Edge

The critical NA loading patterns and resulting contour plots are presented for the hogging longitudinal bending moment at mid-span, at the edge of the carriageway. The hogging longitudinal bending moment refers to the moment to be resisted by the top reinforcement of the carriageway. The results are presented for both the first short span and the first long span of the particular carriageway.

Short Span: The critical NA loading patterns and resulting contour plots are illustrated in Table B.13 on page B-15 for the hogging longitudinal bending moment at mid-span edge, for the first *short span* from the left.

Long Span: The critical NA loading patterns and resulting contour plots are illustrated in Table B.14 on page B-16 for the hogging longitudinal bending moment at mid-span edge, for the

first *long span* from the left.

Angle of Skew (°)	Critical NA Loading Pattern	Resulting Contour Plot (Nm)
0°	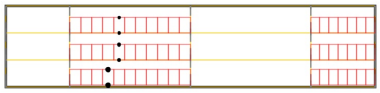 File: 10x8x15x15x8x00.load NA Load Pattern Number: 78	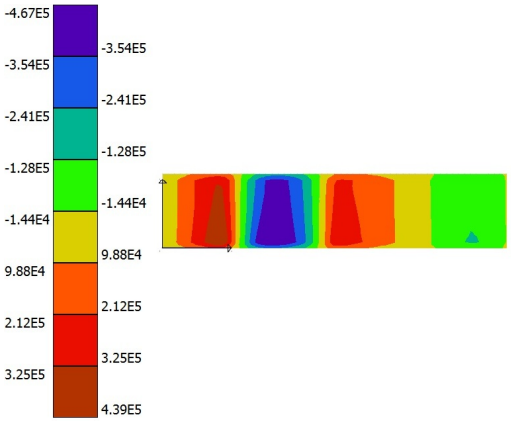
20°	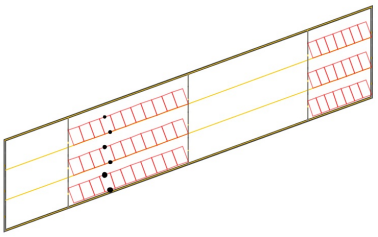 File: 10x8x15x15x8x20.load NA Load Pattern Number: 129	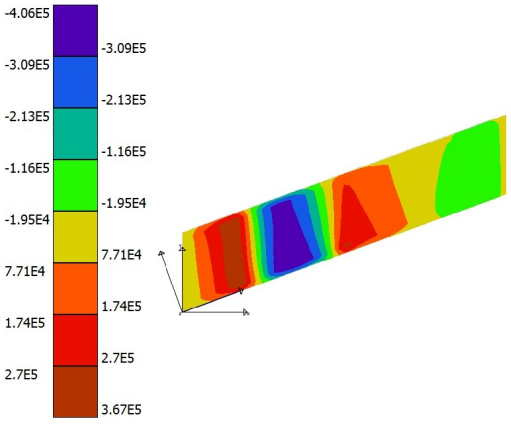
40°	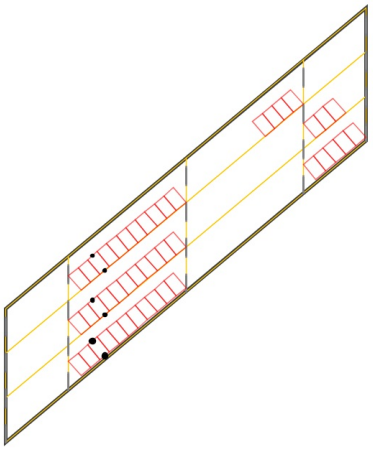 File: 10x8x15x15x8x40.load NA Load Pattern Number: 129	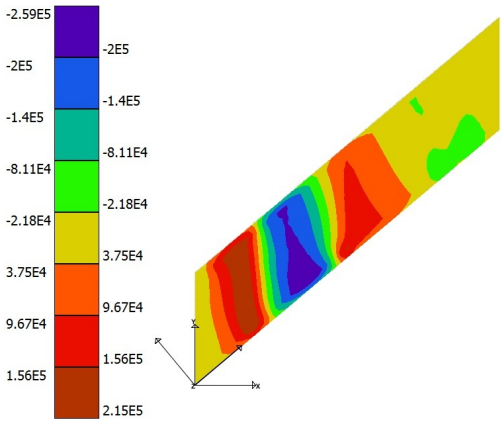

Table B.13: Carriageway $10\,m \times (8\,m + 15\,m + 15\,m + 8\,m)$: Critical NA loading patterns and resulting contour plots for the hogging longitudinal bending moment at mid-span edge, for the first short span

Angle of Skew (°)	Critical NA Loading Pattern	Resulting Contour Plot (Nm)
0°	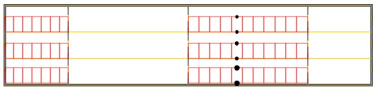 File: 10x8x15x15x8x00.load NA Load Pattern Number: 82	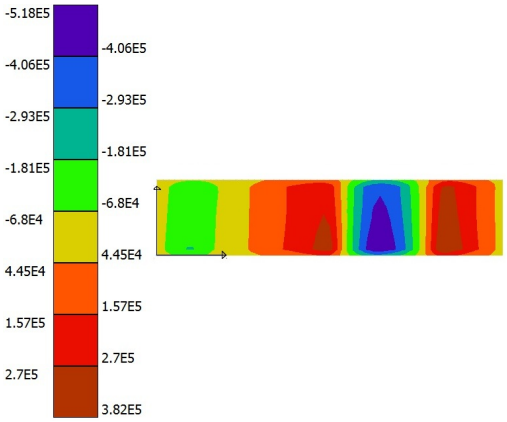
20°	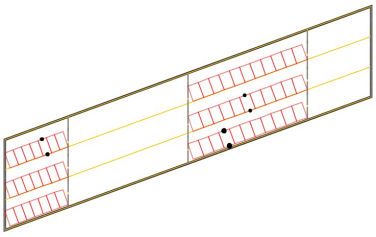 File: 10x8x15x15x8x20.load NA Load Pattern Number: 133	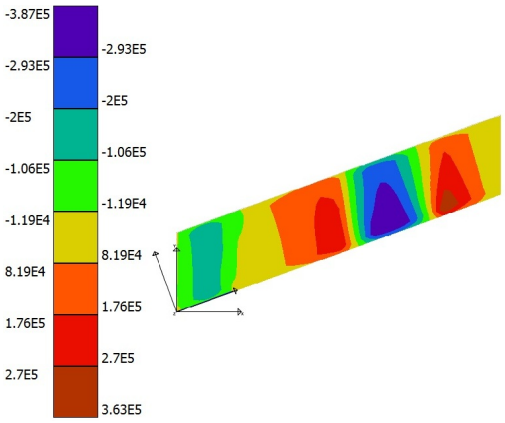
40°	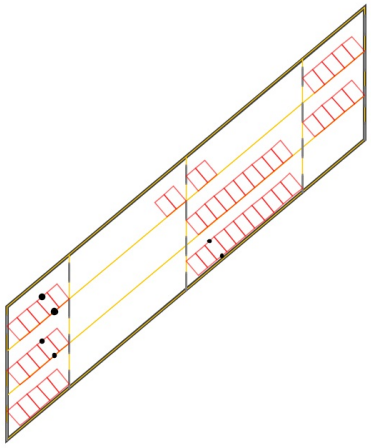 File: 10x8x15x15x8x40.load NA Load Pattern Number: 133	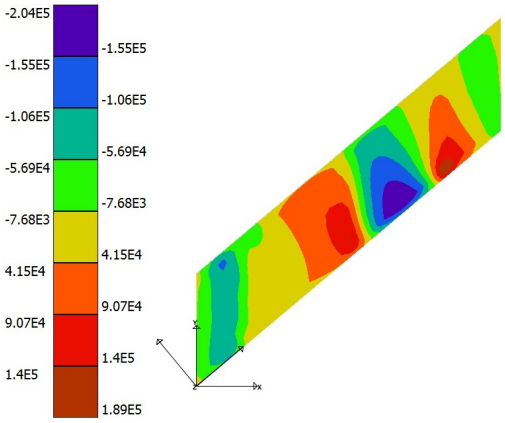

Table B.14: Carriageway $10\,m \times (8\,m + 15\,m + 15\,m + 8\,m)$: Critical NA loading patterns and resulting contour plots for the hogging longitudinal bending moment at mid-span edge, for the first long span

The percentage error of the standard NA loading patterns relative to the critical NA loading patterns is presented as the angle of skew increases from 0° to 40° in increments of 10°. The results include

the actual value at the monitored finite element node, the value of the median in the region of the monitored finite element node as well as the Wood and Armer values for the top reinforcement in the longitudinal direction. The Wood and Armer values have been acquired with the assumption that the reinforcement will be placed parallel to the edges of the carriageway in both directions.

Short Span: The percentage error of the standard NA loading patterns relative to the critical NA loading patterns for the hogging longitudinal bending moment at mid-span edge, for the first *short span*, is presented in Figure B.9.

M_{21}
Hogging - Short Span

	Error (%)		
Angle of Skew (°)	Actual	Median	W & A
0	-6.00%	-6.12%	-7.21%
10	-5.22%	-5.29%	-5.21%
20	-5.22%	-5.20%	-5.30%
30	-5.60%	-5.61%	-5.78%
40	-7.58%	-8.85%	-7.67%

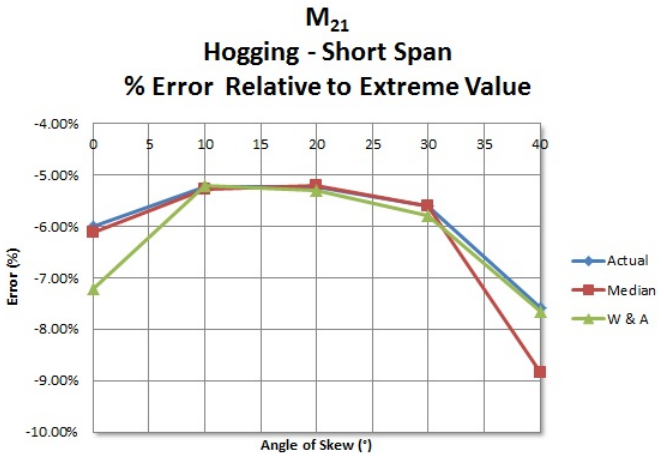

Figure B.9: Carriageway $10\,m \times (8\,m + 15\,m + 15\,m + 8\,m)$: Relative error for the hogging longitudinal bending moment at mid-span edge, for the first short span

Long Span: The percentage error of the standard NA loading patterns relative to the critical NA loading patterns for the hogging longitudinal bending moment at mid-span edge, for the first *long span*, is presented in Figure B.10.

M_{21}
Hogging - Long Span

	Error (%)		
Angle of Skew (°)	Actual	Median	W & A
0	-12.03%	-10.01%	-11.63%
10	-7.99%	-2.80%	-8.18%
20	-10.87%	-8.21%	-13.40%
30	-14.50%	-13.22%	-19.48%
40	-22.25%	-22.45%	-24.99%

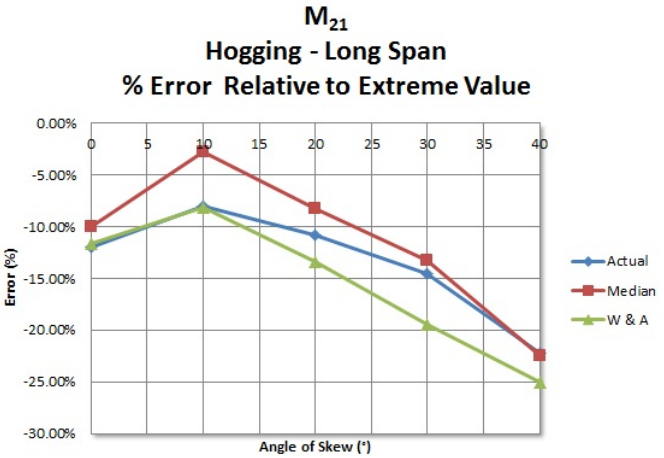

Figure B.10: Carriageway $10\,m \times (8\,m + 15\,m + 15\,m + 8\,m)$: Relative error for the hogging longitudinal bending moment at mid-span edge, the first long span

B.3.3 Support Moment at the Edge

Angle of Skew (°)	Critical NA Loading Pattern	Resulting Contour Plot (Nm)
0°	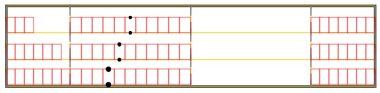 File: 10x8x15x15x8x00.load NA Load Pattern Number: 80	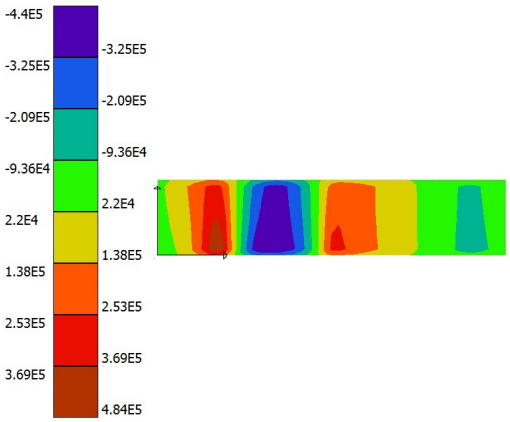
20°	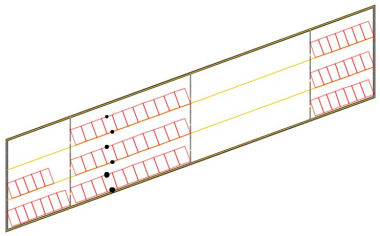 File: 10x8x15x15x8x20.load NA Load Pattern Number: 131	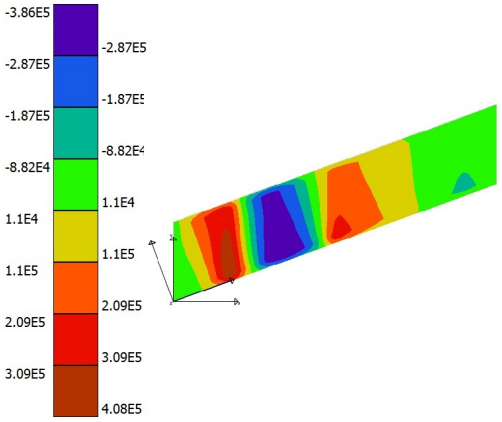
40°	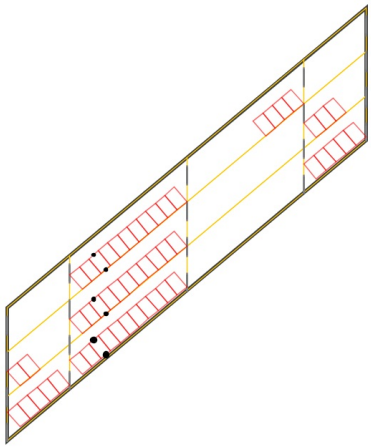 File: 10x8x15x15x8x40.load NA Load Pattern Number: 131	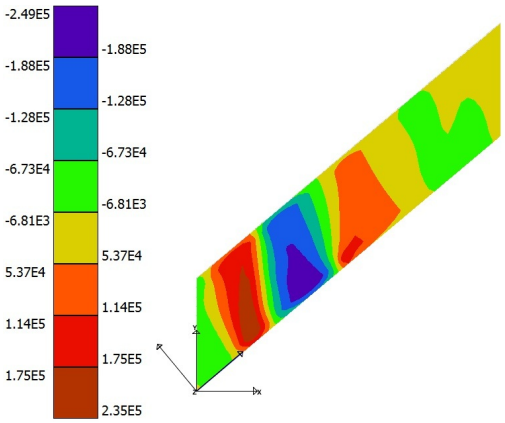

Table B.15: Carriageway $10\,m \times (8\,m + 15\,m + 15\,m + 8\,m)$: Critical NA loading patterns and resulting contour plots for the longitudinal bending moment at the first interior support, at the edge of the carriageway

The critical NA loading patterns and resulting contour plots are presented for the longitudinal bending moment over the supports, at the edge of the carriageway. The longitudinal bending moment over the supports refers to the moment to be resisted by the top reinforcement of the carriageway. The results are presented for the interior support at the first short span and the support at the first long span of the particular carriageway.

Short Span: The critical NA loading patterns and resulting contour plots are illustrated in Table B.15 on page B-18 for the longitudinal bending moment at the first interior support, for the first *short span* from the left.

Long Span: The critical NA loading patterns and resulting contour plots are illustrated in Table B.16 for the longitudinal bending moment at the second interior support, for the first *long span* from the left.

Angle of Skew (°)	Critical NA Loading Pattern	Resulting Contour Plot (Nm)
0°	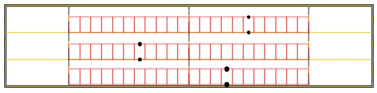 File: 10x8x15x15x8x00.load NA Load Pattern Number: 84	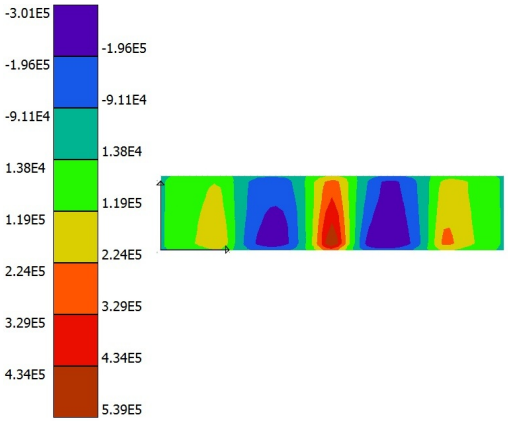
20°	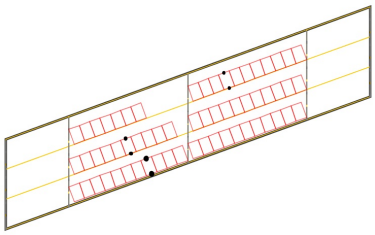 File: 10x8x15x15x8x20.load NA Load Pattern Number: 135	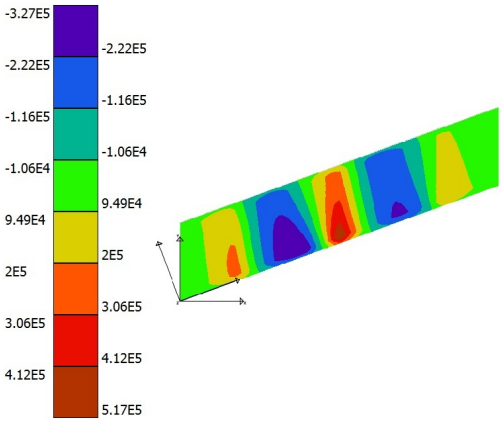

Table B.16: Carriageway $10\,m \times (8\,m + 15\,m + 15\,m + 8\,m)$: Critical NA loading patterns and resulting contour plots for the longitudinal bending moment at the second interior support, at the edge of the carriageway (Continued on the next page)

The percentage error of the standard NA loading patterns relative to the critical NA loading patterns is presented as the angle of skew increases from 0° to 40° in increments of 10°. The results include

the actual value at the monitored finite element node, the value of the median in the region of the monitored finite element node as well as the Wood and Armer values for the top reinforcement, over the supports, in the longitudinal direction. The Wood and Armer values have been acquired with the assumption that the reinforcement will be placed parallel to the edges of the carriageway in both directions.

Angle of Skew (°)	Critical NA Loading Pattern	Resulting Contour Plot (Nm)
40°	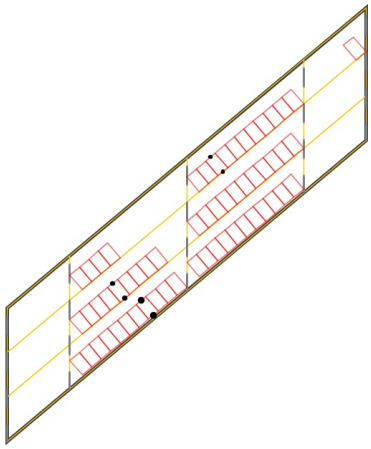 File: 10x8x15x15x8x40.load NA Load Pattern Number: 135	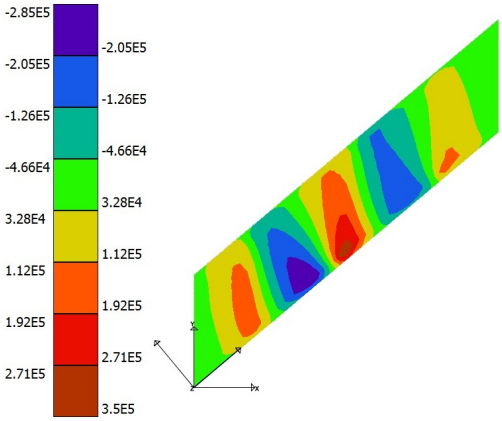

Table B.17: Carriageway $10\,m \times (8\,m + 15\,m + 15\,m + 8\,m)$: Critical NA loading patterns and resulting contour plots for the longitudinal bending moment at the second interior support, at the edge of the carriageway (Continued from the previous page)

Short Span: The percentage error of the standard NA loading patterns relative to the critical NA loading patterns for the longitudinal bending moment at the first interior support, for the first *short span*, is presented in Figure B.11.

M_{21}
Support - Short Span

	Error (%)		
Angle of Skew (°)	Actual	Median	W & A
0	-9.22%	-9.69%	-6.12%
10	-8.75%	-9.02%	-9.23%
20	-8.85%	-8.63%	-9.00%
30	-9.42%	-8.96%	-9.44%
40	-11.27%	-11.07%	-10.98%

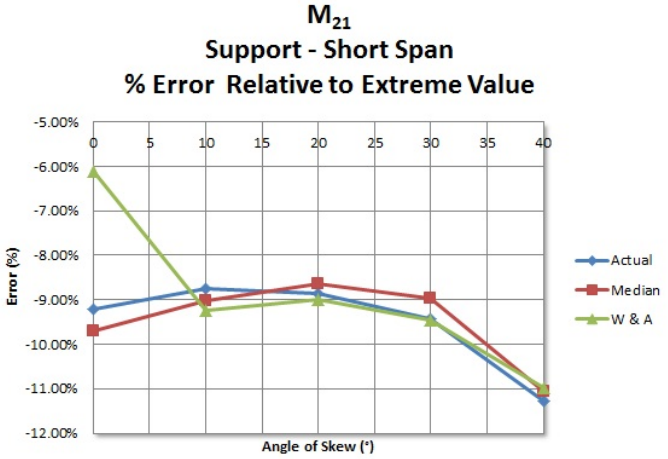

Figure B.11: Carriageway $10\,m \times (8\,m + 15\,m + 15\,m + 8\,m)$: Relative error for the longitudinal bending moment at the first interior support, at the edge of the carriageway

Long Span: The percentage error of the standard NA loading patterns relative to the critical NA loading patterns for the longitudinal bending moment at the second interior support, for the first *long span*, is presented in Figure B.12.

M_{21}
Support - Long Span

	Error (%)		
Angle of Skew (°)	Actual	Median	W & A
0	-14.97%	-16.29%	-13.91%
10	-13.68%	-14.86%	-14.93%
20	-13.19%	-13.18%	-14.05%
30	-13.72%	-11.72%	-14.44%
40	-15.91%	-10.26%	-16.31%

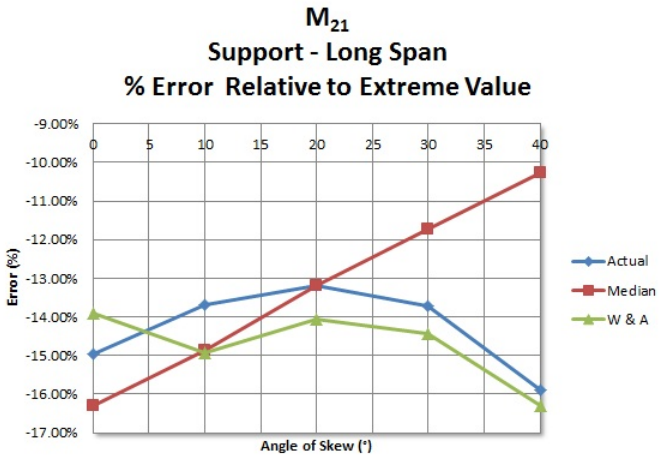

Figure B.12: Carriageway $10\,m \times (8\,m + 15\,m + 15\,m + 8\,m)$: Relative error for the longitudinal bending moment at the second interior support, at the edge of the carriageway

B.4 Normalized Maximum Moments

A multi-span continuous carriageway with an effective width of $10\,m$, two short spans of $8\,m$ and two long spans of $15\,m$ was investigated in this appendix as the angle of skew increases. The two short spans are on either end of the carriageway and the two long spans represent the two centre spans. The critical NA loading patterns were presented for the different moment resultants in each of the critical regions.

The flexural behaviour of the specific carriageway under the effects of normal traffic loading will be presented in this section as the angle of skew increases. The different moment resultant values are normalized and compared *relative* to the largest moment resultant in each of the critical regions for the first short span and the first long span of the particular carriageway.

Short Span: The normalized moment values are shown in Table B.18 for the first *short span* from the left.

	M_{11}	M_{12}		M_{21}		
	Twisting Moment	Bending Moment - Transverse		Bending Moment - Longitudinal		
Angle of Skew (°)	Obtuse Corner	Obtuse Corner	Mid-Span (Center)	Sagging (Edge)	Hogging (Edge)	Support (Edge)
0	0.126	0.133	0.140	0.674	0.471	1.000
10	0.161	0.130	0.151	0.695	0.417	1.000
20	0.222	0.156	0.163	0.708	0.336	1.000
30	0.307	0.213	0.186	0.732	0.243	1.000
40	0.365	0.315	0.217	0.787	0.155	1.000

Table B.18: Carriageway $10\,m \times (8\,m + 15\,m + 15\,m + 8\,m)$: Normalized maximum moments for the first short span

It can be seen from Table B.18 on page B-21 that the longitudinal bending moment over the supports, at the edge of the carriageway, remains the dominant moment resultant for all the angles of skew. The results from Table B.18 on page B-21 are also presented graphically in Figure B.13.

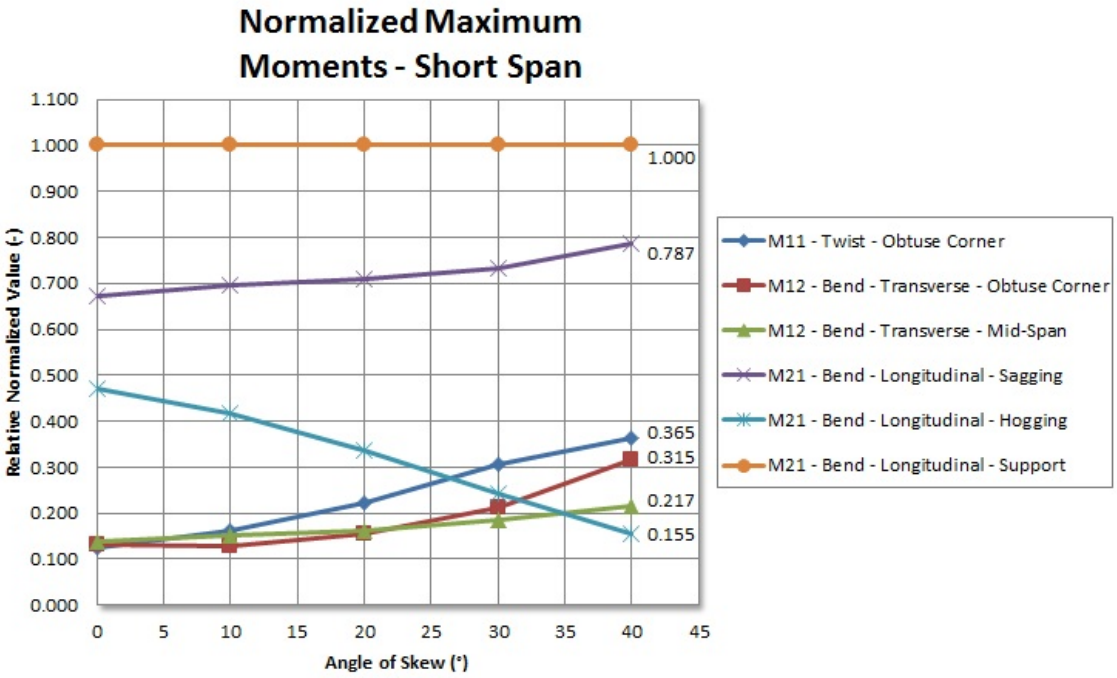

Figure B.13: Carriageway $10\,m \times (8\,m + 15\,m + 15\,m + 8\,m)$: Normalized maximum moments for the first short span

Long Span: The normalized moment values are shown in Table B.19 for the first *long span* from the left.

	M_{11}	M_{12}		M_{21}		
	Twisting Moment	Bending Moment - Transverse		Bending Moment - Longitudinal		
Angle of Skew (°)	Obtuse Corner	Obtuse Corner	Mid-Span (Center)	Sagging (Edge)	Hogging (Edge)	Support (Edge)
0	0.187	0.129	0.179	1.000	0.233	0.996
10	0.271	0.152	0.193	0.979	0.202	1.000
20	0.354	0.209	0.222	0.934	0.160	1.000
30	0.453	0.304	0.268	0.915	0.124	1.000
40	0.543	0.440	0.337	0.911	0.091	1.000

Table B.19: Carriageway $10\,m \times (8\,m + 15\,m + 15\,m + 8\,m)$: Normalized maximum moments for the first long span

It can be seen from Table B.19 that the longitudinal bending moment over the supports, at the edge of the carriageway, remains the dominant moment resultant as the angle of skew approaches and exceeds 10°. The sagging longitudinal bending moment at mid-span, at the edge of the carriageway, is the dominant moment resultant at a 0° angle of skew and remains large relative to the other moment resultants at larger angles of skew.

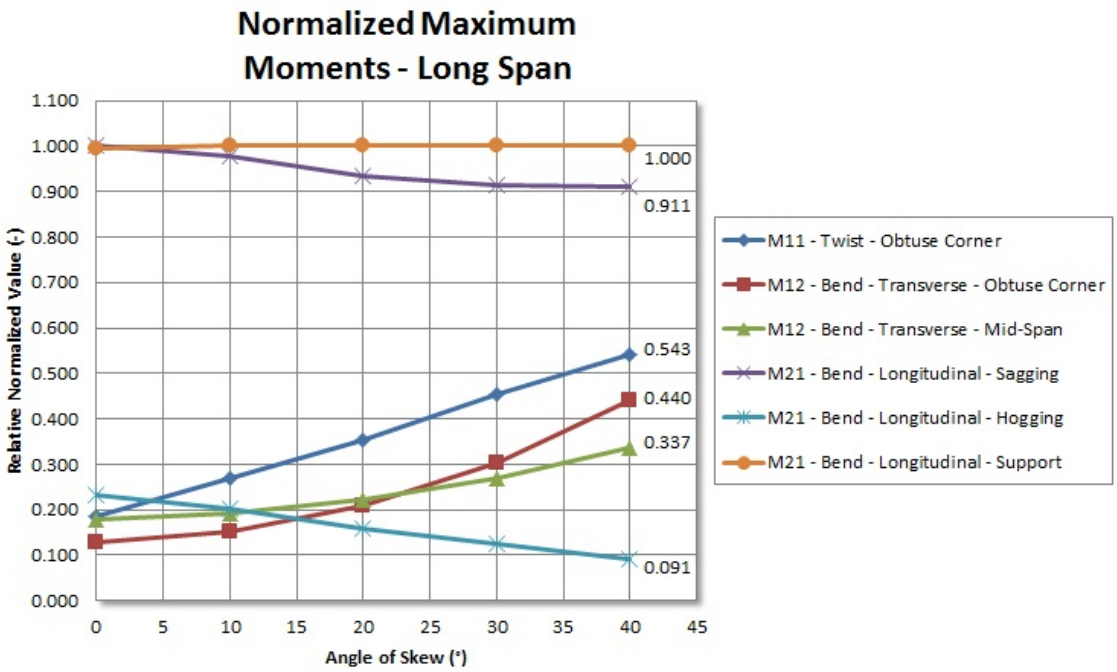

Figure B.14: Carriageway $10\,m \times (8\,m + 15\,m + 15\,m + 8\,m)$: Normalized maximum moments for the first long span

The results from Table B.19 on page B-22 are also presented graphically in Figure B.14.

C Wood and Armer Design Moments

The formulas for acquiring the Wood and Armer design moments according to reference [19] are presented in this appendix. Calculations for the bottom reinforcement and the top reinforcement are presented in the paragraphs below:

Bottom Reinforcement: For the bottom reinforcement the ultimate moments of resistance M_{ux} and $M_{u\alpha}$ are calculated as described below:

$$M_{ux} = M_x + 2M_{xy}\cot\alpha + M_y\cot^2\alpha + \left|\frac{M_{xy} + M_y\cot\alpha}{\sin\alpha}\right|$$

$$M_{u\alpha} = \frac{M_y}{\sin^2\alpha} + \left|\frac{M_{xy} + M_y\cot\alpha}{\sin\alpha}\right|$$

if $M_{ux} < 0$ then $M_{ux} = 0$ with,

$$M_{u\alpha} = \left(\frac{1}{\sin^2\alpha}\right)\left(M_y + \left|\frac{(M_{xy} + M_y\cot\alpha)^2}{M_x + 2M_{xy}\cot\alpha + M_y\cot^2\alpha}\right|\right)$$

if $M_{u\alpha} < 0$ then $M_{u\alpha} = 0$ with,

$$M_{ux} = M_x + 2M_{xy}\cot\alpha + M_y\cot^2\alpha + \left|\frac{(M_{xy} + M_y\cot\alpha)^2}{M_y}\right|$$

Top Reinforcement: For the top reinforcement the ultimate moments of resistance M_{ux} and $M_{u\alpha}$ are calculated as described below:

$$M_{ux} = M_x + 2M_{xy}\cot\alpha + M_y\cot^2\alpha - \left|\frac{M_{xy} + M_y\cot\alpha}{\sin\alpha}\right|$$

$$M_{u\alpha} = \frac{M_y}{\sin^2\alpha} - \left|\frac{M_{xy} + M_y\cot\alpha}{\sin\alpha}\right|$$

if $M_{ux} > 0$ then $M_{ux} = 0$ with,

$$M_{u\alpha} = \left(\frac{1}{\sin^2\alpha}\right)\left(M_y - \left|\frac{(M_{xy} + M_y\cot\alpha)^2}{M_x + 2M_{xy}\cot\alpha + M_y\cot^2\alpha}\right|\right)$$

if $M_{u\alpha} > 0$ then $M_{u\alpha} = 0$ with,

$$M_{ux} = M_x + 2M_{xy}\cot\alpha + M_y\cot^2\alpha - \left|\frac{(M_{xy} + M_y\cot\alpha)^2}{M_y}\right|$$

D User Guide

A user guide is presented in this appendix for the software developed during the course of this study. The user guide consists of two parts:

- A user guide is presented for *viewing* existing loading patterns from files referenced in the body of this document.
- A more detailed user guide is presented for using the software and *generating* new loading patterns for a particular bridge deck.

Each of the user guides are presented using a step-by-step process with illustrations. The software was developed and tested primarily on a Windows operating system. The reader is urged to operate the software in conjunction with this user guide on a Windows system.

D.1 Viewing Existing Loading Patterns

It is not always possible to present NA loading patterns for large bridges, or complex traffic loading patterns, with a sufficient level of detail in printed media, e.g. an A4 page. For the purpose of providing a sufficient level of detail, the NA loading patterns can be viewed in a digital graphical environment. The procedure for viewing existing loading patterns using the software developed during the course of this study is described in this section. Each loading pattern is associated with a specific file and NA loading pattern number. The associated files and NA loading pattern numbers are indicated in the tables that present the results of the various carriageways treated in this study.

Step 1: Start the application by running the SABridgeDesigner.jar file[9]. The graphical user interface will be displayed. Navigate to the File menu and select Open. The procedure is displayed in Figure D.1.

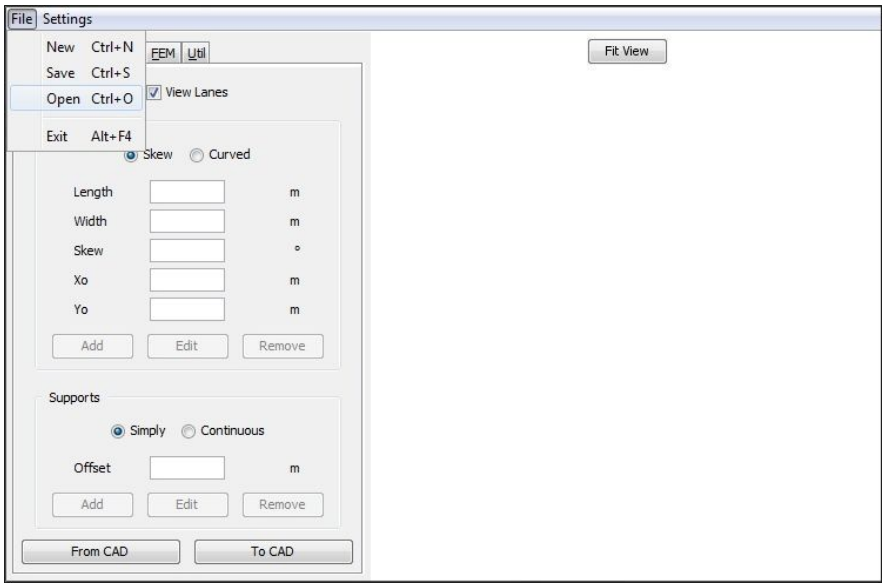

Figure D.1: Step 1: Start the application

[9]When in an Integrated Development Environment start the application by running the file `ui.RunGUI.java`

Step 2: Navigate to and select the file that should be opened, e.g. StandardContinuousPatternsExample.load. Select Open. The procedure is displayed in Figure D.2.

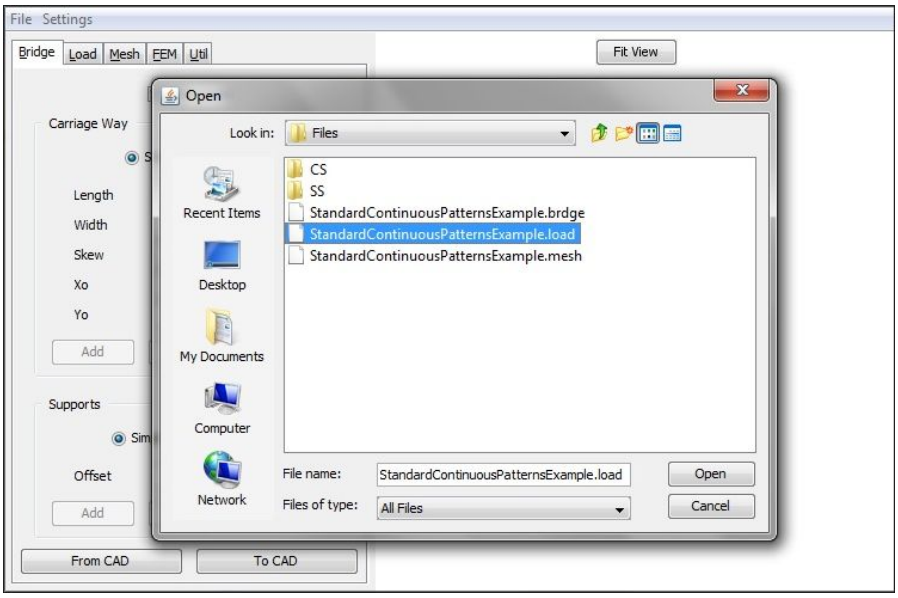

Figure D.2: Step 2: Select the file to open

Step 3: After selecting and opening the file to be viewed, the geometry of the bridge deck will be displayed. The carriageway, supports and notional lanes will be visible. Select the Load tab from the graphical user interface. Then select the Traffic tab and then the NA tab if it is not selected. The procedure is displayed in Figure D.3.

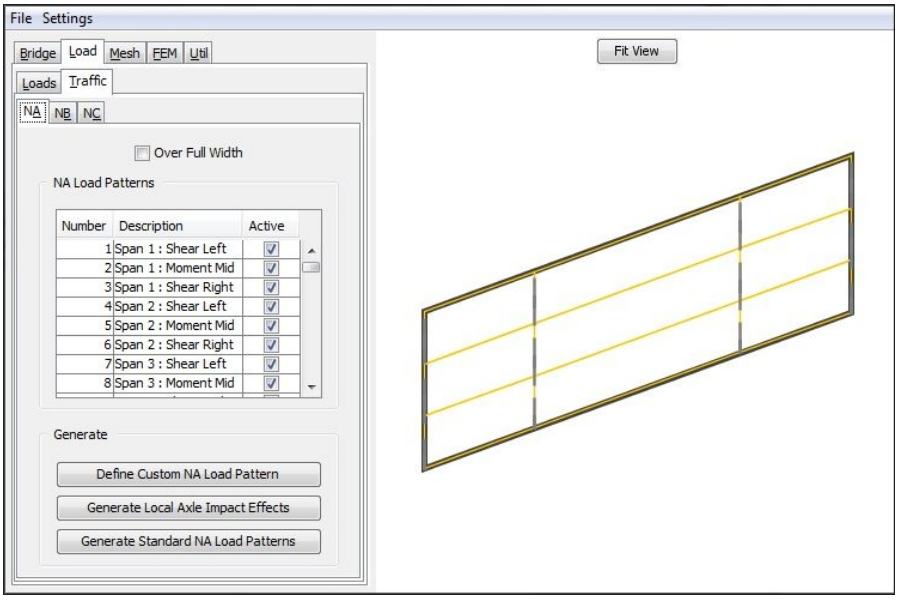

Figure D.3: Step 3: Navigate to the NA traffic load tab

Step 4: After navigating to the NA Traffic Load tab, select the NA loading pattern to be viewed. All the NA loading patterns that were generated for the particular bridge will be displayed in the table. When the mouse is placed over a NA loading pattern a brief description of the pattern will be displayed on the screen. The procedure is displayed in Figure D.4.

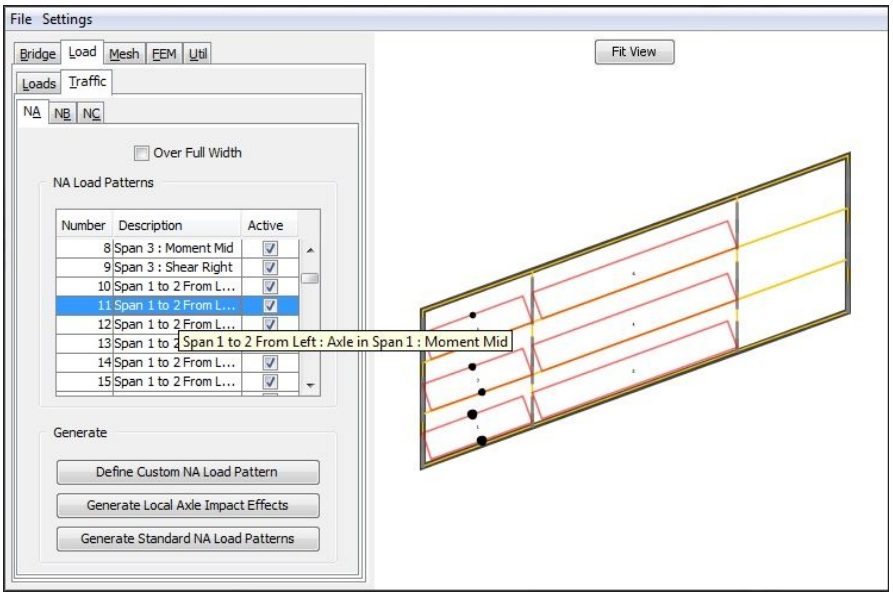

Figure D.4: Step 4: Select the NA loading pattern to view

Step 5: When the NA loading pattern that should be viewed has been selected, the detail of the pattern on the screen may be too small. Navigate to the Settings menu and the Load sub-menu. Select Increase (or Ctrl+I) to increase the graphical indices of the selected NA loading pattern to a sufficient level. The procedure is displayed in Figure D.5.

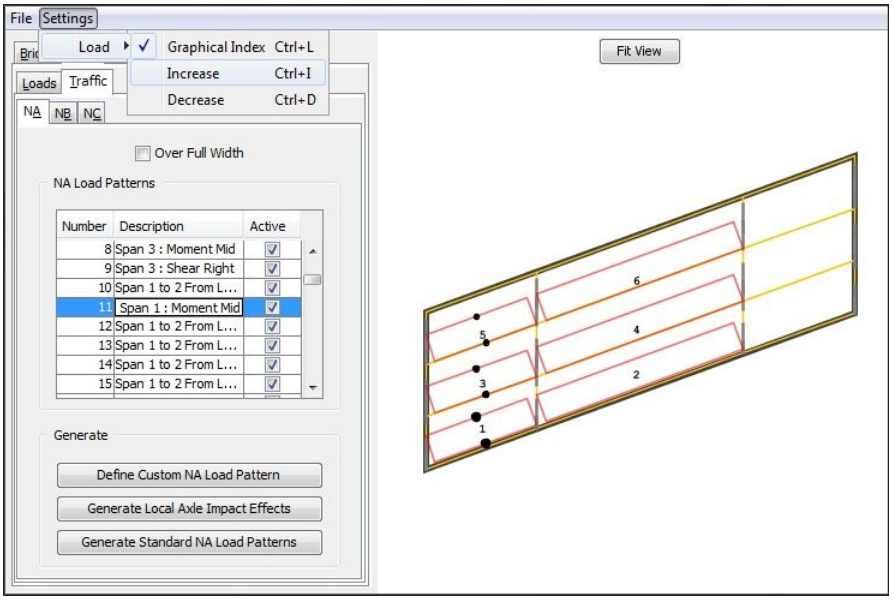

Figure D.5: Step 5: Increase the graphical display of load indices

Step 6: After the NA loading pattern that should be viewed has been selected and the graphical display of the load indices have been increased sufficiently, the NA loading pattern can be viewed in detail. The mouse wheel can also be used to Zoom in on the NA load pattern for a closer view. When the mouse is placed over a part of the NA loading pattern (a distributed part or a concentrated axle part) a full description of that part of the NA loading pattern will be displayed on the screen. Details such as the intensity of the load and the effective loaded length of that part of the load will be displayed. The procedure is displayed in Figure D.6.

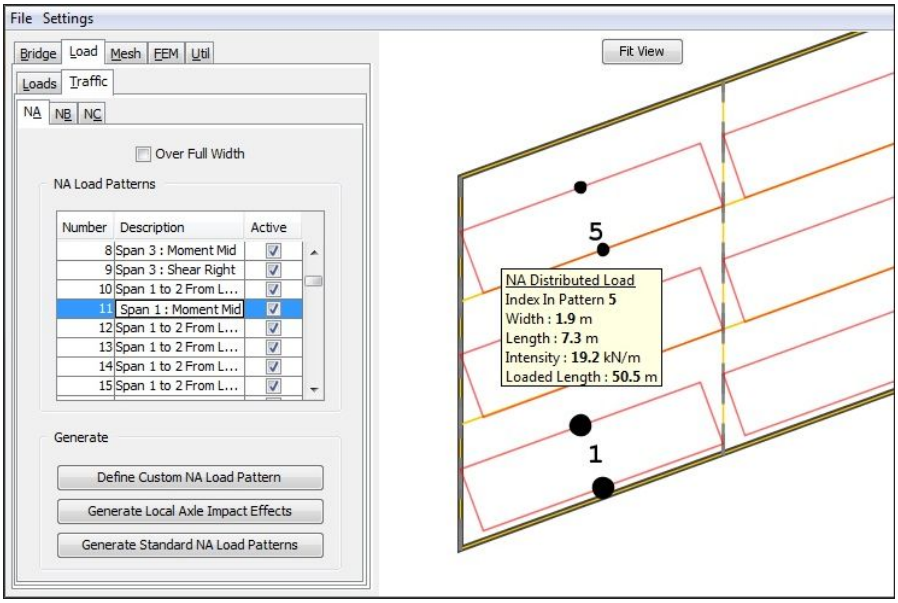

Figure D.6: Step 6: Detailed view of a NA loading pattern

D.2 Generating Extreme Loading Patterns

The basic functionality for using the software was described in the previous section. The procedure for generating new extreme NA loading patterns are described in this section.

D.2.1 Geometry

The geometry of the bridge deck and the position of the supports needs to be defined.

Carriageway: The length, width and angle of skew of the carriageway needs to be defined[10]. An example is developed as an aid to the user guide. A simply supported single span carriageway with the following geometry will be used in the example:

- length of $20\,m$
- width of $15\,m$
- angle of skew of 20°

In the example the carriageway is instantiated with an origin at (0.0, 0.0). The origin can be at different locations for bridges with multiple carriageways. The example is displayed in Figure D.7.

[10]Provision has been made for curved carriageways. Curved carriageways are not treated in this study.

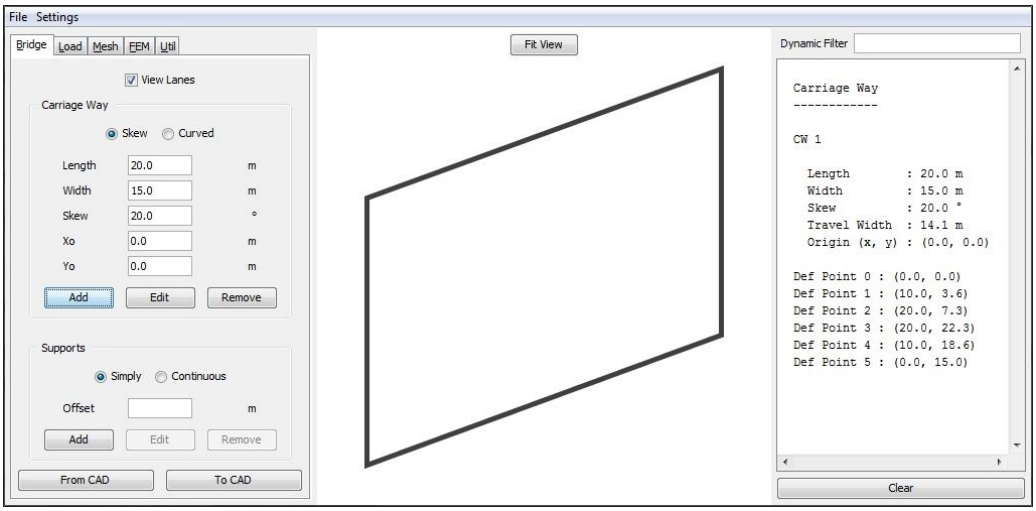

Figure D.7: Step 1: Define the carriageway

After all the data has been typed in the text fields, the carriageway can be added by pressing the Add button in the carriageway section.

Supports: After the geometry of the carriageway has been defined, the offsets of the supports relative to the origin of the carriageway can be defined. In the example the supports are added at the start ($0.0\,m$) and at the end ($20.0\,m$) of the carriageway, as illustrated in Figure D.8.

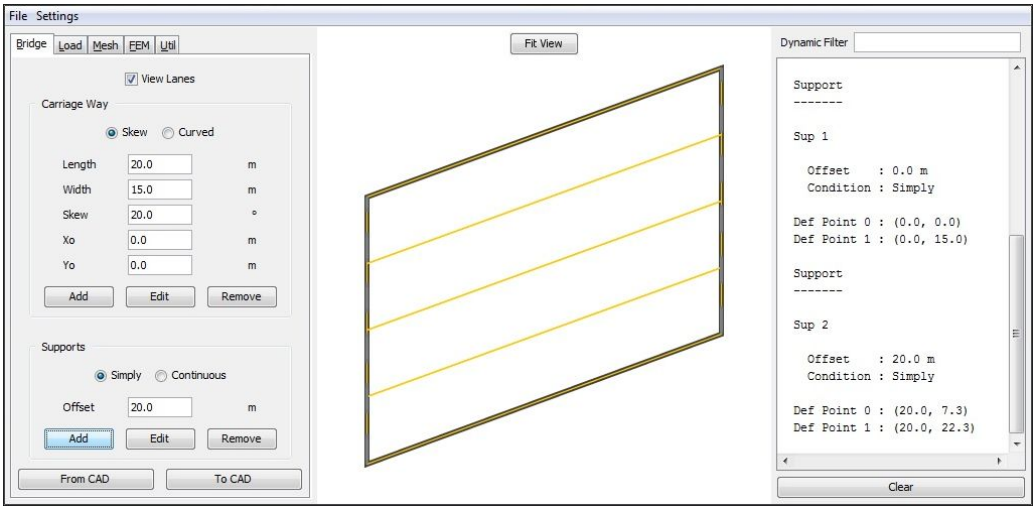

Figure D.8: Step 2: Define the supports

After two or more supports have been added, the notional lanes are calculated based on the effective width of the carriageway. The notional lanes will be displayed if the check box View Lanes is selected. Additional continuous supports can be added for multi-span continuous carriageways.

D.2.2 Mesh Generation

After the geometry of the carriageway has been defined and the supports have been added, the mesh can be generated.

Mesh Parameters: Mesh and material parameters can be set for a specific component by selecting the appropriate component from the Component list on the Mesh tab. For the purpose of this example only the carriageway CW 1 will be in the list. The type of element[11], quality of the mesh and thickness of the elements can be set. The quality of the mesh can be set as a percentage between 50 % and 100 %, while an element width to length ratio of approximately 1.5 is maintained. The material parameters for the specific component can also be set. The procedure for setting appropriate mesh and material parameters are illustrated in Figure D.9.

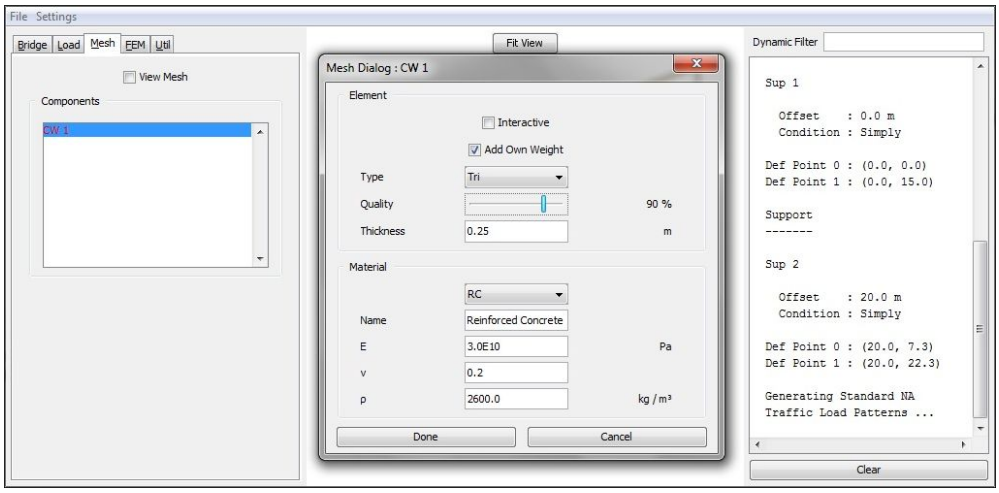

Figure D.9: Step 3: Setting the mesh parameters

The mesh parameters are applied by pressing the Done button. For smaller bridges, the mesh can be generated interactively, by selecting the Interactive check box.

Viewing the Mesh: After appropriate material and mesh parameters are applied, the mesh can be viewed by selecting the View Mesh check box from the graphical user interface on the Mesh tab. The procedure is illustrated in Figure D.10.

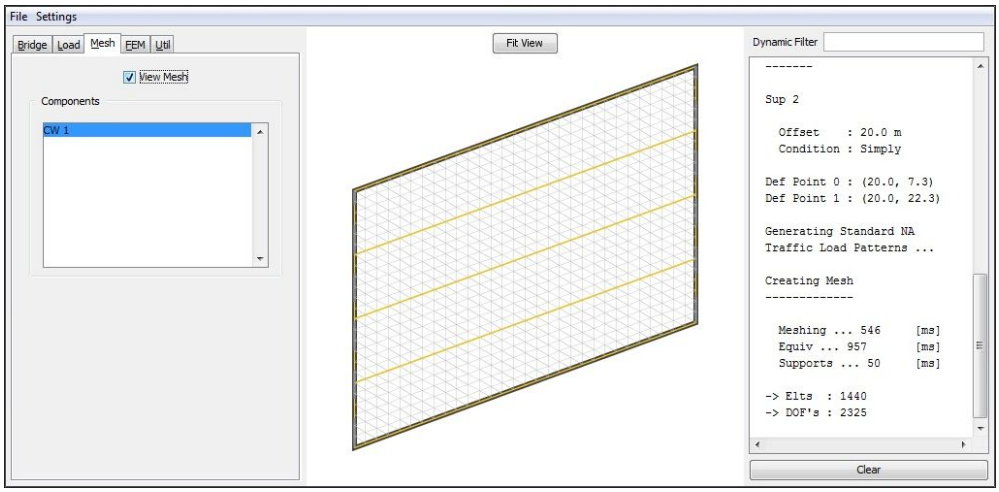

Figure D.10: Step 4: Viewing the mesh

[11] Only triangular plate elements are currently supported.

D.2.3 Load Generation

After the geometry of the bridge deck has been defined and the mesh has been generated, the traffic loads can be generated and applied to the bridge deck. The generation of the standard patterns and the extreme patterns are presented in the paragraphs below.

Standard NA Loading Patterns: The so-called standard NA loading patterns can be generated by navigating to the Load tab, selecting the Traffic tab and then the NA tab. The standard NA loading patterns can be generated by clicking on the Generate Standard NA Load Patterns button. The standard NA loading patterns for the specific carriageway will be generated and displayed in the table. The procedure is displayed in Figure D.11.

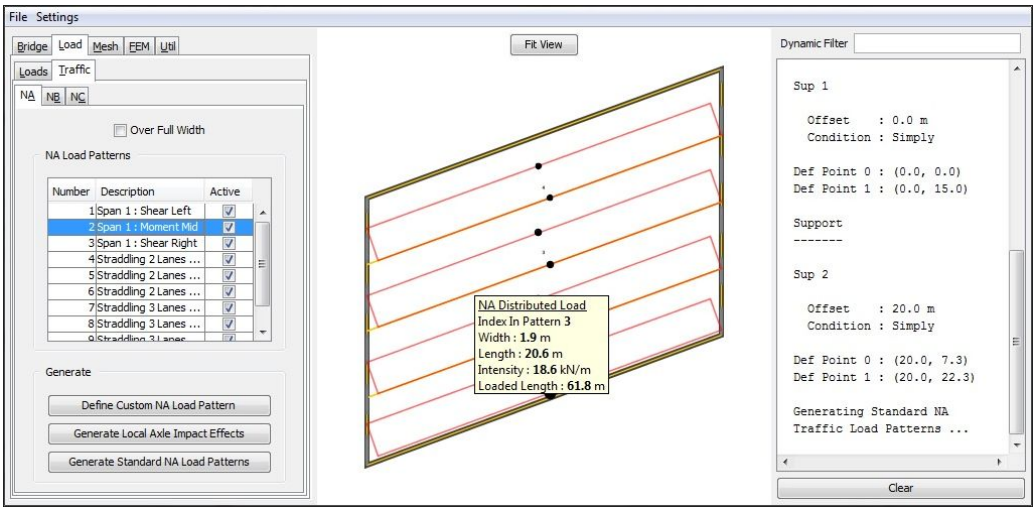

Figure D.11: Step 5: Generate standard NA loading patterns

Extreme NA Loading Patterns: An extreme NA loading pattern can be generated for a specific region of the carriageway, for a selected (flexural) mode of failure.

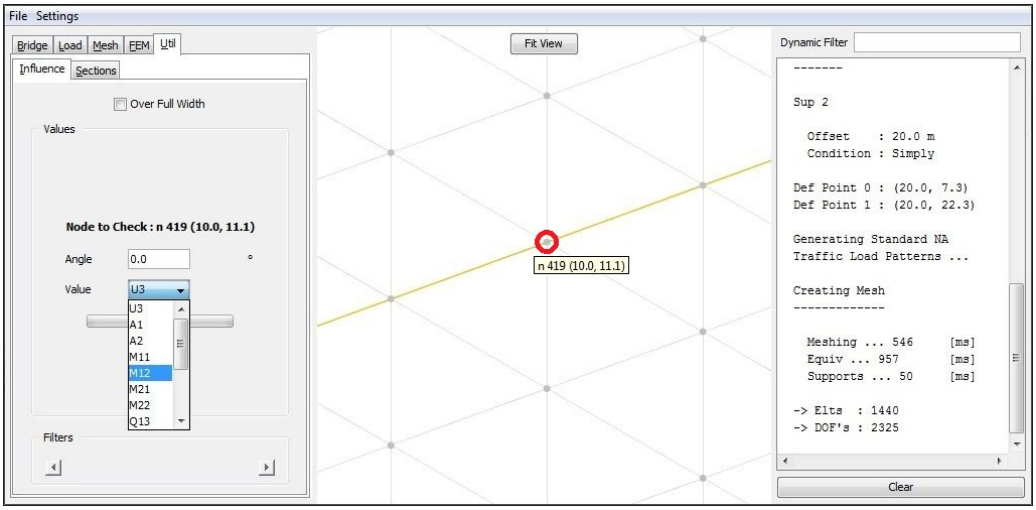

Figure D.12: Step 6: Generate extreme NA loading patterns

Navigate to the Util tab and select the Influence tab. Select the specific finite element node for which the extreme pattern should be generated. In this example the node at mid-span, Node 419, will be selected. The node can be selected by Zooming in and selecting the node by clicking on it, as illustrated in Figure D.12 on page D-7. Next a mode of failure can be selected from the drop down box. For the purpose of this example the transverse bending moment, M_{12}, will be selected. The selected moment resultant can also be rotated to obtain extreme patterns for rotated moment resultants. The extreme NA loading pattern for the specific node and mode of failure will be generated and displayed in the table on the NA Traffic Load tab. Based on the size of the bridge and the quality of the mesh, the generation of an extreme NA loading pattern may take some time to complete. The procedure is illustrated in Figure D.12 on page D-7. The procedure for viewing existing loading patterns was described in section D.1.

D.2.4 Finite Element Analysis

After the geometry of the bridge deck has been defined, the mesh has been generated and the loads defined, a finite element analysis can be performed. Once the finite element analysis has been performed the output can be interpreted. Envelopes of the various load cases can be formed and the NA loading patterns can be compared to each other.

Finite Element Analysis: After the NA loading patterns to be included in the analysis have been selected on the NA Traffic Load tab, the finite element analysis can be performed. Navigate to the FEM tab and select the appropriate load factors. Start the finite element analysis be clicking on the Analyse button on the FEM tab, as illustrated in Figure D.13.

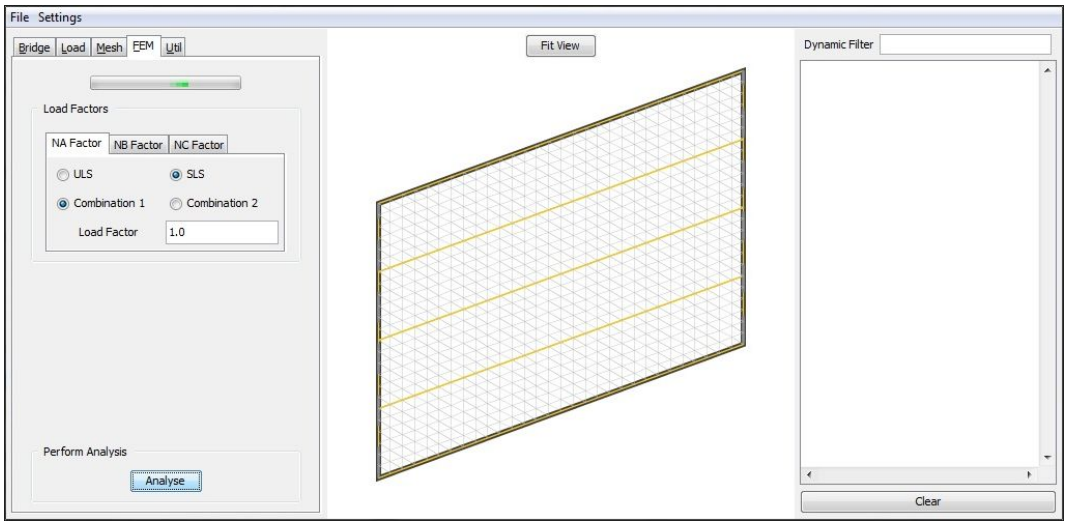

Figure D.13: Step 7: Start the finite element analysis

Only the NA loading patterns marked as Active in the NA Load Patterns table on the NA Traffic Load tab will be included in the analysis.

Viewing Results: After the finite element analysis has been performed, the results from the finite element analysis can be viewed graphically and interpreted. The procedure for viewing the finite element results is illustrated in Figure D.14 on page D-9.

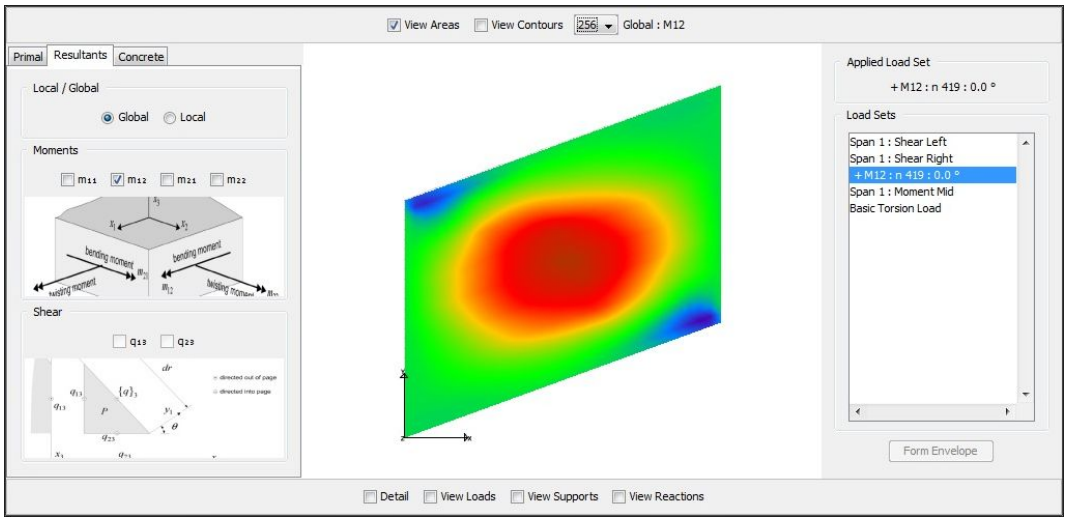

Figure D.14: Step 8: Viewing the finite element results

Additional documentation regarding the functionality and usage of the post-processor can be found in the final year project in reference [12].

E Component Class Diagrams

The object set M, that represents the state of the object model, was described in Chapter 6. An overview of the components[12] of each of the subsets M_{sub_i}, representing each of the sub-models, are presented in this appendix. The overview is presented in the form of UML (Unified Modeling Language) class diagrams. Only the most important classes and interfaces are shown. The reader is referred to the attached source code and the documentation thereof in Appendix F if more detail should be required.

E.1 Bridge Components

The components of the M_{bridge} sub-model are presented in Figure E.1.

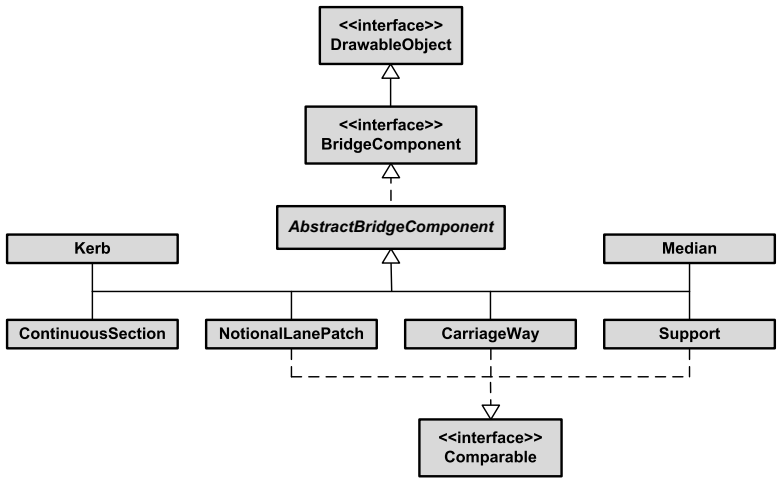

Figure E.1: Class diagram: Bridge components

E.2 Traffic Load Components

The components of the M_{load} traffic load sub-model are presented in Figure E.2.

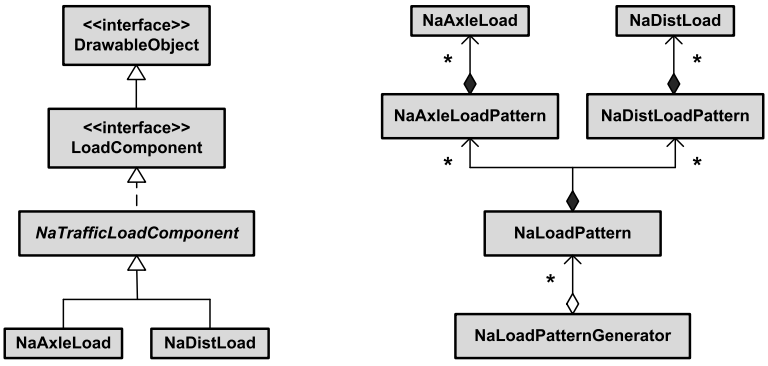

(a) Class diagram **(b)** Association diagram

Figure E.2: Class diagram: Traffic load components

[12]The term "elements of a model" is not used since it may be ambiguous: Finite Element; Mesh Element

E.3 Mesh Components

The components of the M_{mesh} sub-model are presented in Figure E.3. Additional documentation regarding the mesh model implementation can be found in the final year project in reference [13].

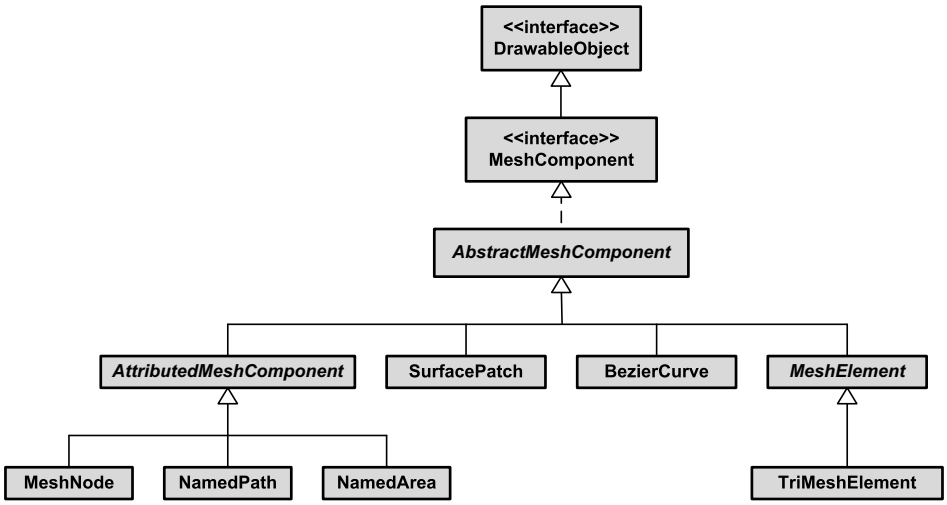

Figure E.3: Class diagram: Mesh components

E.4 Finite Element Components

The components of the M_{fem} finite element sub-model are presented in Figure E.4.

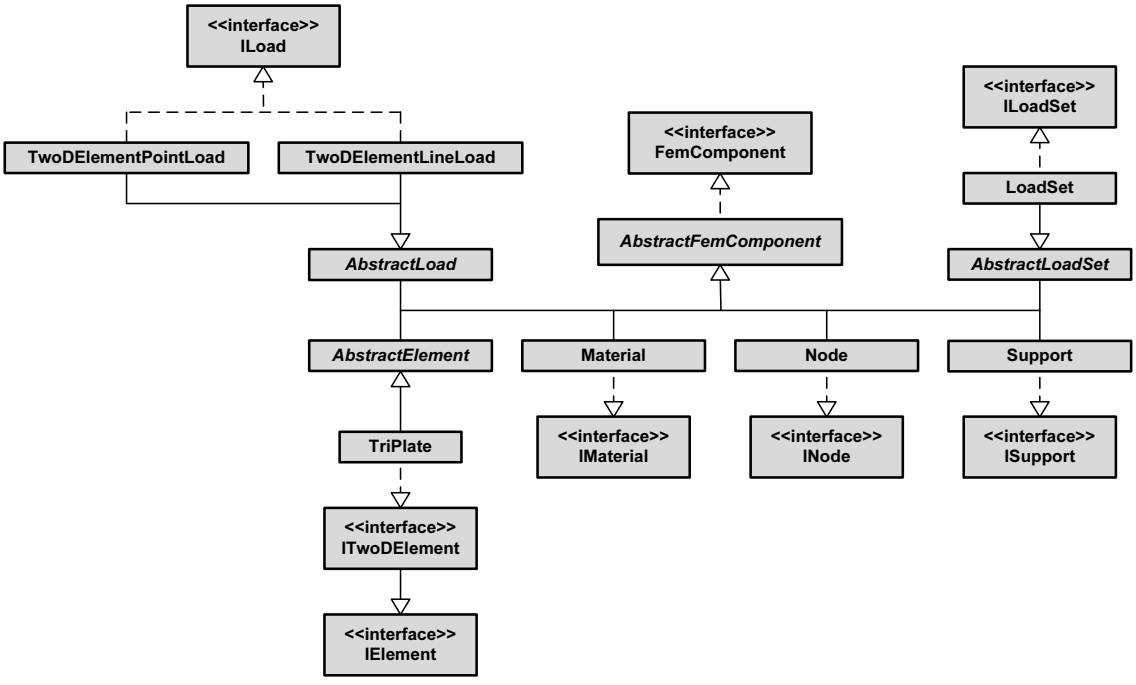

Figure E.4: Class diagram: Finite element components

F Electronic Media

Software, source code, files and results in digital format.